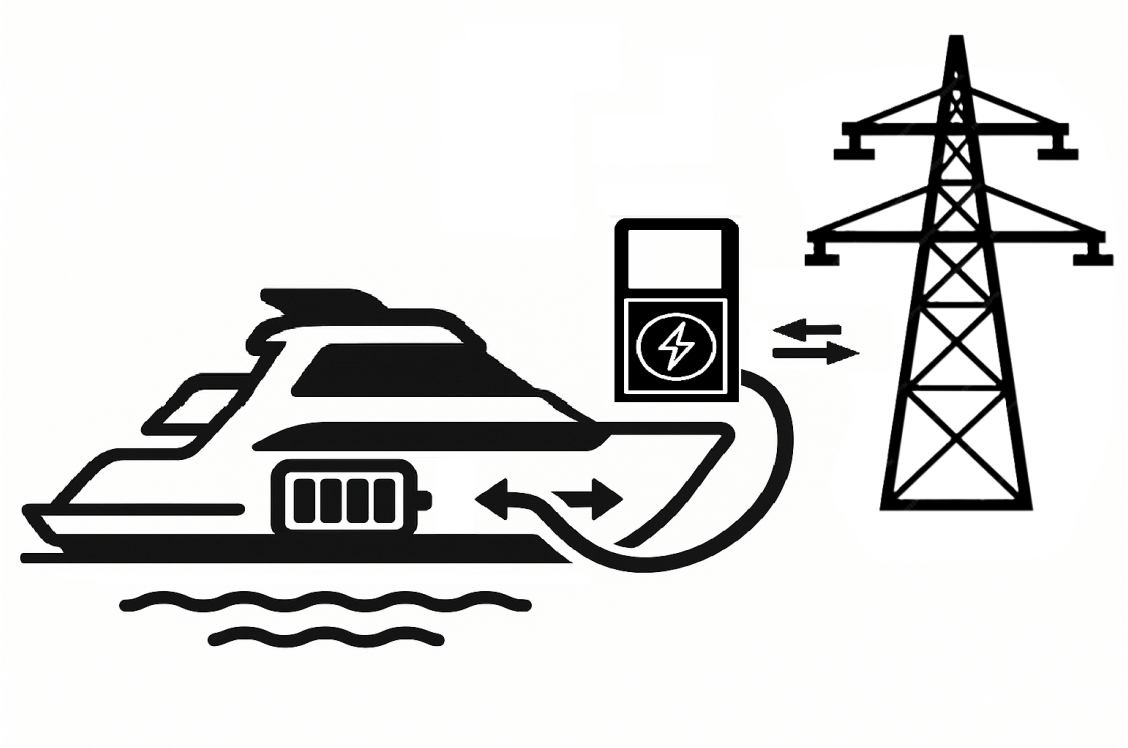

Optimizing B2G Usage to Maximize Revenue and Ensure Warranty Compliance

Master's thesis in Master Mobility Engineering

Peter Mårtensson
Shiyi Qiu

Department of Mechanics and Maritime Sciences

CHALMERS UNIVERSITY OF TECHNOLOGY
Gothenburg, Sweden 2025
www.chalmers.se

Master's thesis 2025

Optimizing B2G Usage to Maximize Revenue and Ensure Warranty Compliance

Peter Mårtensson
Shiyi Qiu

CHALMERS
UNIVERSITY OF TECHNOLOGY

Department of Mechanics and Maritime Sciences
Division of Marine Technology
Chalmers University of Technology
Gothenburg, Sweden 2025

Optimizing B2G Usage to Maximize Revenue and Ensure Warranty Compliance
Peter Mårtensson
Shiyi Qiu

Supervisor: Ringolds Jargans, Volvo Penta
Supervisor: Wengang Mao, Mechanics and Maritime Sciences
Examiner: Wengang Mao, Mechanics and Maritime Sciences

Master's Thesis 2025
Department of Mechanics and Maritime Sciences
Division of Marine Technology
Chalmers University of Technology
SE-412 96 Gothenburg
Telephone +46 31 772 1000

Cover: Visualization of a bidirectional power flow for Boat to Grid.

Typeset in LaTeX
Printed by Chalmers Reproservice
Gothenburg, Sweden 2025

Optimizing B2G Usage to Maximize Revenue and Ensure Warranty Compliance
A Subtitle that can be Very Much Longer if Necessary
PETER MÅRTENSSON, SHIYI QIU
Department of Mechanics and Maritime Sciences
Chalmers University of Technology

Abstract

With the development of maritime electrification, the Boat-to-Grid (B2G) system shows great application potential. The battery is not only used for ship propulsion, but can also participate in grid services. However, B2G usage may accelerate battery degradation. To solve this problem, this thesis builds an optimization model to find the optimal daily usage strategy for boat batteries under B2G. The goal is to maximize profit while protecting battery lifetime. This study selects two typical battery types, Lithium Iron Phosphate (LFP) and Nickel Cobalt Aluminum (NCA), and creates daily usage profiles based on seasonal energy demand in two Swedish cities, Gothenburg and Luleå. The degradation models are considered as constraints. Two optimization methods are used. The first one is based on Model Predictive Control (MPC) with IPOPT solver, using current as the decision variable to maximize daily revenue. The second one is based on Genetic Algorithm (GA) with the DEAP framework, using power as the decision variable to minimize daily cost. In Frequency Containment Reserve (FCR) service, the results show that in most cases both methods can generate optimal charging and discharging strategies under different usage conditions, saving at least 4 % in summer. The battery can still achieve profits while limiting degradation, which reflects that the model has the capability to balance revenue and battery lifetime.

Keywords: electric boats, boat to grid, frequency regulation, battery degradation, LFP, NCA, Model Predictive Control, Genetic Algorithm, bidirectional charging.

Acknowledgements

We are sincerely grateful to our Volvo Penta supervisor, Ringolds Jargans, for his expert guidance and constant encouragement during our thesis work. At the same time, we would like to express our thanks to the Chalmers team, especially Wengang Mao and Chi Zhang, for their kind guidance, valuable suggestions, and continuous support throughout the whole process. We also wish to thank Valeria Castellucci from Uppsala University for her insightful feedback and helpful comments as our subject reader. Finally, we would like to extend our appreciation to Daniel Arnström from Uppsala University, for his support on MPC and CasADi,

Perface

This thesis is a joint Master's thesis project conducted by two students: Shiyi Qiu from Chalmers University of Technology and PETER MÅRTENSSON from Uppsala University. While the work has been carried out collaboratively, the thesis will be submitted separately to each respective university in accordance with their individual academic requirements.

PETER MÅRTENSSON, SHIYI QIU, Gothenburg, June 2025

List of Acronyms

Below is the list of acronyms that have been used throughout this thesis listed in alphabetical order:

FCR	Frequency Containment Reserve
FCR-N	Frequency Containment Reserve Normal
FCR-D	Frequency Containment Reserve Disturbance
B2G	Boat-to-Grid
GA	Genetic Algorithm
MPC	Model predictive control
SEI	Solid Electrolyte Interphase
TSO	Transmission System Operator
SoC	State of Charge
EoL	End of Life
CAGR	Compound Annual Growth Rate

Nomenclature

Below is the nomenclature of indices, parameters, and variables that have been used throughout this thesis.

Indices and notations

i	Index number for boat in fleet
t	Time index
$max(x, y)$	Picks only the largest value of x and y
prim	Primary
secu	Secondary

Parameters

T	Battery temperature [K]
V	Battery pack voltage [V]
η	efficiency
P^{min}	Highest discharge power allowed from wall box
P^{max}	Highest charge power allowed from wall box
K	arbitrary constant
SoC^{min}	SoC floor
SoC^{max}	SoC ceiling
$SoC^{departure}$	SoC required at $t_{departure}$
$t_{departure}$	All values of t for which a boat leaves for sea
$SoC^{docking}$	SoC level when boat docks
$t_{docking}$	All values of t for which a boat arrives back from sea
t_{used}	All values of t for which the boat is at sea
t_{war}	The battery warranty period

I^{min}	Highest output current allowed
I^{max}	Highest charging current allowed
bat^{price}	battery price
deg^{lim}	Degradation level at end of life
Δt	Time discretization step (time interval)
Δf_t	Deviation of frequency

Variables

P^{wall}	Power delivered out from wall box
P^{bat}	Power delivered from battery
SoC	State of charge
C^{bat}	Capacity of battery
I	Current
$C_{rate} = \frac{I}{C^{bat}}$	Current in the case of only primary usage
I^{prim}	
deg^{tot}	Total degradation for a given time step
deg^{h}	Total degradation for the receding horizon
deg^{cal}	Degradation due to calendar aging
deg^{cyc}	Degradation due to cycling aging
deg_{cost}	Cost of degradation
$cost^{el}$	The cost of charging the battery
el^{price}	Electricity price
$cost^{el-FCR}$	The cost of electricity when attending FCR market
R_t	Factor representing how much of the offered power will be consumed
Rev^{FCR}	Revenue gain from attending the FCR market
FCR^{comp}	Compensation for each power unit offered to the grid
P^{size}	Power offered to support the grid
θ	Expression for electricity price as a function of attending the FCR market
δ	Binary constant representing weather or not the battery supports the grid
Rev^{bid}	Final revenue
Pen^{SoC}	Penalty for violating the allowable SoC range

Pen^{deg}	Penalty for exceeding the battery aging limit

Contents

List of Figures

List of Tables

1
Introduction

To justify the time and effort devoted to this thesis, it begins with an introduction chapter. This chapter will provide the necessary background, overall aims and define the specific goals of this work.

1.1 Background

The maritime sector plays a vital role in global transportation and is a significant contributor to greenhouse gas emissions. The International Maritime Organization (IMO) has recognized this challenge and, under its Greenhouse Gas Strategy, aims to reduce CO_2 emissions from international commercial shipping by at least 40 % by 2030 compared to 2008 levels, with a long-term goal of reaching net-zero emissions by 2050 [1]. While these goals specifically address the commercial shipping sector, the transition towards electrification also influences the maritime industry more generally. Electricity is becoming increasingly important in the move towards cleaner energy, not only for commercial ships but also for leisure boats and small-scale transport vessels. This reflects a growing shift across the maritime sector towards low-carbon, sustainable solutions.

Electric boats are expected to grow significantly in the coming years. According to market research, the global electric ship market size is expected to reach USD 14.2 Billion by 2030 from USD 3.3 Billion in 2022 growing at a Compound Annual Growth Rate of 20.0% from 2022 to 2030. This growth is being driven by both policy regulations and advances in battery and charging technology [2].

Meanwhile, the global power generation sector is undergoing a significant transition which has historically been the largest source of CO_2 emissions. From 2018 to 2023, the installed capacities of solar photovoltaics and wind energy more than doubled, and their contribution to electricity generation nearly doubled as well. However, since these variable renewable sources depend on weather conditions, they introduce fluctuations in power supply. As a result, enhancing the flexibility of the entire power system is becoming increasingly essential [3].

One promising solution is to utilize distributed energy storage systems to increase demand side flexibility. In this case, electric boats equipped with high capacity batteries can be used as mobile energy storage assets. In traditional electric boat design, especially for leisure applications, it is assumed that boats are used only a

short time every year, usually between 40 and 90 hours. When the boats are at the dock and connected to power, these boats can be charged at times of low power demand and discharged to the grid at times of high power demand, providing the basis for Boat-to-Grid applications.

However, the increased usage of batteries introduces new challenges. Lithium-ion batteries are one of the most expensive components in the boat. Frequent charge and discharge will increase batteries' degradation [4]. Battery degradation not only increases operational costs but also causes environmental problems, as battery manufacturing and recycling batteries need a lot of energy and materials [5].

1.2 Literature Review

Boat-to-Grid (B2G) technology is a concept where electric boats not only draw energy from the grid but can also feed power back to the grid.

Several projects and modeling studies have shown that Boat-to-Grid (B2G) operations are both technically viable and economically beneficial. Roy et al. [6]propose that the onboard energy storage of a marine microgrid can be utilized as FCAS (frequency control ancillary service) by regulating system voltage and frequency of shore side local grid. The study developed two simulation models using MATLAB/Simulink: one focused on onboard zonal electric distribution (ZED), and the other on ferry-to-grid (F2G) operations. In the F2G model, a coordinated charging of 4 MW BESSs (Battery Energy Storage Systems) of 40 electric vessels to provide frequency control ancillary services (FCAS) to the shore side grid. The results demonstrated that these ferries could significantly contribute to voltage and frequency stabilization during peak load periods, thereby acting as distributed, mobile energy storage units within the power system. The results showed the technical feasibility of integrating maritime transport with grid service, which extended the idea of vehicle-to-grid (V2G) to maritime applications. However, the study did not include battery aging or economic analysis, which are important for real world applications.

Roy et al. [7] investigated the effects of coordinated electric ferry charging on the local distribution network in Gladstone, Queensland, Australia. The authors used OpenDSS software to do power flow analysis based on actual load data. In the model, four battery energy storage systems (BESSs) were implemented, each representing a proposed EF charging station. A dynamic model of the BESSs was developed using MATLAB Simulink and linked to the OpenDSS environment. The simulation results showed that with the coordinated control, the bus voltage increased about 1%–1.5%, the load current decreased around 2%–2.5%. Also,the total power consumption and losses were reduced, especially when the load increased by 80%. The results showed that the control method could keep system parameters within the acceptable range. Moreover, electric ferries can work in both Grid-to-

Ferry (charging) and Ferry-to-Grid (discharging) modes, which means they have the potential to act as distributed energy storage systems and help support the grid [7].

Pintér et al. [8] studied the potential of small electric boats to support the power grid at Lake Balaton in Hungary. Their results showed that small electric boats in the sailing marinas can offer lots of energy storage capacity and interact with the grid. The study estimated that by 2030, the cumulative energy storage potential of these boats could reach up to 15.6 MWh, especially in connection with the promotion of micro-grid solutions, local energy communities, and virtual production integration [8].

Korsner Johansson and Petersson [9] carried out a thorough evaluation of electric boats in Sweden, focusing on their capability to support grid services like frequency containment reserve (FCR). The study found that frequency containment reserve (FCR) currently offers the most favorable revenue potential due to its high compensation and relatively low energy throughput.

Boat to grid applications introduce additional charge discharge cycles beyond normal use. This increase in battery usage accelerates battery degradation. According to the cycle-life modeling study by Wang et al. [10], battery aging is significantly influenced by cycling conditions such as temperature, depth of discharge (DoD), and charge/discharge rate (C-rate). Battery degradation consists of both cycle aging, which is usage dependent, and calendar aging, which is related to time, state of charge (SoC), and temperature.

Wang et al. [11] conducted an empirical study to quantify lithium-ion battery degradation under different operational scenarios, comparing standard driving cycles with participation in vehicle-to-grid (V2G) services, specifically frequency containment reserve (FCR). Their results revealed that daily involvement in FCR for up to two hours imposed only minor additional wear compared to conventional driving. This suggests that participation in ancillary services may be economically viable, as the incremental degradation cost is outweighed by potential revenue, particularly when service duration and current levels are kept within moderate thresholds.

Han et al. [12] proposed an economic model to evaluate the profitability of V2G frequency regulation services while considering battery degradation. Their model estimated degradation costs using a fixed cost per kilowatt-hour of energy discharged. Although their battery testing procedure included both shallow and deep cycling profiles, the economic analysis did not explicitly account for the varying impacts of cycle depth, state-of-charge (SoC), or temperature on battery aging. The simplified degradation representation may limit the model's accuracy under diverse operating conditions and may not fully reflect the nonlinear nature of real-world battery wear.

Previous studies either ignore battery degradation, use overly simple models, or do not apply their results to the maritime field. Few of them considered operational constraints, such as ensuring daily usage requirements or meeting a battery warranty

when analyzing the economic benefits of B2G.

1.3 Goals

This thesis aims to fill the gaps that remain after the literature review. It proposes an optimization framework for electric ships to participate in grid services. The framework includes two main constraints. The first is to guarantee the passing of a minimum battery lifetime for boat. The second is to make sure that the ship is available for daily usage. The model combines real electricity prices, battery degradation model, and primary operations.

The goals for this thesis are:

- Develop battery usage strategies that extend operational lifetime while ensuring effective participation in B2G services.
- Design an optimization framework that maximizes revenue from ancillary services without accelerating battery degradation.
- Establish a control approach that balances grid energy demands with long term battery health.

1.4 Delimitations

The thesis will be bounded by the following general delimitations:

- The aggregator of boat is assumed to be able to provide frequency regulation services and is assumed to not cause any frequency imbalances. All offered bids are assumed to be procured.
- Day-ahead electricity market prices are provided in SEK, with a fixed exchange rate of 10 SEK to 1 EUR applied throughout the study.

Additional delimitations and assumptions will be introduced in the Methodology Chapter.

1.5 Thesis Outline

Chapter 1 introduces the readers to the thesis objectives and provides the necessary background. This is followed by Chapter 2, which sets the stage for understanding the thesis by presenting all necessary theory. Chapter 3 describes the overall methodology, including the adaptation of degradation models and the optimization scenarios evaluated. Chapter 4 presents the results obtained by applying the methodology presented in Chapter 3. These results are interpreted and discussed in Chapter 5, with a discussion summary and conclusions given in Chapter 6. Finally, Chapter 7 proposes potential future work that builds on the findings in this thesis.

2
Theory

This chapter provides the theoretical foundation for understanding the subsequent work in this thesis. It begins by introducing battery structure and two specific battery chemistries. It then shifts focus to aging/degradation and presents two aging models. Following this, there is an introduction of the Swedish frequency regulation market, with emphasis on the specific services and products. The section ends with some theory about Model Predictive Controller (MPC) and Genetic Algorithm (GA).

2.1 Battery structure

As this paper has its core in batteries, this theory section will begin with a short general description of the structure of battery cells. The general structure of battery cells can be seen in Figure 2.1 below. A battery needs to have two electrodes, one positive and one negative. They are commonly referred to as anode and cathode. These are the materials that exchange charge during charging and discharging. The anode is the electrode where oxidation occurs, while the cathode is where reduction occurs. These two electrodes are separated by a thin layer called the separator. The separator is mixed with the electrolyte whose task is to enable ion transportation between the two electrodes. Both electrodes are connected to current collectors, which are the attachment between the electrodes and the external circuit [13].

When a battery is discharged, material in the negative electrode undergoes oxidation and releases an electron. This travels through the circuit to the positive electrode, where it enables a reduction reaction. For discharging, it is therefore the negative electrode that is referred to as anode and the positive electrode that is referred to as cathode. The opposite process and labeling are true during battery charging. This time, it is the negative electrode material that oxidizes and the positive electrode that gets reduced. The chemical reaction in batteries that results in this exchange of charge is usually called a redox reaction. In the continuation of this thesis, the anode and cathode will correspond to the anode and cathode during discharge, hence representing the negative and positive electrode, respectively.
Alongside the redox reaction, ion diffusion takes place using the electrolyte as its medium. This diffusion of positive ions (cations) and negative ions (anions) (if present) is absolutely necessary to maintain charge neutrality in the two electrodes. Keeping the charge of the electrodes constant enables the redox reaction to continue [13].

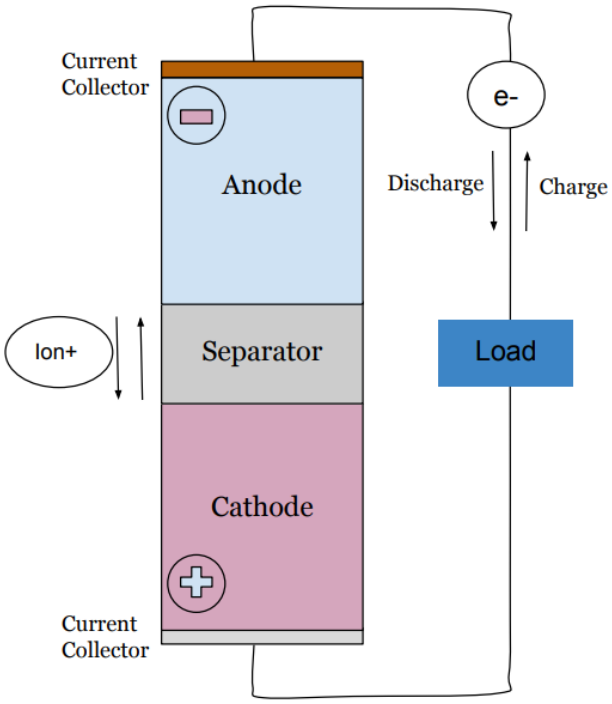

Figure 2.1: Illustration of a general battery structure

Lastly, the purpose of the separator and current collectors is briefly examined. The separator acts as an electrical isolation between the two electrodes, meaning it prevents electrons from passing through it. While being electrically insulating, it should still allow for ionic transport, for the reasons explained previously. By preventing electron transport between the electrodes, using the electrolyte as medium, the separator ensures that any current must flow through the external circuit. Here, the current can be used to provide useful work and power an attached load. Current collectors, on the other hand, are integrated into or attached to the electrodes to enhance their electrical conductivity. This minimizes resistive losses during both charge and discharge [13].

With a general structure of a battery cell presented, we now briefly examine the origin of the induced electron flow. This flow originates from a potential difference between the two electrodes, depending on the materials involved. Each electrode's potential cannot be assigned any absolute value; however, the electrode potential for different materials can be quantized with the use of a reference material. The most commonly used reference is the "standard hydrogen electrode (SHE)", whose potential is set to zero. Using this reference, the relative potential of any other material can be easily found and measured using a voltmeter. This measured potential is called the standard potential for that specific material. For a more detailed description, see Chapter 2 of "Electrochemical engineering" by Fuller eta al. In the same book, Appendix A contains a table of some standard potentials [14].

With standard potentials known for two electrodes, it becomes straightforward to calculate the total cell voltage. It is done by subtracting the half-cell standard potentials, as in Equation (2.1). As a final remark, it is worth noting that other reference electrodes may be used to decide an electrode's potential. As long as both electrodes use the same reference material to decide their potential, the difference in potential will be the same [15].

Table 2.1: Table presenting some of the standard potentials given in [16]

Element	Oxidant	$\rightleftharpoons$	Reductant	Standard potential
F	$F_2 + 2e^-$	$\rightleftharpoons$	$2F^-$	2.87
Cl	$Cl_2 + 2e^-$	$\rightleftharpoons$	$2Cl^-$	1.3595
Cu	$Cu^+ + e^-$	$\rightleftharpoons$	Cu	0.521
H	$2H^+ + 2e^-$	$\rightleftharpoons$	H_2	0
Zn	$Zn^{2+} + 2e^-$	$\rightleftharpoons$	Zn	-0.763
Na	$Na^+ + e^-$	$\rightleftharpoons$	Na	-2.714
Li	$Li^+ + e^-$	$\rightleftharpoons$	Li	-3.045

$$U_{cell} = U^{ref}_{electrode1} - U^{ref}_{electrode2} \tag{2.1}$$

2.1.1 Battery Chemistries

Batteries come in many different forms and sizes, varying in both chemical composition and active material used. Today, lithium ion batteries (LIBs in short) are the most widely used secondary battery chemistry in markets such as consumer electronics, electric vehicles, and grid storage applications. This popularity comes from their high gravimetric and volumetric energy density in combination with their moderate cost [17]. LIBs themselves can be divided into several different types, each with slightly different molecular composition. Some of the most common ones are listed in Table 2.2 together with their abbreviations.

Table 2.2: Different LIB chemistries with their notation and molecular composition[18].

Battery chemistry	Notation
$LiFePO_4$	LFP
$LiMn_2O_4$	LMO
$Li_4Ti_5O_{12}$	LTO
$LiCoO_2$	LCO
$LiNi_xCo_yAl_zO_2$ $(x+y+z)=1$	NCA
$LiNi_xMN_yCo_zO_2$	NMC
$LiNi_{0.5}Mn_{1.5}O_4$	LNMO

In Table 2.2, five out of the six compositions refer to the cathode material used in the specific cell type. LTO is the only composition that is not used as a cathode,

but rather as an anode material [18].

In this report, the focus will exclusively be on LFP and NCA type cells. In 2016, these battery chemistries accounted for 36 respectively, 9 mass % of the LIBs market share [19]. Both chemistries can be found in EVs [19], and are used by companies such as Volvo.

2.1.2 LFP

Lithium-locaion batteries having a cathode made of $LiFePO_4$ are usually referred to as "LFP" cells, and were first introduced in 1997 [17]. The half cell voltage for LFP cathodes, when using Li/Li^+ as reference, is 3.45 volts. A common choice for the anode material is graphite, and the voltage for graphite, using the same reference, is 0.1 volts [18].

This battery chemistry has very long cycle life and is relatively safe [20]. Describing LFP batteries as safe is somewhat misleading, a point highlighted in "The Handbook of Lithium-Ion Battery Pack Design". The book emphasizes that all lithium-ion chemistries exhibit similar failure modes. On the other hand, LFP has lower energy density compared to some of its competitors, which results in less energy dissipation during failure events[21].

Article [20] provides additional arguments, other than that of low energy density, as to why LFP cells are a safer option compared to other competitors. It states that LFP batteries are resistant to many chemicals, making them more chemically stable and less flammable than many other battery chemistries. These properties result in high temperature tolerance and less risk of thermal runaway.

The relatively low price and good environmental profile of LFP batteries are a consequence of iron's high abundance. This contrasts with other materials such as cobalt needed in chemistries such as NCA, NMC, and LCO [17]. Further comparisons between LFP and other lithium-ion chemistries can be made by analyzing Table 7.5 in Chapter 7 in "The Handbook of Lithium-Ion Battery Pack Design". The table shows the fact that LFP has relatively low energy density; however, simultaneously it exhibits high power density. It also highlights the long cycle life of LFP together with its low cost per kWh [21]. Additional relevant properties of LFP cells include their theoretical capacity limit of roughly 170 $mAhg^{-1}$ [20] and its maximum voltage of 3.45 volts [18].

Finally, the major disadvantages of LFP cathodes are examined. One of the primary limitations with LFP cells is their poor electronic conductivity, typically ranging from 10^{-6} to 10^{-10} scm^{-1}. Additionally, LFP has the issue of poor lithium diffusion, limiting the speed of the redox reactions.

The electrical conductivity can be significantly improved by adding carbon materials, which was first postulated by Prof Michael Armand together with his coworkers.

Examples of other measures improving both the electrical conductivity and diffusion length of lithium include the addition of metal oxide, reduction of LFP particle size, and finally doping the electrode material [20].

2.1.3 NCA

As seen in Table 2.2 NCA is the abbreviation for $LiNi_xCo_yAl_zO_2$. The sum of x, y and z should equal one just as for $LiNi_{0.8}Co_{0.15}Al_{0.05}O_2$. This specific combination of NCA has been used as the cathode material in Tesla EVs since the beginning of 2010.

One advantage with NCA compared to LFP is its high theoretical capacity of $280 mAhg^{-1}$. The difference in practical capacity is slightly smaller because LFP cells operate closer to their theoretical capacity limit than NCA cells. According to Table 1 in article [18], the voltage of NCA is also higher than that of LFP [22].

When it comes to batteries using NCA as the cathode material, one has the opportunity to choose between high energy density or high stability. The origin of this tunability follows from the fact that x, y and z can be varied in the chemical formula. Increasing x raises the concentration of nickel which results in a higher energy density. This correlation between nickel concentration and energy concentration follows from the fact that nickel is the primary redox active material in NCA. Unfortunately, a higher nickel concentration also results in more weak bonds in the form of nickel to oxygen bonds(Ni-O), which lowers the overall stability of the cell by increasing the risk of unwanted chemical reactions [23].

2.1.4 Aging

As batteries age, they degrade, and their performance gradually declines. This is often quantified and/or measured by either capacity or power fade. Aging is commonly separated into two categories, namely calender aging and cycle aging. Calender aging refers to the degradation originating from the passing of time. No current has to flow to or from the battery in order for calendar aging to occur. Cycle aging, on the other hand, is the degradation originating from the flow of current [24].
To accurately model battery degradation, both of these contributions should be considered. Therefore, this thesis will account for both calendar and cycling aging when analyzing the degradation of LFP and NCA battery cells. These aging processes are commonly defined by mathematical expressions, four of which are presented below.

LFP calendar aging

The primary factors contributing to calendar aging are storage time, SoC, and temperature. All of these are incorporated into the LFP calendar aging model presented in article [25], as shown in Equation (2.2).

$$C_{fade}(t, SoC, T) = (0.019 \cdot SoC^{0.832} + 0.5195) \cdot (3.258 \cdot 10^{-9} \cdot T^{5.087} + 0.295) \cdot t^{0.8} \quad (2.2)$$

Units for each of the parameters found in Equation (2.2) are presented in Table 2.3. In Equation (2.2) all the parameters are intrinsic and does not depend on the

Table 2.3: Units of parameters and output value for Expression (2.2)

Parameter	t	SoC	T	C_{fade}
Unit	[months]	[%]	[C°]	[%]

battery size. Hence it can be applied for any battery size.

LFP cycling aging

When batteries are frequently used, calendar aging alone is no longer sufficient to model their degradation. In these cases, cycling aging must be included. For LFP batteries, the cycling aging model used in this thesis is taken from article [10] and is presented in Equation (2.3) below. In the paper the allowed C_{rate} (current/capacity) range is between C/2 and 10C, and the current throughput, denoted as Ah, is defined only as the current going into the battery. The other parameters found in Equation (2.3) are temperature denoted as "T", number of cycles denoted as "n", depth of discharge denoted as "DOD" and the battery capacity used in article [10] denoted as C_0. Equation (2.3) also includes a variable denoted B. This variable depends on C_{rate} and its expression was deduced based on interpolation of values listed in Table 3 of article [10]. Equation (2.3) and the expression for B are depicted below.

$$C_{fade}(C_{rate}, n, DOD, T, C_0,) = B \cdot exp(\frac{-31700 + 370.3 \cdot C_{rate}}{R \cdot T}) \cdot Ah^{0.55} \tag{2.3}$$

$$Ah = C_0(DOD \cdot n) \quad , \quad B = 522 \cdot C_{rate}^2 - 7383 \cdot C_{rate} + 3.742 \cdot 10^4$$

Similarly to the calendar aging model, this cycling aging model gives an output in percentage. This unit together with the units for the input parameters for Equation (2.3) are provided in Table 2.4.

Table 2.4: Units for the parameters used in Expression (2.3)

Parameter	C_{rate}	number of cycles (n)	T	DOD	C_0= 2	C_{fade}
Unit	[Ah]	[-]	[C°]	[-]	[Ah]	[%]

NCA calendar aging

Calendar aging for NCA cells is modeled using the expression presented in Equation (2.4), taken from article [26]. Similarly to Equation (2.2), it depends on storage time, SoC, and temperature; however, its appearance differs somewhat.

$$C_{remain}(t, SoC, T, C_0) = C_0 \cdot exp(-k \cdot t^{0.548}) \tag{2.4}$$

$$k = exp(\frac{0.092 \cdot SoC + 170.22 - \frac{72580}{T}}{R})$$

The output of Equation (2.4) represents the remaining battery capacity after subtracting the capacity loss due to previous calendar aging. With this in mind, it becomes clear that C_0. corresponds to the initial capacity and the exponential term

in Equation (2.4) corresponds to the system's degradation factor. This factor is independent of the nominal battery capacity and can therefore be applied to NCA batteries of any size. The units for the parameters found in Equation (2.4) are provided in Table 2.5 below.

Table 2.5: Units for the parameters found in Expression (2.4)

Parameter	t	SoC	T	C_0	C_{remain}
Unit	[days]	[%]	[C°]	[Ah]	[Ah]

NCA cycling aging

In article [27] a cycling aging model for NCA cells is presented. It is given by Equation (2.5) and holds great similarities with Equation (2.3). However, one important difference is that while Equation (2.3) outputs capacity fade in percentage, Equation (2.5) provides the absolute capacity loss.

$$C_{fade}(I, Ah, T) = 130 \cdot exp(\frac{-18461 + 32|I|}{R \cdot T}) \cdot Ah^{0.4} \quad , \quad Ah = C_0(DOD \cdot n) \quad (2.5)$$

Table 2.6 below presents the units for each parameter used in Equation (2.5).

Table 2.6: Units for parameters given in Equation (2.5)

Parameter	I	Ah	T	C_0=7	C_{fade}
Unit	[A]	[Ah]	[C°]	[Ah]	[Ah]

2.1.5 Frequency Regulation and Batteries

In the electricity grid the production and consumption of electricity must always remain balanced. Any mismatch causes the grid frequency and system voltage to change [28]. For a higher demand than supply of electricity, the frequency drops, increasing the risk of blackouts. When supply is higher than the demand for electricity, frequency instead rises, potentially damaging devices connected to the grid [29]. In the Nordic electricity grid the frequency is always balanced around a value of 50 Hertz [30]. This means that if the frequency level is below 50 then production should be increased to exceed the contemporary demand. Having a frequency above 50 calls for the opposite case where production has to be reduced below the size of the contemporary demand. The grid's ability to minimize frequency change and also to restore the frequency to its intended value is what frequency regulation is all about [30, 31].

Factors affecting the frequency change, following a system perturbation, primary include the characteristics of the grid system itself, the access to stabilizing reserves, and the magnitude of the perturbation/disturbance. The deciding factor in determining the frequency robustness of a grid is the total rotational inertia present

in the system [30].

As discussed in article [31] frequency instability can be either short-term, lasting only for a few seconds, or long term, lasting up to several minutes. This is one of the reasons why frequency regulation calls for multiple different types of stabilizing resources [30].

Batteries generally have short activation times, and different batteries can have a variety of power capacities. This makes batteries suitable for a handful of grid stabilization services. In article [32] grid services and resources are sorted into three different categories: high frequency with low intensity, high frequency with high intensity, and low frequency with high intensity. A fourth category can can be added, namely the one with low frequency and low intensity, see Figure 2.2.

The article provides examples such as energy arbitrage, which usually requires high frequency and high intensity, while frequency regulation fits more into the category of high frequency and low intensity. Finally, it presents black start as one of the applications that requires high intensity and low frequency [32].

While batteries offer a wide range of potential applications, certain use cases are more commonly studied and implemented. Since 2010, there has been a clear trend in research and publications on Battery Energy Storage Systems (BESS), with power support, frequency regulation, and voltage support being the most frequently addressed and published applications [33]. As frequency regulation is the primary focus of this thesis, the following two sections will discuss two stabilizing services commonly used for frequency regulation.

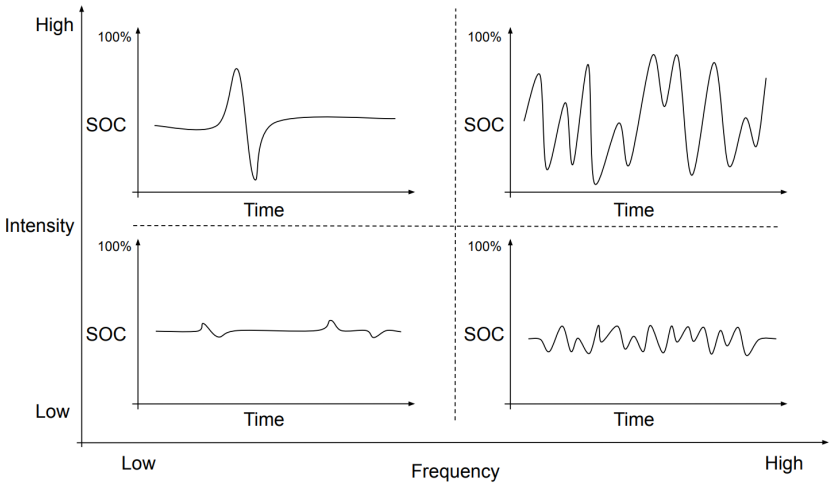

Figure 2.2: Four different types of battery usage profiles that could conduct grid services.

Energy storage using batteries

One tool that can be applied to help optimize the frequency in a grid is to implement energy storage (ES) units. Energy storage units can act as buffers by demanding energy/charging when the production is to high in the system and similarly it can discharge when the production is too low. In doing so ES units can minimize the mismatch between demand and production. Additionally ES systems can be made to have fast response times, enabling accurate and frequent stabilization [28].

Frequency Containment Reserve using batteries

Frequency Contamination Reserves (FCR) aim to stabilize the frequency in the event of frequency deviations and are fundamental to balancing the electricity system. They are activated automatically if the frequency deviation is measured to be within their predefined frequency window. According to the Frequency quality analysis 2022 from Fingird [34], the total number of frequency deviations in 2022 is shown in the Table 2.7. These results show that although extreme deviations rarely occur, frequent small deviations still reflect the necessity of implementing effective frequency control strategies to ensure the stability of the system.

Table 2.7: Total number of frequency deviation in 2022.

f (Hz)	**Total amount**	**Max duration (s)**	**Average duration (s)**
> 50.1	51348	800.80	6.21
> 50.2	211	140.10	5.28
> 50.3	7	10.10	5.34
< 49.9	45398	756.60	5.60
< 49.8	131	83.9	6.92
< 49.7	12	11.80	5.45
< 49.6	3	8.70	6.37
< 49.5	2	4.30	0

2.1.6 Frequency Regulation Markets

The Nordic synchronous power system is a jointly operated electricity network that includes Sweden, Finland, Norway, and Eastern Denmark. Within this synchronous area, all transmission grids are interconnected through an AC network and operate at a common frequency of 50 Hz. Maintaining frequency stability across the region is a shared responsibility among the national Transmission System Operator (TSOs), and is essential for ensuring reliable power system operation [35].

The role and responsibility of Transmission System Operator(TSOs) is to control and operate the transmission grid and transport electricity to regional or local distribution networks [36]. In Sweden, Svenska Kraftnät, have several different an-

cillary services including Fast Frequency Reserve (FFR), Frequency Containment Reserve(FCR), automatic Frequency Restoration Reserve (aFRR), and manual Frequency Restoration Reserve (mFRR). These products are traded in markets where participants bid by offering specific capacities at chosen prices. There is also a minimum bid size requirement for products that can be offered on the market. In order for biders to participate in the market for ancillary services they need to get a permission and a approved result from the prequalification. Prequalification is the process used to test the unit or group that plans to deliver ancillary services [37]. In the following Table 2.8 there is the overview of three different Frequency Containment Reserve products [38].

Table 2.8: Overview of the requirements for reserves.

	FCR-D upward	**FCR-D downward**	**FCR-N**
Description	Upward regulation	Downward regulation	Symmetrical upward and downward regulation
Minimum bid size	0.1 MW	0.1 MW	0.1 MW
Activation	Automatic linear activation within the frequency interval 49,90 - 49,50 Hz	Automatic linear activation within the frequency interval 50,10 - 50,50 Hz	Automatic linear activation within the frequency interval 49,90 - 50,10 Hz
Activation time	Presented in the document with technical requirements for FCR	Presented in the document with technical requirements for FCR	Presented in the document with technical requirements for FCR
Volume requirements	Up to 542 MW for Sweden	Up to 542 MW for Sweden	224 MW for Sweden
Endurance	At least 20 minutes	At least 20 minutes	1 hour

2.1.7 Bidding Procedure

The reserves for FCR-N, FCR-D upward, and FCR-D downward are secured through two complementary day-ahead auctions. The majority of the required capacity is acquired during the first auction, while the remaining portion is acquired in the second round. The volume of FCR that may be provided per unit is limited to a maximum of 5% of the total FCR requirement. For instance, if the Nordic region requires 600 MW for FCR-N and 1450 MW for FCR-D upward, a single unit can provide maximum 30 MW and 72.5 MW, respectively [39].

The procurement and pricing of these reserves are based on market mechanisms. The up regulating price is the price of the most expensive up regulating energy bid accepted, whereas the down regulating price is the price of the cheapest down regulating energy bid accepted [40]. The following Table 2.9 provides an overview

of how different ancillary services are procured and priced [41]. FCR full activation frequency deviation for FCR-N is ± 100 mHz. The activation within the interval 49.9 to 50.1 Hz must be proportional to the frequency deviation. 0% activation is required at 50.0 Hz. When the frequency drops to 49.9 Hz or lower, the 100% FCR-N capacity in upward direction should be activated.When the frequency equal to or above 50.1 Hz 100% of the FCR-N capacity being activated in the downward direction should be activated. The control response follows a linear relationship within the 49.9 Hz to 50.1 Hz [42].

Table 2.9: Procurement and pricing of reserves.

Feature	**FCR-D upward**	**FCR-D downward**	**FCR-N**
Procurement	Bids on capacity market	Bids on capacity market	Bids on capacity market
Capacity remuneration	Pay as cleared. Prices per MW are published on Mimer	Pay as cleared. Prices per MW are published on Mimer	Pay as cleared. Prices per MW are published on Mimer
Energy compensation	No energy remuneration	No energy remuneration	According to up or down regulating prices. Prices are published on Mimer
Time for trade	1 day (closure 18h) or 2 days (closure 16h) ahead of the hour of delivery	1 day (closure 18h) or 2 days (closure 16h) ahead of the hour of delivery	1 day (closure 18h) or 2 days (closure 16h) ahead of the hour of delivery

2.2 Optimization models

2.2.1 Model predicting control (MPC)

Model Predictive Control is a control method that originates from the late seventies. While it is an umbrella term including a lot of different controllers, each with minor differences, they all follow the same fundamental structure. The structure is well described in [43], where the first step is to mathematically define/predict the future system states. This prediction is then compared to the desired future system states. The obtained error between these two is then sent to an optimizer as input. The optimizer minimizes a predefined cost function, which depends on the prediction error and incorporates system constraints. The output is a sequence of future system control inputs. The length of this sequence is called the predilection horizon. Of all the control inputs obtained only the first control input is applied, after which the process is repeated with updated system information. The process of a MPC is illustrated in Figure 2.3.

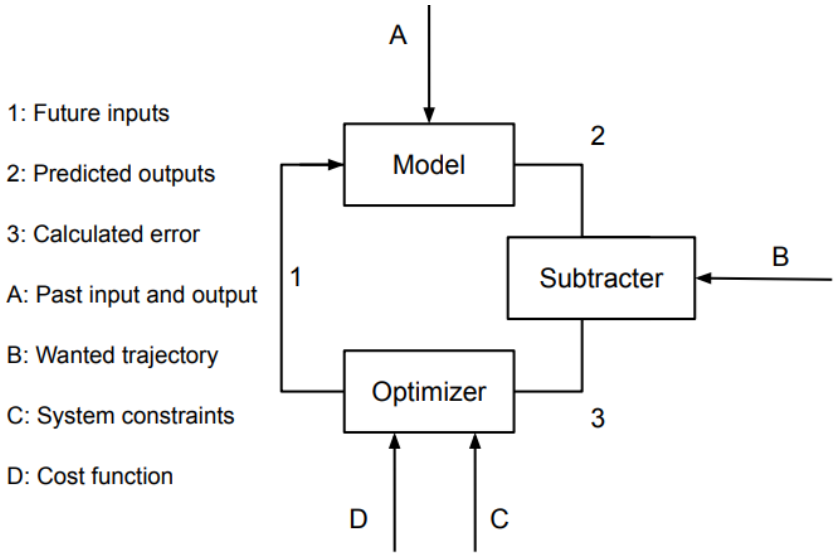

Figure 2.3: General flow of a MPC, based on figure in book [43].

Knowing the overall structure of MPC, the next step is to explain how to construct an MPC. First, building an MPC requires the system in question to be represented by a mathematical model. This model should be able to accurately predict the future state and behavior of the system. The extent of this prediction, whether it is in time or some other unit, is usually referred to as the prediction horizon.

Having the system model, the second part needed is the cost function. The cost function should depend on the system's states, which themselves depend on the system control inputs. Having this dependence essentially results in the cost function being dependent on the system's control inputs.

The constructed cost function can now be minimized with an optimizer that in addition to the cost function, considers all the system constraints. The optimizer output will be the optimal control inputs over the prediction horizon. When having these inputs, merely the first one will be applied, changing the system state and shifting the prediction horizon one step forward. The process can now be repeated with the additional system information. Shifting the prediction horizon forward one step for each iteration is known as the receding horizon principle. What this principle does is making sure that the controller continuously adapts and considers all available system information [43].

Being reliant on the accuracy of the system model, the MPC does not become any better than the system model it exploits. For complex systems and problems, the derivation and development of a accurate model can be time consuming and is often cited as one of the mayor disadvantages with MPC. Depending on the complexity of the model and the length of the chosen horizon utilizing MPC can also require large computational power. This is especially true when using non linear MPC (NMPC). The required computational power especially goes up when the introduced nonlinearities converts the problem from being convex to nonconvex. A

nonconvex problem contains local maximum and minimum points which can result in suboptimal solutions, moreover stability issues [43].

To implement MPC in Python the open source package CasADi can be used. CasADi is capable of solving nonlinear problems, as well as including an arbitrarily large number of equality and inequality constraints. For detailed information about CasADi the reader is refer to its own documentation site, see [44].

2.2.2 Genetic Algorithm (GA)

Genetic Algorithm (GA) is a population-based metaheuristic inspired by the principles of natural selection and evolution, originally introduced by Holland [45]. GA has been used in many fields such as engineering design, operations research, artificial intelligence, and energy systems optimization.

Unlike traditional gradient-based optimization methods, GA does not require derivative information, making it suitable for non-linear, multi-modal, and black-box optimization problems. GA operates on a population, which is a group of individuals. Each individual represents a potential solution to the optimization problem. Individuals are usually encoded as binary strings or real-valued vectors. The quality of each individual is evaluated using a fitness function, the score of the fitness function based on how well the solution meets the optimization objective.

The algorithm improves the population over generations by applying three main operators:

- **Selection**: This step chooses individuals with higher fitness scores. These individuals are more likely to be used as parents for the next generation. This simulates the evolutionary concept of "survival of the fittest."
- **Crossover**: Combines genetic information from two parents to produce new offspring. This encourages the inheritance of beneficial traits and exploration of new solutions.
- **Mutation**: This introduces small random changes to maintain genetic diversity and avoid premature convergence. Mutation helps explore new areas of the solution space.

There are common stopping conditions for GA, including:

- The algorithm reaches a predefined maximum number of generations.
- The best fitness value does not improve significantly over several consecutive generations.
- The fitness of the best solution reaches a predefined threshold or target value.

The performance of GA is highly influenced by its parameter settings. Parameters are essential to balance exploration and exploitation and to achieve good optimization results.

- **Population Size**: Defines the number of individuals in each generation. A larger population increases genetic diversity and exploration ability but requires more computational resources. A smaller population reduce computation time but may lead to premature convergence.
- **Crossover Rate**: Indicates the probability of applying crossover between selected parents. Higher crossover rates tend to encourage exploration by creating new genetic combinations , while lower crossover rates limit diversity and may slow down search.
- **Mutation Rate**: Defines the probability of random changes in the offspring. Mutation introduces randomness and helps maintain genetic diversity. If the rate is too low, the population may converge prematurely; if too high, the search may become unstable.
- **Selection Method**: Determines how individuals are chosen to become parents. Common methods include roulette wheel selection, tournament selection, and rank-based selection. The choice of selection strategy can influence convergence speed and the quality of solutions.

The general structure of a genetic algorithm is shown below Figure 2.4:

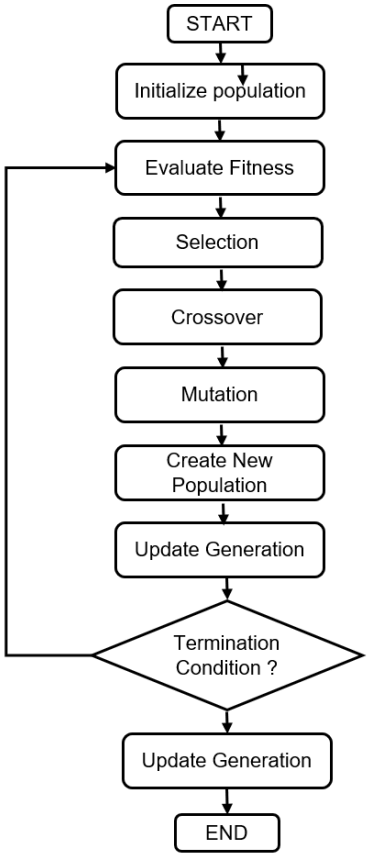

Figure 2.4: GA Flow Chart

In this thesis, Genetic Algorithm is implemented using the DEAP (Distributed Evolutionary Algorithms in Python) framework, DEAP is a open source evolutionary

computation framework library for Python. The functionalities provided by DEAP are organized into several modules. These modules work together to support the flexible design and extension of algorithms. Users can customize their own algorithm structures based on these strategy module. The tools module includes used genetic operators such as initialization, crossover, mutation, and selection. These operators can be easily registered into the toolbox and used during the algorithm process[46]. DEAP also support single-objective and multi-objective optimization and allows for easy tracking of algorithm performance through built-in logging tools such as Logbook.

3
Methodology

To determine the optimal usage for boat batteries capable of B2G, multiple factors must be considered. These include electricity price, battery chemistry, external limitations, and a few more. An effective approach to successfully considering all these parameters and identifying the best usage profile would be to develop a simulation tool using all these parameters as input values.

While the scope of this thesis was to develop a method for determining the optimal B2G usage for an arbitrary use case, specific cases were also required to run, test and validate the developed code. The methodology, process, and system limitations applied in this thesis are presented in the following sections. However, a brief summary of the problem formulation is first provided.

3.1 Problem formulation

Fundamental problem formulation

Even within a maritime system following tight restrictions, many different secondary usage profiles might be possible. All of these would together with the the fixed primary usage result in different interactions between the grid and the boats. Therefore the question arises: "what is the optimal way for the boat/boats to interact with the grid". To answer this question a better understanding of what the word "interaction" refers to, and what information it includes is necessary.

The interaction between the boat batteries and the grid embed information such as the charging and discharging power at different time instances. Furthermore it contains information on how much energy the battery can provide/reserve for ancillary services during each time step. Finding the optimal secondary usage profile, and as a consequence the most optimal interaction, requires one to find and quantify the advantages and disadvantages of utilizing as well as not utilizing the battery for B2G. These contributions must then be compared to eventually find the balance point giving the highest ratio of advantages over disadvantages.

Mathematical interpretation

A mathematical description of the more fundamental problem formulation stated above is necessary, in order for the possibility to solve it. The first step in this transition is to converted each advantage and disadvantage into either cost or revenue. These can then be added together to constitute the systems cost function. In this thesis the cost is the sum of electricity cost and the indirect cost of degradation. Gained revenue on the other hand is the result of attending ancillary services and getting compensated for these services. Adding these two contributions gives the system's cost function.

Solver approach

With a constructed cost function, a controller, such as MPC or a algorithm such as GA, can be used to minimize the cost function. The optimization might be restricted to follow some system constraints such as allowed SoC interval and/or allowed charging power so these constraints are also essential to include in the optimization problem. With the cost function minimized and all the constraints obeyed, the optimal solution and with that the best secondary usage profile is found.

With the problem formulation postulated and the core objective defined, system boundaries can be introduced.

3.2 System boundaries

To conduct an extensive analyzes of the potential of B2G and how to optimize its use, the system size had to be reduced by either limiting or fixing some parameters. The assumptions and specifications made in this thesis are all presented in the following sections. The technical specifications postulated in this thesis are introduced first.

3.2.1 Battery Types and Degradation Models

When deciding which batteries to analyze, the attention quickly went to LIBs. This was because they are the most widely used secondary batteries. Moreover, out of these, LFP and NCA both account for a large part of the market share [17] [19]. These arguments, combined with the fact that Volvo Penta uses both NCA and LFP batteries, made these chemistries a suitable choice to analyze.

Having determined which battery chemestries and degradation models to implement, the next step was to decide on specific battery packages. Since this thesis investigates two different cell chemistries it is reasonable to use two different battery packages, one utilizing LFP and one utilizing NCA. With this in mind the cube battery and the Peninda (K01) battery were chosen. Both of these are delivered by Volvo Penta and suitable for maritime applications. Some general information about the two batteries are presented in Table 3.1, shown below.

Table 3.1: Battery specification

Battery model	Cell chemistry	Capacity [kWh]	Voltage [V]
Cube	NCA	90	650
Peninda	LFP	73.6	620

The above numbers are used as reference numbers for both the MPC and GA later in this thesis. However, some adjustments will be made for whenever MPC is used. In these cases each boat battery will be assumed to have the same specifications as the cube battery. The remaining difference is, of course, the fact that LFP degradation models will be used. This choice was made to more easily isolate the difference between the degradation models itself rather than obtaining differences in the result due to differences in battery specifications. For GA on the other hand the specifications will be exactly as shown in Table 3.1. This to represent a more realistic scenario and by doing so map the difference between the optimal secondary usage case for not only two separate chemistries, but rather these two very specific battery packages.

In terms of configuration, it is assumed that all battery cells of the same type have the same behavior and degradation profiles. In other words, each cell of the same type is identical in its performance, specifications and degradation. It will be assumed that the two batteries presented above, the cube and peninda battery, are made from the cells used in article [27] and [10]. There overall specifications is given in Table 3.2.

Table 3.2: Cell specification

Cell chemistry	Capacity [Ah]	Voltage [V]
NCA	7	3.6
LFP	2.2	3.3

Based on this information, the required cell configuration to obtain the two assumed battery packages can be determined.
For **NCA battery:**
The number of cells connected in series was

$$N_s = \frac{650\,\mathrm{V}}{3.6\,\mathrm{V}} \approx 180 \text{ cells in series.}$$

The number of cells connected in parallel was

$$N_p = \frac{90000\,\mathrm{Wh}}{650\,\mathrm{V}} \cdot \frac{1}{7\,\mathrm{Ah}} \approx 19 \text{ strings in parallel}$$

Now the same calculations can be done for the Peninda **LFP battery:**
The number of cells connected in series was

$$N_s = \frac{620\,\mathrm{V}}{3.3\,\mathrm{V}} \approx 188 \text{ cells in series.}$$

The number of cells connected in parallel was

$$N_p = \frac{620000\,\text{Wh}}{620\,\text{V}} \cdot \frac{1}{2.2\,\text{Ah}} \approx 46 \text{ strings in parallel}$$

The battery and cell specifications assumed in this thesis is summarized in the following Table 3.3.

Table 3.3: Battery pack properties for simulations.

Chemistry of battery cells	**LFP/C**	**NCA/C**
Capacity of the battery	2.2 Ah	7 Ah
Number of cells in series	188	180
Number of parallel branches	46	19
Energy of the pack	73.6 kWh	90 kWh
Nominal voltage of the pack	620 V	650 V

The degradation models used in this thesis were divided into two types, namely calendar and cycling degradation, see section 2.1.4. Degradation due to mechanical stress and other factors were excluded. Having determined the battery chemistries and what degradation types to be considered, the next step was to construct the degradation models. In this thesis, these models were obtained from existing literature. For specific cells, a more rigorous approach would have be to conduct degradation experiments and derive the degradation models from the obtained results. However, such an approach would be both time-consuming and require advanced equipment, and was therefore left outside the scope of this thesis.

To choose between different degradation models presented in various scientific papers and books, a couple of requirements were defined. Firstly, it was decided that the calendar aging model should only depend on time, SoC, and temperature, while the cycling aging should depend on current or C_{rate}, current throughput, and temperature. This decision was based on the observation that these terms appeared frequently in the literature and were always primary contributors to the degradation. The degradation models should also have all their coefficients defined and be semi-empirical. This ensures that no further battery testing is required before the models can be applied for calculations. Among the models fulfilling these requirements, the newest ones were chosen to minimize the error due to recent developments in battery technology. The four degradation models used in this master thesis are based on those presented in the theory section.

A couple of assumptions regarding the batteries were also made. First of all, the voltage is assumed to be constant and independent of factors such as SoC and age. The batteries are also assumed to have the same temperature as their environment (ambient temperature). Yet another battery assumption that has a large impact on the results is the assumption that the batteries follow the chosen degradation models. The fact that the models are roughly 10 years old makes the reader justified

in questioning their accuracy; however, since they are simply inputs values, their accuracy does not really affect the simulation tool itself.

3.2.2 Locations

Deciding on what locations to be analyzed, a couple of factors were considered. Firstly, the locations analyzed should be complementary to each other, hence have large differences in most if not all aspects and parameters. The locations in question should also have data available for all of the parameters required to conduct this study, and furthermore, have close access to water. The required parameters are listed below. Based on these requirements, Gotheburg and Luleå turned out to be suitable choices. While they might not differ significantly in all aspects, differences do exist, and both have the necessary data. Once again, it should be stated clearly that, even tough only the two locations, Gothenburg and Luleå, were tested, the final simulation tool should work just as well for B2G optimization at other locations, as long as data for the parameters listed below are available:

- Temperature
- Electricity price
- B2G compensation (dependent on what grid service)
- Real time grid frequency

3.2.3 Time Discretization and Data Simplification

In the process of converting continuous time to discrete time, an appropriate step size needs to be chosen. Since the data used in this thesis, day-ahead market price of electricity, temperature, and the consumption of energy are provided on an hourly basis, a step size of one hour seems appropriate. This setting makes it easy to implement the data in the model.

For the frequency deviation, the data collected from Fingrid [47]had a resolution of 3 minutes. Because other data is only available per hour, it is not necessary to keep the high resolution of the frequency data. To simplify, the maximum deviation from the 50.00 Hz in each hour is selected.

Furthermore, in each hour, the charging or discharging power is assumed to stay constant. This means the power does not change during that hour. Based on this assumption, the SoC change caused by charging during this hour will appear at the start of the following hour. This approach matches the hourly time resolution.

3.2.4 Primary Usage and Energy Consumption

When expanding the usage of an electric boats to also do B2G, the factors to be considered increase. In this thesis it will be assumed that the primary usage can not be trumped by the secondary usage. This says that independently on how profitable it would be to attend the FCR market, this will never happen for hours where the boat will either be used or has to prepare to meet any upcoming SoC target. The

primary usage represents all the usage patterns that would be found for the boat if it were not able to perform B2G. The secondary usage on the other hand represents only the usage following the expansion of using the boat for B2G. Not only will the secondary usage not trump the primary usage, it will also be assumed that the primary usage is set by the boat owner and therefore seen as a fixed input parameter into the optimization problem.

To estimate how daily sailing affects the battery's SoC, several power levels were considered. These values reflect imaginary power demands under different operational conditions. In each case, a certain amount of sailing time is assumed, following the arrival and departure time presented in the previous section. The energy consumed during each hour is easily calculated from the power. They relate one to one since the power is assumed to be constant during each hour. The battery's remaining energy after each hour is calculated by deducting the consumed energy from the initial energy level that hour. The SoC is calculated by dividing the remaining energy by the total battery capacity. The energy remaining in the boat batteries for each hour, season and location is assumed to follow the profiles illustrated in Figures 3.1-3.2. These profiles are not based on actual data, but were instead artificially created to approximate a plausible usage profile for each season at the two locations of Gothenburg and Luleå.

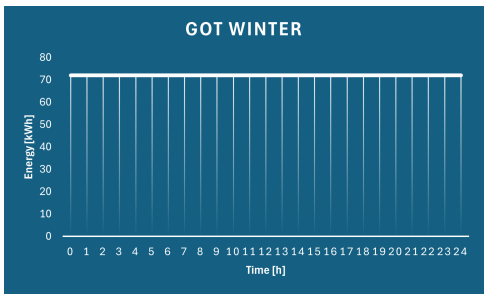

(a) Primary usage for winter in Gothenburg.

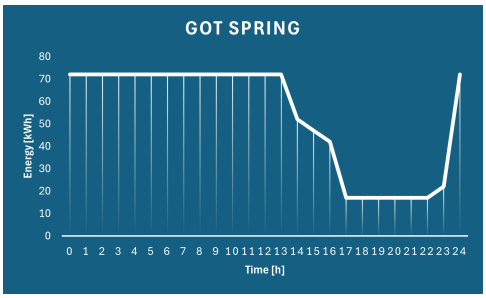

(b) Primary usage for spring in Gothenburg.

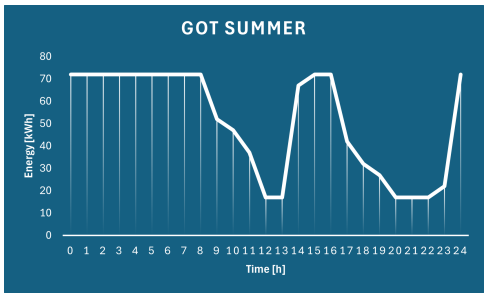

(c) Primary usage for summer in Gothenburg.

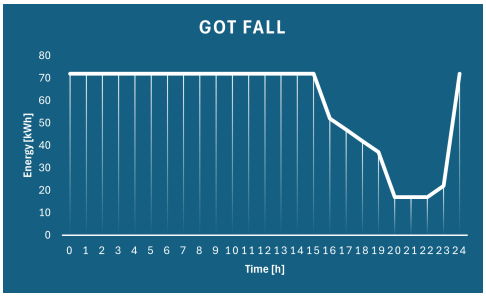

(d) Primary usage for autumn in Gothenburg.

Figure 3.1: All four seasonal primary usage profiles for Gothenburg.

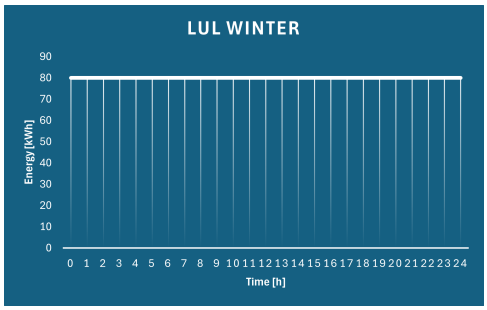

(a) Primary usage for winter in Luleå.

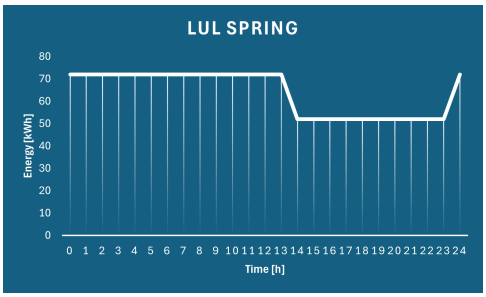

(b) Primary usage for spring in Luleå.

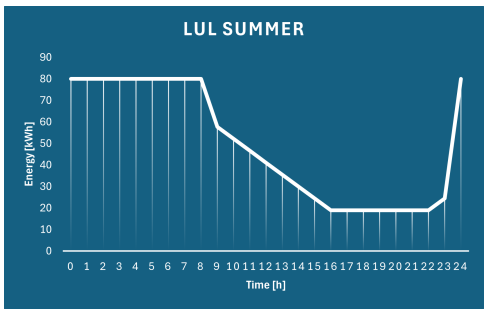

(c) Primary usage for summer in Luleå.

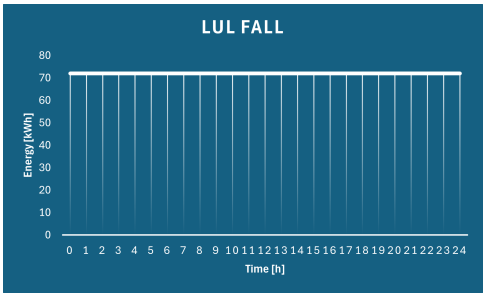

(d) Primary usage for autumn in Luleå.

Figure 3.2: All four seasonal primary usage profiles for Luleå.

3.2.5 Overview

All the parameter constraints are found below in Table 3.4.

Table 3.4: Parameter values used in B2G.

Parameter	Value	Unit
Δt	1	h
Charging/discharging efficiency	1	-
Minimum allowed SoC	0.15	-
Maximum allowed SoC	0.9	-
EOL capacity fade	0.2	-
Maximum discharging power	-50	kW
Maximum charging power	50	kW
Battery cell charge capacity (NCA)	7	Ah
Battery cell charge capacity (LFP)	2.2	Ah
Battery pack voltage (NCA)	350	V
Battery pack voltage (LFP)	320	V
Battery energy capacity (NCA)	90	kWh
Battery energy capacity (LFP)	73.6	kWh
Battery pack cost (NCA)	10000	Eur
Battery pack cost (LFP)	10000	Eur

3.3 Modification of degradation models

With all system limitations defined, the focus now shifts to the degradation models. In order for the simulation tool, developed in this thesis, to be applicable for all battery capacities, modifications to Equations (2.3) and (2.5) are required. These modifications are explained in the following two sections.

3.3.1 Modification of LFP cycling model

Since C_{rate} is an intensive quantity that does not depend on system size, it might appear that Equation (2.3) can be applied to batteries regardless of their capacities. However, this overlooks the fact that current throughput must be scaled in accordance with the chosen battery capacity. The need for scaling current throughput is illustrated in Figure 3.3. Figure 3.3 can be used to illustrate that C_{rate} is an inten-

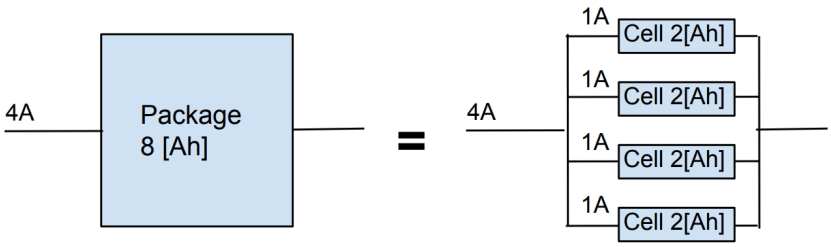

Figure 3.3: Battery package separated into parallel cells.

sive quantity however, more importantly it illustrates that the current throughput differs between the cells and the total battery package. For example, if after one hour the current throughput for each cell is 1 Ah, then after the same time the current throughput reaches 4 Ah for the whole battery package. Using Equation (2.3) together with the fact that a single cell has the same C_{rate} but different current throughput compared to the whole battery package, it follows that the cells and package degrade at different rates. This is not possible because the battery package has to degrade in accordance with the cells from which it is made. This statement holds true only if the degradation is expressed as a percentage and not as an absolute value. If the capacity loss is given as a absolute value the package will degrade in a rate equal to that of each individual cell times the numbers of cells in the package. If the package contains more than one cell this loss will for obvious reasons assume a value other than that of the individual cell.

Based on previous arguments, Equation (2.3) has to be modified. Specifically, a scaling factor must be introduced before current throughput. This scaling factor is calculated as $2.2/C$, where 2.2 represents the battery capacity used in article [25] and C the battery capacity of the battery tested. This fraction therefore represents the hypothetical current passing through each imaginary 2.2 Ah cell in which the tested battery is conceptually divided.

Yet another factor has to be added into Equation (2.3) before it can be applied

in this thesis. This factor comes from the fact that in article [10] only the current entering the battery is assumed to result in degradation. This differs from the assumption made in this thesis, where both charging and discharging will degrade the battery equally. Therefore Equation (2.3) has to be divided by two and applied not only for charging events, but also for discharging events. This adaptation of Equation (2.3) to fit the assumptions of this thesis results in a negligible difference.

By adding the scaling factor and dividing Equation (2.3) by two, the final expression for the LFP cycling degradation model is obtained, see Equation (3.1). Equation (3.1) also includes the conversion factor 1/100, which converts the unit from percentage to a fractional changing factor.

$$C_{fade}(C_{rate}, Ah, T) = \frac{1}{100 \cdot 2} \cdot B \cdot exp(\frac{-31700 + 370.3 \cdot C_{rate}}{R \cdot T}) \cdot (Ah \cdot \frac{2.2}{C})^{0.55} \quad (3.1)$$

3.3.2 Modification of NCA cycling model

In order to use Equation (2.5) for degradation calculations regardless of battery size, a couple of modifications must be made. First, the current throughput must be scaled to account for any differences between the studied battery capacity and the capacity of 7 Ah used in article [27] from which Equation (2.5) originates. This is done similarly to the LFP cycling case by introducing a scaling factor before the current through put in Equation (2.5). The intention of this scaling factor is, as previously mentioned, to divide the battery into imaginary cells with the same capacity as those used in the derivation of Equation (2.5). Since this original capacity was 7 Ah, the correct scaling factor becomes $7/C$, where C again is the capacity of the battery tested. If the tested cells have a capacity of 7 Ah then the original expression is recovered, as expected.

Next the current must be scaled. Unlike C_{rate}, used in the LFP model, current is dependent on the system size. Fortunately the scaling factor for current becomes trivial after realizing it scales the same way as current throughput. Hence multiplying the current by $7/C$ makes this equation competent independent on system size. In article [27] only charging current is accounted for. In contrast, this report assumes that degradation depends solely on current magnitude and not the direction (sign). To represent this, Equation (2.5) is divided by two, just as was done for the previously modified LFP model.

One might be tempted to stop here and simply implement these changes. However, it is important to also consider the output unit. The output from Equation (2.5) is in absolute capacity loss and not in relative loss. Moreover, due to the previous scaling of extensive parameters, the absolute loss is in relation to a capacity of 7 Ah. To obtain the relative capacity loss, the result and therefore Equation (2.5) has to be divided by 7.

Rewriting the original expression according to the changes above, while leaving it in the unit of absolute degradation for a single 7 Ah cell, yields the final expression

shown in Equation (3.2).

$$C_{fade}(C_{rate}, Ah, T) = [C_{rate} = \frac{|I|\cdot 7}{C}] = \frac{130}{2} \cdot exp(\frac{-18461 + 32 \cdot C_{rate}}{R \cdot T}) \cdot (Ah \cdot \frac{7}{C})^{0.4} \tag{3.2}$$

3.4 Testing and Verification of degradation models

With four applicable degradation models, the next step becomes to implement these in Python for testing, visualization, and verification. In order to test the models and create plots visualizing the degradation over time, artificial usage profiles must be created. The artificial usage profiles used are depicted in Figures 3.1-3.2. Each profile was made in Excel and includes information about the hourly SoC, current, power consumption, etc, see Figure 3.4. Notice that 72 kWh is equivalent to 80 SoC in these files. Hence the verification of the degradation models uses the MPC approach where both the cube and Peninda battery has the same specifications. The result of the verification should be independent on whether the MPC or GA approach is applied since everything is given in percentage.

Battery Specifications:	time_hour	Power_used: [kW]	Energy_left: [kWh]	SOC: [%]	SOC_diff	Voltage: [V]	Current: [kA]	C-rate: [-]
Capacity: 140 [Ah]	0	0	72	80	0	650	0	0
Energy: 90[kWh]	1	0	72	80	0	650	0	0
Voltage: 650[V]	2	0	72	80	0	650	0	0
Charge_max: 50[kW]	3	0	72	80	0	650	0	0
Discharge_max: 100[kW]	4	0	72	80	0	650	0	0
	5	0	72	80	0	650	0	0
	6	0	72	80	0	650	0	0
	7	0	72	80	0	650	0	0
	8	0	72	80	0	650	0	0
	9	0	72	80	0	650	0	0
	10	0	72	80	0	650	0	0
	11	0	72	80	0	650	0	0
	12	0	72	80	0	650	0	0
	13	-20	72	80	0	650	-0.03076923	-0.34188
	14	-5	52	57.7778	-22.2222	650	-0.00769231	-0.08547
	15	-5	47	52.2222	-5.55556	650	-0.00769231	-0.08547
	16	-25	42	46.6667	-5.55556	650	-0.03846154	-0.42735
	17	0	17	18.8889	-27.7778	650	0	0
	18	0	17	18.8889	0	650	0	0
	19	0	17	18.8889	0	650	0	0
	20	0	17	18.8889	0	650	0	0
	21	0	17	18.8889	0	650	0	0
	22	5	17	18.8889	0	650	0.00769231	0.08547
	23	50	22	24.4444	5.555556	650	0.07692308	0.854701
	24		72	80				

Figure 3.4: Artificial daily data for spring day in Gothenburg.

To achieve a verification of the degradation models, such a calculation will be conducted. It will be done by implementing the degradation models in a simple Python script taking in all necessary input values. For the usage profiles, one will be created by repeatedly applying the daily spring profile for Gothenburg, while the second will do the same for Luleå.

The degradation results obtained using the above Python script should now be validated. This is done by comparing the obtained degradation output with the degradation output from Cassandra (Volvo's own degradation simulation program).

Cassandra can simulate degradation for both NCA and LFP type batteries. Except from specifying the battery chemistry, Cassandra also requires the usage profile and temperature data. Requiring the same input data as the used Python script implies that the two calculations are similar in nature, hence their results are comparable. If the overall appearance and magnitudes are similar between the Cassandra output and the results obtained from the constructed Python script, then that would indicate accurate degradation models. If they were to differ then this can be kept in mind for the analysis of the results and/or used to correct the degradation models. Cassandra was not used directly in this thesis because important parts such as degradation models are not presented but rather integrated in the program.

3.5 Model and Optimization

Having validated the used degradation models, the next step becomes to introduce secondary usage and optimize its profile. Before choosing a controller and optimizer the problem/situation should be analyzed. In the case of optimizing B2G one should realize that most of the parameters are known or accurately predicted for the near future. Therefore in order to achieve as good results as possible it would be wise to exploit all the credible data available. A strong candidate to achieve this is to implement MPC, see subsection 2.2.1. Before choosing MPC as the control method it is important that non linear models, such as our degradation models, can be taken as input values. With this concern in mind the Python package CasADi was found and can be used to solve non linear problems just as the one we are facing using MPC [44]. Another algorithm that can be used is Genetic algorithm (GA). Both these models and their design is presented in the following sections.

3.5.1 MPC code design

In order to design the code implementing the MPC. An overview of how it should work is shown in Figure 3.5.
Having the wanted work flow each segment has to be designed and/or defined. Since MPC serves as the core, being the solver, of the code developed in this thesis, its design is presented first. When implementing MPC in Python, a couple of design choices must be made. First of all, the receding horizon will be set to x hours, where x is a number between $12 - 35$. This interval comes from the fact that Nordpool releases 24 hours of electricity prices at roughly 12.45 every day [48]. Before the release, at 12 o'clock, 12 hours remain until midnight where the last known electricity price is found. Then, at 13 o'clock, these 12 hours have reduced to 11 hours. However, now the release has taken place, hence another 24 hours are known. This gives $11 + 24$ hours, resulting in a known horizon of 35 hours. The MPC step size is set to one hour in accordance with the technical assumptions stated earlier. Therefore, the way in which the horizon changes is by counting down from x in steps of one for each iteration except the one where new data is released. At that point, 24 new hours are added, extending the horizon length to 35. From there, the countdown restarts, and the process continues accordingly.

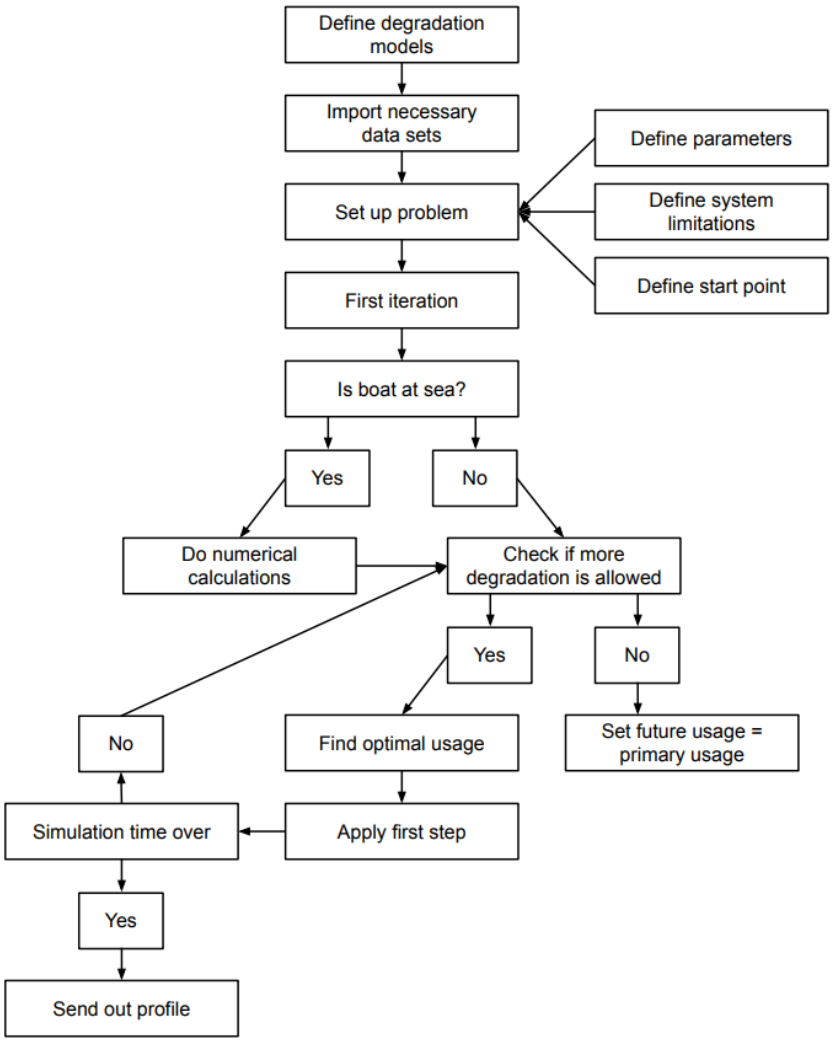

Figure 3.5: Illustration of the MPC does work flow.

Another design choice that has to be made is the construction of the cost function. As previously mentioned, only the cost from electricity price and degradation will be considered in the cost function. As for the revenue, compensation for ancillary services is the only contributor. Adding the cost and revenue gives the cost function used in this thesis, which is shown in Equation (3.24) below. The first term corresponds to the revenue, while the second and third correspond to the cost of electricity and degradation, respectively. Depending on the simulations specifications, additional punishment terms might be added to Equation (3.24) in order to achieve soft limits. In order for the optimization problem to be totally defined, some additional equations must be introduced, and furthermore, some parameters must be assigned values. These additional equations are all presented together with the cost function below in Equations (3.4) - (3.24).

The only parameter not given in Table 3.4 that has to be defined in the simulation tool is the solver tolerance, the scaling factor and the amounts of allowed iterations. The tolerance has to be chosen with the following knowledge in mind.

Lower tolerance results in a harder problem and might result in solver failure. Too high tolerance, on the other hand, might result in poor solutions, too far from the optimal one. In order to find a suitable tolerance, this thesis contains a short investigation testing the solutions obtained using different tolerances. The investigation was made by creating twelve different scenarios, varying in solver tolerance, degradation limit, and scaling factor. The scaling factor is a factor multiplied with the cost function to change its magnitude. The appropriate scaling factor will also be deducted from this tolerance investigation. The scenarios together with their respective results are presented in Figure 3.6. Had the pattern not been clear after the twelve simulations, additional runs would have been necessary to perform.

Scenario specification			tol_sol2 = 1e-9			Revenue:	Successfull solver
T_sim = 48	t_start = 1440	deg = limited	tol = 1e-13	scaling = *10**0	max_iter = 5000	-0.001788612	7/41
T_sim = 48	t_start = 1440	deg = limited	tol = 1e-13	scaling = *10**(-6)	max_iter = 5000	-0.001878112	48/0
T_sim = 48	t_start = 1440	deg = limited	tol = 1e-11	scaling = *10**0	max_iter = 5000	-0.001824608	48/0
T_sim = 48	t_start = 1440	deg = limited	tol = 1e-11	scaling = *10**(-6)	max_iter = 5000	-0.001647541	48/0
T_sim = 48	t_start = 1440	deg = limited	tol = 1e-9	scaling = *10**0	max_iter = 5000	-0.001768387	48/0
T_sim = 48	t_start = 1440	deg = limited	tol = 1e-9	scaling = *10**(-6)	max_iter = 5000	-0.001427485	48/0
T_sim = 48	t_start = 1440	deg = unlimited	tol = 1e-13	scaling = *10**0	max_iter = 5000	-0.001714861	6/42
T_sim = 48	t_start = 1440	deg = unlimited	tol = 1e-13	scaling = *10**(-6)	max_iter = 5000	-0.001878469	48/0
T_sim = 48	t_start = 1440	deg = unlimited	tol = 1e-11	scaling = *10**0	max_iter = 5000	-0.001824285	48/0
T_sim = 48	t_start = 1440	deg = unlimited	tol = 1e-11	scaling = *10**(-6)	max_iter = 5000	-0.001649206	48/0
T_sim = 48	t_start = 1440	deg = unlimited	tol = 1e-9	scaling = *10**0	max_iter = 5000	-0.001721223	48/0
T_sim = 48	t_start = 1440	deg = unlimited	tol = 1e-9	scaling = *10**(-6)	max_iter = 5000	0.000679333	48/0

Figure 3.6: Twelve use cases tested to determine suitable tolerance. Parameters used: [T_{war} = 3 years]

The last column in Figure 3.6 above represents how many of the iterations that are being solved by solver 1 respective solver 2. Solver 2 has a tolerance of $1e-9$ which is always higher or equal to that of solver 1. Consequently, a problem solved entirely by solver 1 is always more or equally accurate than one solved partially or solely by solver 2. Based on this one can draw the conclusion that a tolerance of $1e-13$ is too low, both in the case of limited and unlimited degradation with a scaling factor of 1. Therefore, the lowest tested tolerance that manages to solve the problem independently of scaling factor is $1e-11$. Looking only at a tolerance of $1e-11$ and $1e-9$ one can see that a scaling factor of 10^0 always gives a revenue/cost function that is lower compared to the scaling factor of 10^{-6}. For this reason a scaling factor of 10^0 is the preferred choice when conducting future simulations. Having decided on the tolerance and the scaling factor, the only remaining parameter to define is the number of iterations. The number 5000 was chosen solely based on the experience gained during the development of the simulation tool. However, the reader should be aware that this number, as for the rest, might have to be changed if the simulated scenarios are changed drastically, either in terms of imposed constraints or, for example, the implemented degradation models.

Verification of MPC code

Having designed the MPC it is time to validate the MPC code. This is done to ensure that the code is performing as expected and does not produce any obvious shortcomings.

Scenarios with trivial solutions

The first way for which the MPC will be verified is by making sure it works for very simple scenarios. Two very simple scenarios will be constructed, each having a known trivial solution. Applying the MPC code to these simple scenarios, the obtained solutions can be compared with the trivial solution. If the MPC code is incorrectly constructed it will not work and this verification will have proved that it has to be revisited and corrected. If the code produces the correct solutions, then this validates its ability for at least simple scenarios. The following discusses these simple scenarios and how they will be constructed in this thesis.

To construct the simple scenarios used for the above verification requires simple inputs. Therefore, parameters such as temperature, electricity price and frequency regulation compensation are all set to constant values. Furthermore, the grid frequency is set to a step function going between 50 ± 1 Hz, where 50 is the nominal frequency. The nature of the primary usage should also be simple; however, it is important to ensure that primary usage is not being trumped by secondary usage, since this is a constraint previously imposed. For this reason, the profile that will be used for the simple scenarios verification is the GOT spring profile. Simplifying the problems in this way enables rigorous calculations and/or a trivial solution which can be used to validate the result. The simple scenarios are described in more detail below, along with the solutions they should lead to.

The first simple use case is constructed to have the trivial optimal solution of constant max charge and discharge. For this to be true, the revenue from frequency regulation must be high, and the cost of degradation should be low. The first can easily be implemented simply by having a large FCR compensation term. The cost of degradation can also be manipulated easily, with the most effective solution being to simply modify the degradation models to always give out a degradation of zero. By doing so the optimization problem will never see any degradation cost and can focus only in maximizing the revenue. The parameters that represent these changes/implementations are presented in Table 3.5.

Table 3.5: Parameters used for obtaining trivial solution with high charging and discharging.

Parameter	Value or interval
Cal_{deg} for each iteration	0.0
Cyc_{deg} for each iteration	0.0
Electricity price	1
Frequency pattern	Step function [49,51]
FCR compensation	40
Battery price	$1e4$
Tolerance	$1e-11$
Warranty period	1 year

The second scenario is constructed in a way, such that as little charge and/or dis-

charge as possible will take place. To achieve this, it is important to minimize the gain of charging and discharging frequently. This is easily done by setting the FCR compensation to a negative value. Furthermore, one can increase the cost of degradation by increasing the battery prices. Having a higher degradation will not have any effect if the degradation is constantly kept at zero. It is therefore changed to always give a degradation of 0.00001 every hour/iteration. Considering the above, a set of parameters was chosen for this second simple use case, and its parameters are shown in Table 3.5.

Table 3.6: Parameters used for obtaining trivial solution with low charging and discharging.

Parameter	Value or interval
Cal_{deg} for each iteration	0.00001
Cyc_{deg} for each iteration	0.00001
Electricity price	1
Frequency pattern	Step function [49,51]
FCR compensation	-0.01
Battery price	$1e12$
Tolerance	$1e-11$
Warranty period	1 year

The resulting usage profile implementing these scenarios are shown in the upcoming result section 4. This verification method only ever captures the accuracy for simplified scenarios. Therefore, it would be of value to also verify the MPC code for more realistic scenarios. The way in which this will be done is by comparing the results produced by the MPC code with the results obtained using GA. If these are producing similar results for different scenarios, then that would at least indicate that the solution they produce is close to the real one. If they are not similar, at least one can draw conclusions about which of the applied codes that performs the best.

3.5.2 Genetic Algorithm Design

In this thesis, the Genetic Algorithm (GA) was developed using the DEAP framework to solve the optimization problem. Each individual in the GA represented a charging strategy, starting from the time the boat arrives at the dock until it departs. During this 24-hour period, two types of time were defined:

- **Uncontrollable period:** When the boat was sailing, the battery used for propulsion. The model used real SoC and current data from input data.
- **Controllable period:** When the boat was docked, the GA was allowed to optimize battery charging strategy.

For each hour, the GA controls three decision variables. It meant there were 3 values per hour, and 72 values in total for a full day.

- Operational Mode: A binary vector where 0 indicated normal charging and 1 indicated participation in FCR services.

- Normal Charging Power (kW): A vector of length 24. Each element represented the charging power for that hour.
- FCR Power (kW): A vector of length 24. Each element represented the charging or discharging power for that hour attending the FCR service.

Constraints and Fitness Function

In the model, main constraints were as follows:

- Charging or discharging power should be within the minimum and maximum limits of the wallbox.
- SoC should always remain within allowed range from 15 to 90 % during the whole operation.
- At departure times, SoC should not be lower than the target SoC.
- The initial SoC used in optimization should be the same as the SoC when the boat returns to the dock.
- Daily battery degradation should not exceed the allowed limit.

The fitness function was designed to minimize the total cost. There were included electricity cost, FCR cost and revenue, battery degradation, and penalties. Electricity cost under normal charging was calculated by multiplying power and electricity price. Electricity cost under FCR mode was calculated by multiplying power, electricity price, and an activation coefficient. Revenue from FCR was determined by compensation and actual power used. Penalty terms were used to enforce constraints in fitness function:

- SoC Target Penalty: If the SoC at the end of a controllable window does not meet the target, a penalty is added.
- Degradation Limits:
  - Daily battery degradation
  - Cumulative degradation

The total cost equation, see equation (3.3), is shown below. Each term is defined in Equations (3.4)–(3.20) for GA.

$$\text{Total Cost} = cost^{el} + cost^{el-FCR} - Rev^{FCR} + deg^{cost} + Pen^{SoC} + Pen^{deg} \quad (3.3)$$

For each hour, the following steps were taken:

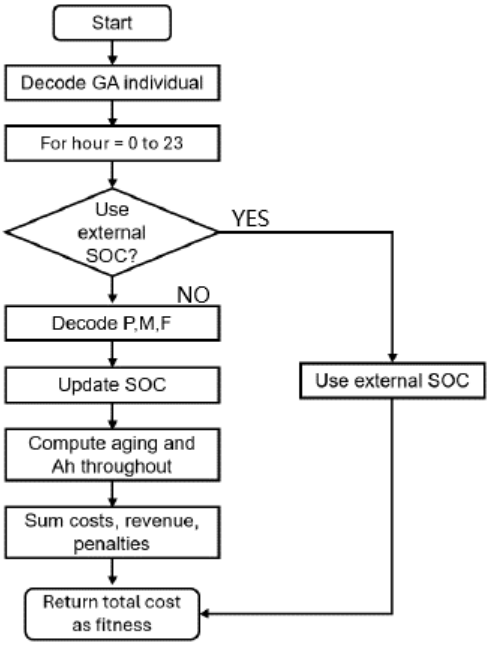

Figure 3.7: Fitness function Flow Chart.

The initial population was created using a custom initialization method. This method was designed to ensure both feasibility and diversity across the decision variables. During controllable hours, the charging power was initialized using a uniform distribution between 0 W and the maximum allowable charging power. For uncontrollable hours, the charging power was fixed to 0 W. The operational mode was initialized with a bias. For each controllable hour, there is an 80% probability to assign FCR mode and a 20% probability to assign normal charging mode. This bias encouraged early exploration of FCR services. The FCR power values were initialized using a uniform distribution between the maximum allowable discharging power and the maximum allowable charging power. The genetic algorithm used the following parameter settings:

- Population size: 400 individuals
- Number of generations: 600
- Crossover probability: 0.7
- Initial mutation probability: 0.2, linearly decreasing to 0.05

To maintain diversity and prevent early convergence, the mutation probability was linearly reduced over generations. The population diversity was monitored using the standard deviation of individual fitness values. In addition, every 50 generations, 10% of the population was replaced by newly generated random individuals to reintroduce changes in case of stagnation.

Performance Evaluation

To ensure effective optimization and avoid early convergence, the performance of GA was monitored throughout the whole process. For each generation, the average fitness was recorded. The average fitness showed the overall population per-

formance. These values were automatically recorded using DEAP's built-in tool Logbook. Through the average fitness curve, the optimization effect could be understood. This also provided a reference for fine tuning.

At the same time, in order to evaluate the effectiveness of the optimized strategy, the following key performance indicators were tracked:

- SoC progression curve: The SoC curve helped to visualize whether the SoC kept in the limited range or whether the SoC target was met at the specific time.
- Mode selection: This illustrated how the GA selected between normal charging and FCR participation.
- Power and FCR deviation: The charging/discharging power was compared with the FCR deviation. A positive deviation should correspond to positive power, and a negative deviation to negative power.
- Cost: The total cost was broken down into electricity cost, FCR compensation, and battery degradation cost. This helped to assess the economic benefit.

Mathematical Framework

$$P_{t,i}^{bat} = \eta \cdot P_{t,i}^{wall} \qquad \forall\, t,i \qquad MPC, GA \qquad (3.4)$$

$$SoC_{t+1,i} = \frac{I_{t,i}}{C_{t,i}^{bat}} \Delta t + SoC_{t,i} \qquad \forall\, t,i \qquad MPC, GA \qquad (3.5)$$

$$P_i^{min} \leq P_{t,i}^{wall} \leq P_i^{max} \qquad \forall\, t,i \qquad GA \qquad (3.6)$$

$$SoC_{0,i} = K \qquad \forall\, t = 0, i \qquad MPC, GA \qquad (3.7)$$

$$SoC^{min} \leq SoC_{t,i} \leq SoC^{max} \qquad \forall\, t,i \qquad MPC, GA \qquad (3.8)$$

$$SoC_{t,i} \geq SoC_{t,i}^{departure} \qquad \forall\, t \in t_{departure}, i \qquad MPC, GA \qquad (3.9)$$

$$SoC_{t,i} = SoC_{t,i}^{docking} \qquad \forall\, t \in t_{docking}, i \qquad GA \qquad (3.10)$$

$$I_{t,i} = I_{t,i}^{prim} \qquad \forall\, t \in t_{used}, i \qquad MPC \qquad (3.11)$$

$$I_{t,i}^{wall} = \frac{P_{t,i}^{wall}}{V} \qquad \forall\, t \in t_{used}, i \qquad GA \qquad (3.12)$$

$$I^{min} \leq I_{t,i} \leq I^{max} \qquad \forall\, t,i \qquad MPC \qquad (3.13)$$

$$deg_{t,i}^{tot} = deg_{t,i}^{cal} + deg_{t,i}^{cyc} \qquad \forall\, t,i \qquad MPC, GA \qquad (3.14)$$

$$deg_{t+x,i}^{tot} = \sum_{t=t}^{t=t+x} deg_{t,i}^{cal} + deg_{t,i}^{cyc} \qquad \forall\, t,i,x \in [11,35] \qquad MPC, GA \qquad (3.15)$$

$$deg_{t+x,i}^{tot_{prim}} = \sum_{t=t}^{t=t+x} deg_{t,i}^{cal_{prim}} + deg_{t,i}^{cyc_{prim}} \qquad \forall\, t,i,x \in [11,35] \qquad MPC, GA \qquad (3.16)$$

$$deg_{t+x,i}^{tot} \leq deg_{t+x,i}^{tot_{prim}} \qquad \forall\, t,i,x \in [11,35] \qquad MPC, GA \qquad (3.17)$$

$$deg_{t,i}^{cost} = deg_{t,i}^{tot} \cdot \frac{bat^{price}}{deg^{lim}} \qquad \forall\, t,i \qquad MPC, GA \qquad (3.18)$$

$$R_t = \frac{|\Delta f_t|}{50.0 - 49.9} \qquad \forall\, t,i \qquad MPC, GA \qquad (3.19)$$

$$cost_{t,i}^{el} = el_t^{price} \cdot max(0, P_{t,i}^{wall}) \cdot \Delta t \qquad \forall\, t \qquad MPC, GA \qquad (3.20)$$

$$cost_{t,i}^{el-FCR} = el^{price} \cdot R_t \cdot P_{t,i}^{wall} \cdot \Delta t \qquad \forall\, t,i \qquad MPC, GA \qquad (3.21)$$

$$Rev_{t,i}^{FCR} = FCR_t^{comp} \cdot P_{t,i}^{size} \qquad \forall\, t,i \qquad MPC, GA \qquad (3.22)$$

$$\theta = \delta \cdot cost_{t,i}^{el-FCR} + (1-\delta) \cdot cost_{t,i}^{el} \qquad \forall\, t,i,\delta \in [0,1] \qquad MPC \qquad (3.23)$$

$$Rev_{t,i}^{bid} = Rev_{t,i}^{FCR} - \theta - deg_{t,i}^{cost} \qquad \forall\, t,i \qquad MPC \qquad (3.24)$$

The parameter values used in the optimization problems are presented in Table 3.7.

Table 3.7: Default values used in this thesis for input parameters to the simulation tool.

Parameter	Value
Charging/discharging efficiency	1
Δt	1
El price SE1 & SE3	2024 vector repeated MPC:[EUR/Wh], GA:[EUR/kWh]
FCR price SE1 & SE3	2024 vector repeated MPC:[EUR/W], GA:[EUR/kW]
Frequency	2024 vector repeated [Hz]
Temperature for GOT & LUL	Values for 2024 repeated [C°]
Receding horizon	x $\in [12, 35]$
Cells	1 [-]
Battery price	10000 [EUR]
Total degradation limit	20 [%]
Daily degradation limit	none
Warranty period	10 [years]
Ah start	2000/2 [Ah]
Max charge and discharge	50 [kW]
Initial battery capacity	90 [kWh]
Initial SoH	100 [%]
SoC interval	15-90 [%]
Tolerance	10^{10}

3.6 Collection of real data

Until this point simple, moreover made up values and profiles/patterns have been assigned to almost all the variables/parameters. Both in a try to increase readability, controllability, and to minimize problem complexity. The next logical step in order to produce more realistic results is to start collecting real data for external parameters such as electricity price, primary usage and more. The collection of real data will be for the two locations chosen, Gothenburg and Luleå. The time for which data is collected is between 2024-01-01 to 2024-12-31. For simulations longer than one year the collected data is concatenated with itself to obtain lager data sets.
What data and where it was collected from is presented in Table 3.8 below.

Table 3.8: Parameters and there references

Parameter	Gothenburg source	Luleå source
Electricity price	Entsoe [49]	Entsoe [49]
Temperature	SMHI [50]	SMHI [50]
Frequency value	Fingrid [51]	Fingrid [51]
FCR compensation	Miner [52]	Miner [52]

3.7 Test scenarios

Having adapted degradation models, collected real data and two verified simulation codes, more realistic simulations can be performed. The simulations conducted in this study all fell into one of two categories. The first having no short term degradation limit while the second use case/category had. The difference is that the first category, denoted as Use Case 1, implements B2G and attends the FCR-N market as soon as it is profitable. The second category, denoted as Use Case 2, have an additional constraint implemented that might hinder the otherwise optimal charge profile. The additional constraint ensures that the degradation over the receding horizon does not become larger than a predefined limit/value. The two categories are described in more detail in the following sections.

Use Case 1: B2G as soon as it is profitable

When using a battery for B2G the future information is limited. Therefore, instead of relying on predictions, the argument can be made that it is best to implement B2G as soon as it is profitable and not put too much weight on limiting degradation. This is exactly what the first use case represents. The only thing stopping B2G from being implemented, for scenarios where B2G otherwise would have been profitable, is if the code calculates an end of life (EOL) shorter than the warranty time. In this thesis the EOL was calculated by assuming solely primary usage for each of the remaining iterations. Reaching this EOL limit, no further degradation will be permitted, and all B2G operations stopped.

This use case was represented within the MPC code by implementing the default values given in Table 3.7. The GA imposed the same values, however it always contain a short term degradation limit, so to realize this use case it was chosen to be a large value. It was decided based on the following calculation: Each simulation period covers a single day, starting from the boat arrival at the port until its arrival the next day. Based on a 10 year battery warranty and a total allowable degradation of 20%, the theoretical daily degradation limit would be approximately 0.000055 %. In this use case, the goal is to allow the battery to participate in B2G as soon as it becomes profitable. Therefore, a much higher daily aging limit of 0.001 % was applied. This constraint enables more frequent participation in B2G without considering long term degradation.

Further parameter differences between the GA and MPC will be presented in the end of Use Case 2.

Use Case 2: Additional degradation constraint

Within the MPC and GA model, the second approach is exactly the same as for the first one, with the only exception being one additional constraint. In contrast to many other constraints imposed in this study, such as allowed SoC interval, this additional constraint is limiting the degradation for the whole receding horizon. This choice results in more hourly flexibility. Limiting the horizon enables some hours to have very high degradation as long as other hours have low degradation. The limit is put equal to the degradation achieved applying only primary usage for the next 24 hours.

This limit and use case was designed to test whether B2G can be performed without causing more battery degradation than that for primary usage. Limiting the degradation according to this limit ensures that B2G does not introduce any additional degradation. This setup is intended to evaluate whether the battery can still participate in B2G while staying within or lower than the lifetime obtained using only primary usage.

Following the same use cases, the GA and MPC codes only differ by a few parameters. Specifically, the GA code does not incorporate a tolerance parameter, a variable horizon length, or a defined warranty period.

Yearly simulations

The final set of simulations conducted in this thesis were yearly simulations. The yearly simulations were conducted both for Use Case 1 and 2 using only the MPC code.

The MPC code continuously updates its decisions through a receding horizon approach, making it applicable on long-term as well as short-term simulations. In contrast, the GA code used in this study implements a fixed 24 hour optimization window and simulates each day independently. As a result, the GA code used in this thesis is not suitable for long-term simulations.

All the simulations were carried out for LFP cells in Luleå and used almost only the default parameters given in Table 3.7. One major difference from the default scenario was the reduced warranty time. It was changed from a value of ten years to one year. The primary usage applied in the simulations was constructed by initially setting all days to follow the winter profile, which corresponds to no boat usage. Subsequently, every seventh day during spring was replaced with the spring usage profile. In the summer season, every fourth day was instead replaced by the summer usage profile. During the fall season, every tenth day was assigned the fall usage

profile. However, in the case of Luleå, this profile also corresponds to no boat usage and therefore results in no effective difference.

In addition to the above changes, a degradation factor was introduced. The degradation factor simply scaled the degradation obtained from both calendar and/or cycling aging. This enabled more control of the simulations and made it possible to map the difference between Use Case 1 and 2 for both low and high degradation scenarios. The values imposed for the degradation factors are given in Table 3.9.

Table 3.9: Degradation factors introduced in this thesis.

Degradation factor	Description
1	No scaling of the degradation
$5 \cdot [1.39]$	Both calendar and cycling degradation scaled with the factor $(5 \cdot 1.39)$
$5 \cdot [1.45]$	Both calendar and cycling degradation scaled with the factor $(5 \cdot 1.45)$
$5 \cdot [1.45, 1.65]$	Calendar degradation scaled with $(5 \cdot 1.45)$ and cycling degradation scaled with $(5 \cdot 1.65)$

3.8 Comparison MPC and GA

For both Use Case 1 and 2, daily simulations were made using both MPC and GA. This enables a comparison between the two methods based on their produced results.

In this thesis, the results obtained using MPC were indeed compared to those obtained using GA. One advantage of comparing the two algorithms is that if they produce similar solutions, it indicates that the solutions are likely close to the correct solution. This or they are always equally inaccurate however, this would be an unlikely outcome. If they differ, the comparison provides insight into which method that is more suitable for the optimization problem at hand.

The comparison was based on daily simulations conducted for four different dates: January 1st, April 1st, June 1st, and September 1st. These dates are in different seasons and helped to capture how well the two models perform under different seasonal conditions. All test scenarios applied in this thesis are presented in the following subsection.

4

Results

Using the theory in section 2 together with the tools constructed in section 3.5 it is possible to conduct simulations on the two use cases and start obtaining results. All the verification and final results will be presented in this section.

4.1 Validation Results

Before running and trusting this thesis's constructed tools, it's components and inputs should be validated. The two validation steps applied in this thesis will be presented in the following subsections.

4.1.1 Validation of Degradation Models

This subsection starts with presenting the degradation over a ten year period using the models chosen for this thesis, see Figures 4.5 - 4.6. The figures show the total degradation for both LFP and NCA for the locations of Gothenbrug and Luleå.

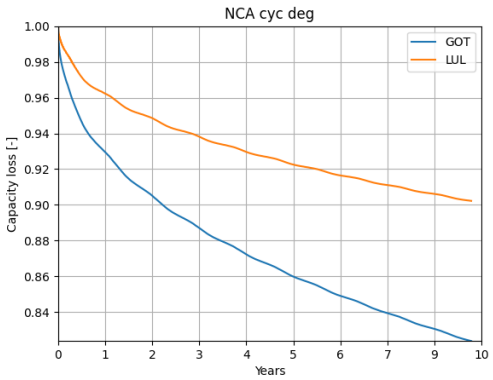

Figure 4.1: Cycling degradation over 10 years for NCA.

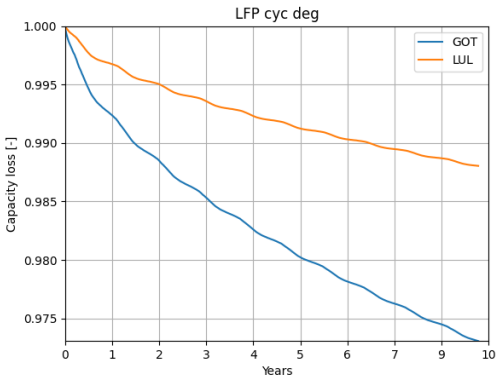

Figure 4.2: Cycling degradation over 10 years for LFP.

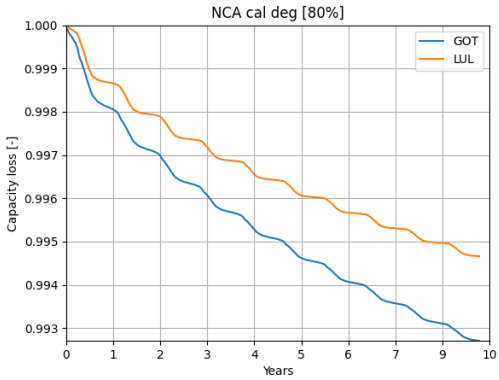

Figure 4.3: Calendar degradation over 10 years for NCA.

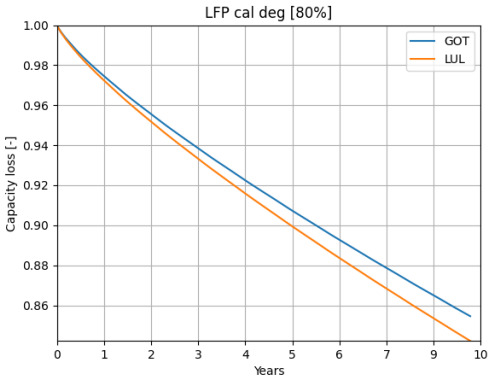

Figure 4.4: Calendar degradation over 10 years for LFP.

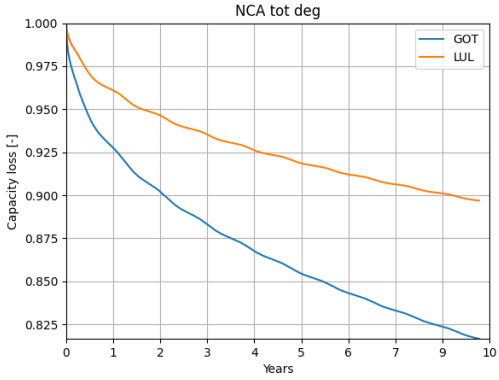

Figure 4.5: Total degradation over 10 years for NCA cells.

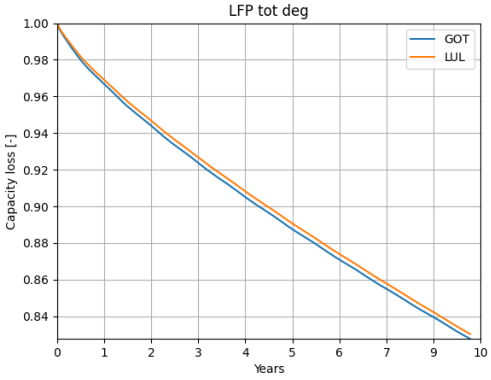

Figure 4.6: Total degradation over 10 years for LFP cells.

Having the degradation curves obtained using the models chosen for this thesis, the same results using Cassandra will now be presented. In Cassandra, Luleå was not avaliable as an optional city, so Stockholm was selected instead. However, the average temperature was changed to match that of Luleås. This shifts the histogram used by Cassandra to closer match the real weather in Luleå. The obtained degradation using Cassandra is presented in Figures 4.7 - 4.10.

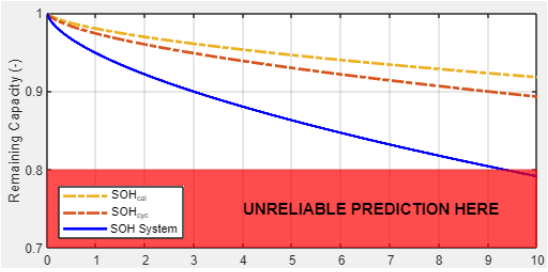

Figure 4.7: Total degradation over 10 years in GOT for NCA cells using Cassandra.

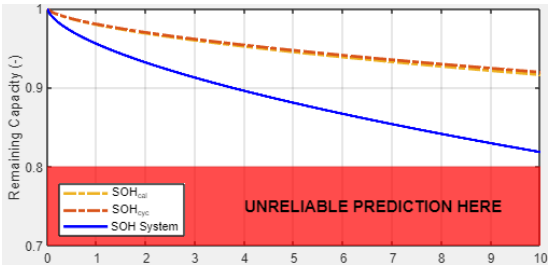

Figure 4.8: Total degradation over 10 years in LUL for NCA cells using Cassandra.

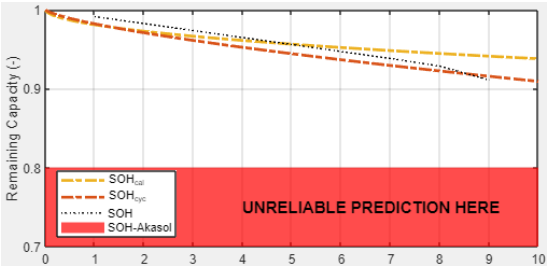

Figure 4.9: Total degradation over 10 years in GOT for LFP cells using Cassandra.

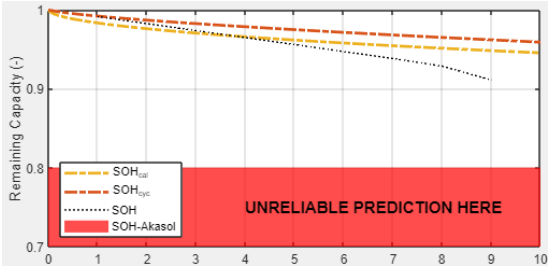

Figure 4.10: Total degradation over 10 years in LUL for LFP cells using Cassandra.

The degradations obtained using the Python script and Cassandra will be compared more in detail in the following discussion section 5.

4.1.2 Verification of MPC model

Now with the necessary results for the degradation models validation, it is time to present the results for the verification of the MPC code. Using the numbers presented in Table 3.5 as input values to the code one obtains the result illustrated in Figure 4.11. The scenario represented by Table 3.5 is the one where frequently charging and/or discharging is very profitable, hence the advantageous choice. In

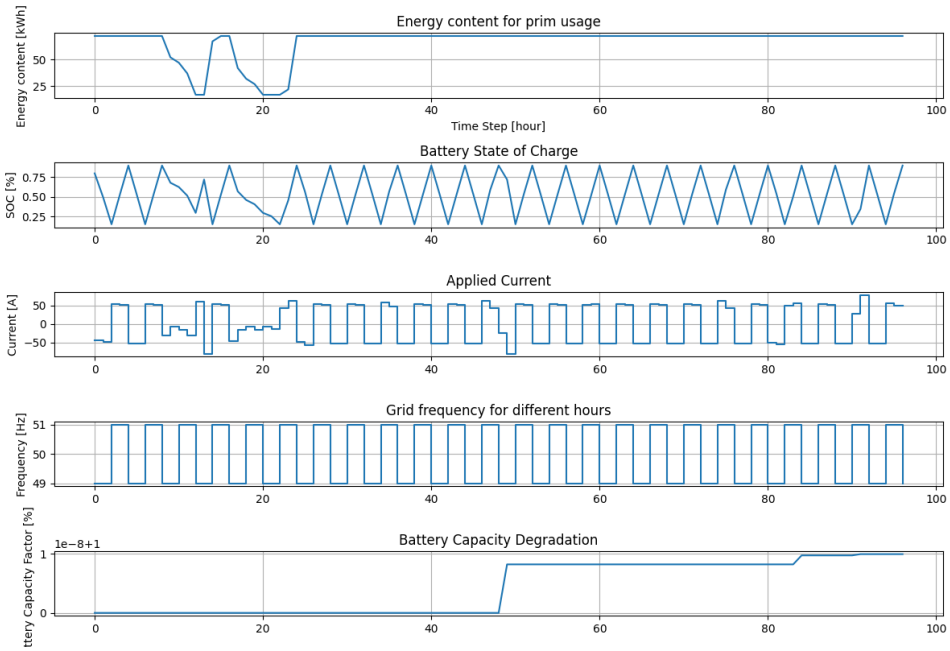

Figure 4.11: Optimal solution when having high FCR compensation. Unit of x-axis [h]

Figure 4.11 no primary usage is compromised; however, for non-primary usage intervals there are a lot of charging and discharging.
Using the numbers presented in Table 3.6 gives the usage profile illustrated in Figure 4.11 below.

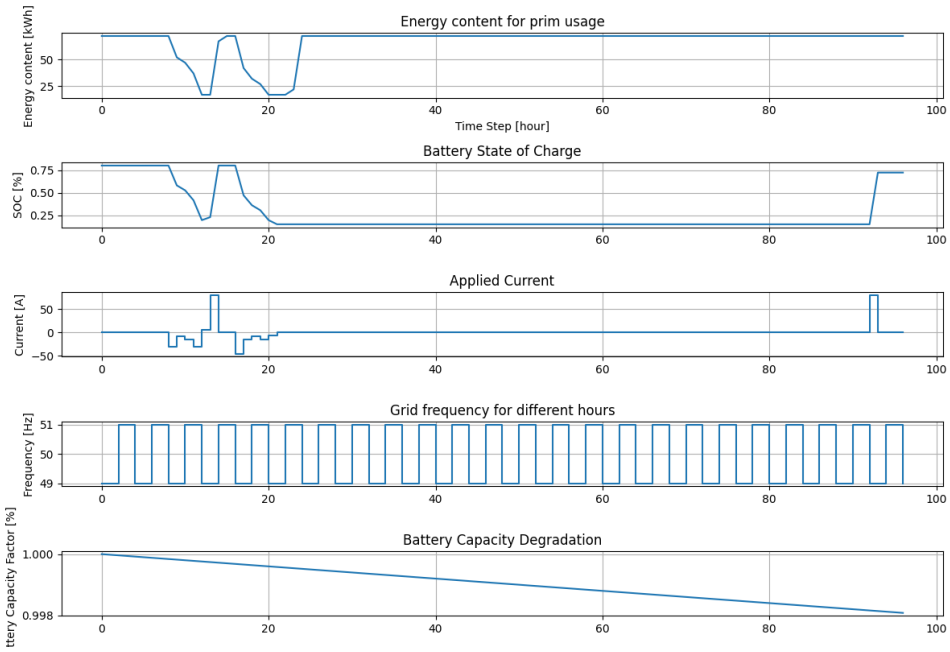

Figure 4.12: Optimal solution when having high degradation cost. Unit of x-axis [h]

In Figure 4.12, as for Figure 4.11, no primary usage is compromised. For intervals without any primary usage, close to no charging or discharging is taking place. This is in well accordance with the trivial solution of this specific scenario.

4.1.3 Evaluation of GA model

In order to evaluate the GA model, the average cost of each generation was recorded. Figure 4.13 showed the cost curve for one example case. From the figure, it could be seen that the average cost decreased rapidly during the first 300 generations and became stable after around generation 450. This indicated that the GA was able to find better solutions step by step and eventually reached convergence. Some peaks could also be observed in the curve. These peaks were caused by randomly adding new individuals to the population every 50 generations. The figure shown here was only from one case. The same method was applied to all cases. The figures were provided in the Appendix A.

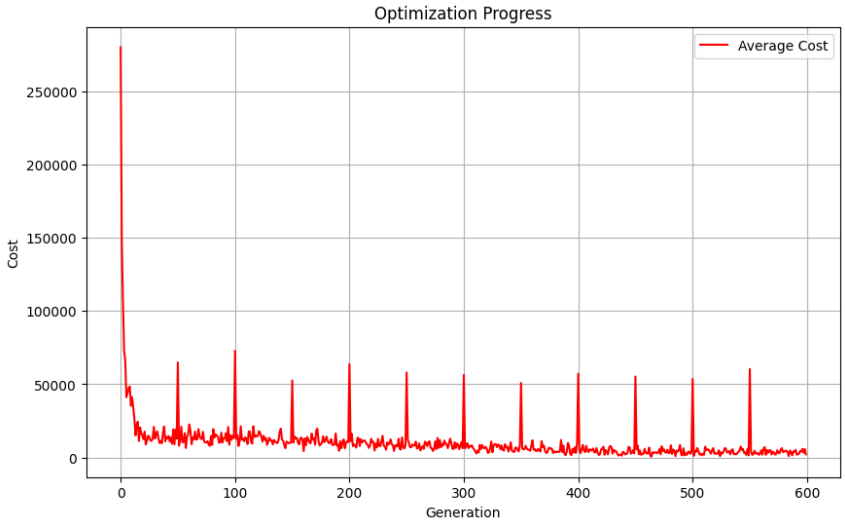

Figure 4.13: GA optimization progress over 600 generations for one day.

4.2 Daily simulations

Having validated the MPC for simple scenarios, it is time for the comparison of the MPC and GA. As described in the method section, merely four days will be used for this MPC and GA comparison. The results obtained using the two models, in the case of only primary usage, are presented in Table 4.1 and 4.2. The tables present the battery degradation cost and electricity cost for each of the four days. Remember these numbers are only correct for primary usage, hence for days without FCR service participation.

4.2.1 Primary Usage only

Results using MPC

Table 4.1: Battery Degradation and Cost of Daily Usage Without Optimization (MPC).

Season	Location	Battery	Daily aging[%]	Electricity cost[EUR]	Degradation cost[EUR]	Total cost[EUR]
Winter	LUL	NCA	4.4e-04	0.0	0.22	0.22
(1 Jan)	LUL	LFP	0.023	0.0	12	12
	GOT	NCA	0.0054	0.0	2.7	2.7
	GOT	LFP	0.023	0.0	12	12
Spring	LUL	NCA	0.016	0.0073	8.1	8.1
(1 Apr)	LUL	LFP	0.023	0.0073	11	11
	GOT	NCA	0.066	0.041	33	33
	GOT	LFP	0.025	0.041	12	12
Summer	LUL	NCA	0.089	0.73	45	45
(1 Jun)	LUL	LFP	0.026	0.73	13	14
	GOT	NCA	0.19	1.2	96	97
	GOT	LFP	0.040	1.2	20	21
Fall	LUL	NCA	0.011	0.0	5.5	5.5
(1 Sep)	LUL	LFP	0.024	0.0	12	12
	GOT	NCA	0.084	0.33	42	42
	GOT	LFP	0.028	0.33	14	14

Results using GA

Table 4.2: Battery Degradation and Cost of Daily Usage Without Optimization (GA).

Season	Location	Battery	Daily aging [%]	Electricity cost[EUR]	Degradation cost[EUR]	Total cost[EUR]
Winter	LUL	NCA	4.4e-04	0.0	0.22	0.22
(1 Jan)	LUL	LFP	0.023	0.0	12	12
	GOT	NCA	0.0054	0.0	2.7	2.7
	GOT	LFP	0.023	0.0	12	12
Spring	LUL	NCA	0.010	0.0073	5.1	5.1
(1 Apr)	LUL	LFP	0.0078	0.0073	3.9	3.9
	GOT	NCA	0.029	0.041	15	15
	GOT	LFP	0.0098	0.041	4.9	5.0
Summer	LUL	NCA	0.035	0.73	17	18
(1 Jun)	LUL	LFP	0.010	0.73	5.1	5.8
	GOT	NCA	0.049	1.2	25	26
	GOT	LFP	0.014	1.2	7.0	8.1
Fall	LUL	NCA	5.2e-04	0.0	0.26	0.26
(1 Sep)	LUL	LFP	0.0063	0.0	3.1	3.1
	GOT	NCA	0.012	0.33	5.8	6.1
	GOT	LFP	0.0076	0.33	3.8	4.1

4.2.2 Case study 1 for profitable B2G

Result using MPC

Using MPC one obtains the results, for Use Case 1, that are given in Table 4.3. Each combination of season, location and battery chemistry have results regarding the total daily aging, degradation cost, revenue and total savings given in both euros and percentage. In addition the results for winter will be graphically illustrated while the plots for the remaining seasons can be found in the Appendix B.

Table 4.3: Battery Degradation and Cost of Daily Usage without degradation limit (MPC).

Season	Location	Battery	Daily aging [%]	Degradation cost [EUR]	Total Revenue [EUR]	Total secu Cost [EUR]	Total prim Cost [EUR]	Savings [EUR]	Savings [%]
Winter	**LUL**	**NCA**	0.0094	4.7	4.5	0.20	0.22	0.014	6.5
(1 Jan)	**LUL**	**LFP**	0.025	12	10	2.2	12	9.6	82
	GOT	**NCA**	0.0054	2.7	7.4e-07	2.7	2.7	4.2e-04	0.016
	GOT	**LFP**	0.025	12	9.6	2.9	12	8.9	76
Spring	**LUL**	**NCA**	0.018	9.1	2.3	6.8	8.1	1.2	15
(1 Apr)	**LUL**	**LFP**	0.024	12	23	-11	11	23	200
	GOT	**NCA**	0.0622	31	5.5	26	33	7.3	22
	GOT	**LFP**	0.024	12	6.3	5.4	12	6.9	56
Summer	**LUL**	**NCA**	0.089	45	4.6	40	45	5.4	12
(1 Jun)	**LUL**	**LFP**	0.030	15	7.5	7.7	14	6.2	45
	GOT	**NCA**	0.19	96	7.5	89	97	8.1	8.4
	GOT	**LFP**	0.040	20	9.1	11	21	10	48
Fall	**LUL**	**NCA**	0.011	5.5	6.9e-07	5.5	5.5	0.0031	0.057
(1 Sep)	**LUL**	**LFP**	0.028	14	3.8	10	12	1.8	15
	GOT	**NCA**	0.081	41	1.1	40	42	2.8	6.7
	GOT	**LFP**	0.029	14	7.3	7.1	14	7.1	50

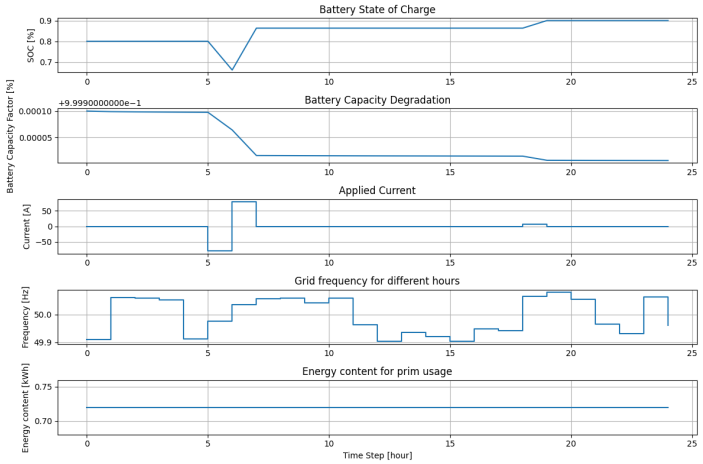

(a) Use Case 1: NCA – LUL

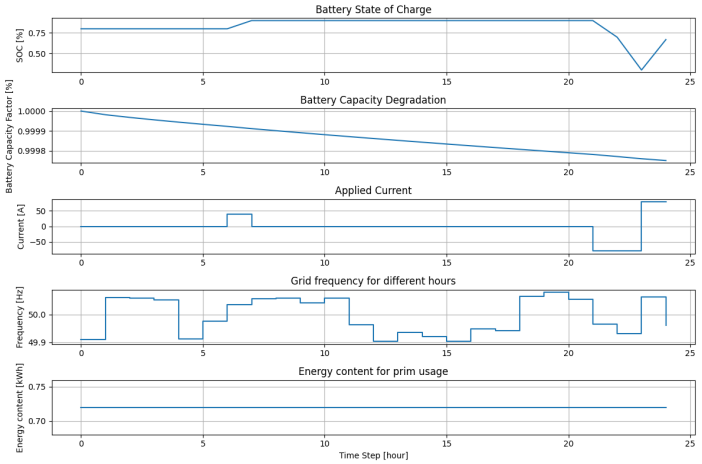

(b) Use Case 1: LFP – LUL

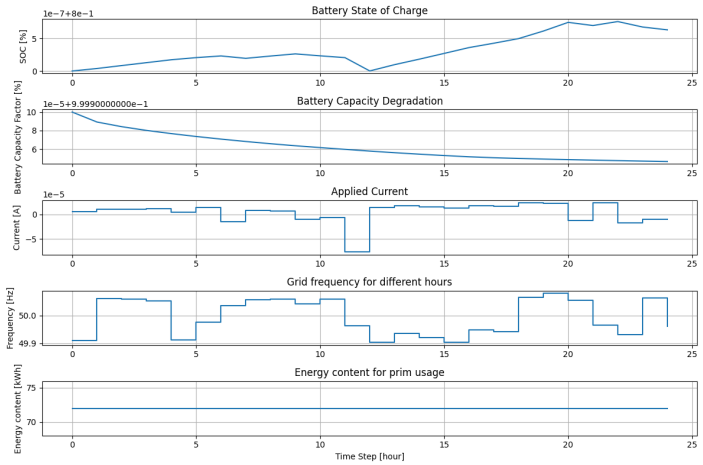

(c) Use Case 1: NCA – GOT

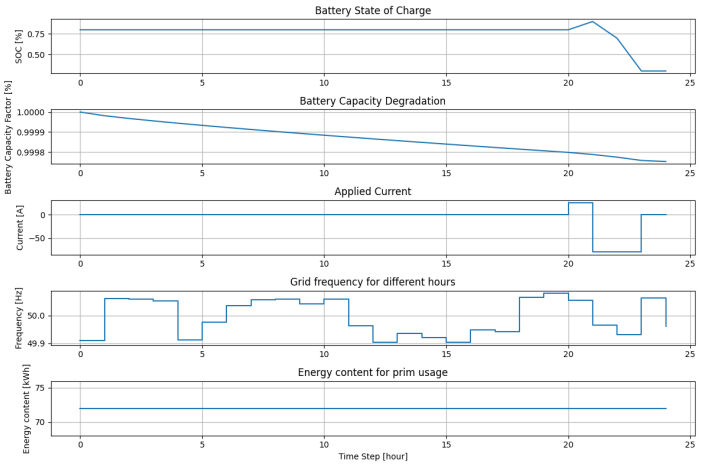

(d) Use Case 1: LFP – GOT

Figure 4.14: Results for a winter day using MPC and Use Case 1. The x-axis in all subfigures represents time, while the y-axes vary: the top graph shows the state of charge (SOC), the second shows battery capacity, the middle graph presents current, the second-to-last shows grid frequency, and the last graph shows battery energy content.

The daily simulations using MPC for Use case 1 can be summarized as a color map and is illustrated in Figure 4.15.

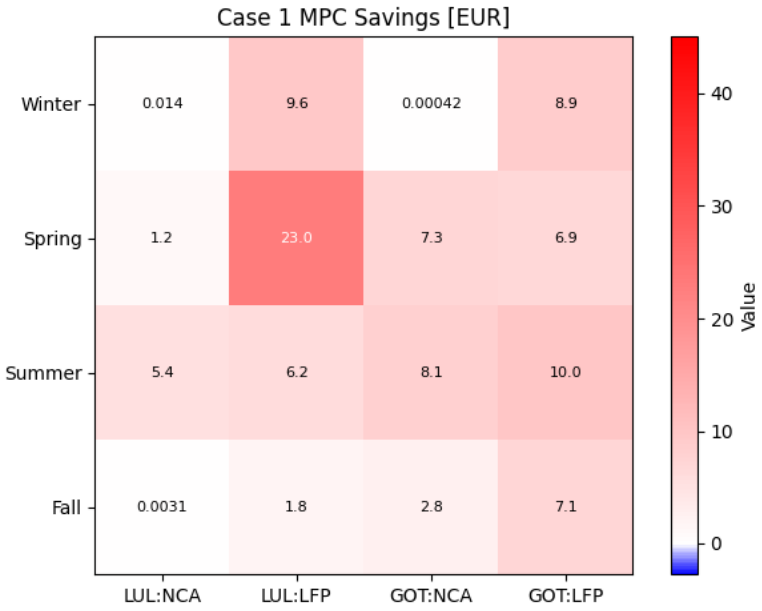

Figure 4.15: Color map summarizing the daily simulations done with MPC, for Use Case 1.

Result using GA

Now switching the controller into GA the same set of results are produced and presented in Table 4.4 and Figure 4.16.

Table 4.4: Battery Degradation and Cost of Daily Usage Without degradation limit (GA).

Season	Location	Battery	Daily aging[%]	Degradation cost[EUR]	Total Revenue[EUR]	Total Cost[EUR]	Savings [EUR]	Savings %
Winter	**LUL**	**NCA**	0.011	5.6	5.6	0.021	0.20	91
(1 Jan)	**LUL**	**LFP**	0.026	13	23	-11	22	191
	GOT	**NCA**	0.014	7.0	2.2	4.8	-2.1	-80
	GOT	**LFP**	0.035	17	24	-6.2	18	154
Spring	**LUL**	**NCA**	0.048	24	20	4.5	0.62	12
(1 Apr)	**LUL**	**LFP**	0.017	8.6	50	-41	45	1155
	GOT	**NCA**	0.029	15	8.5	6.1	8.7	59
	GOT	**LFP**	0.019	9.5	39	-29	34	694
Summer	**LUL**	**NCA**	0.040	20	5.7	14	3.9	22
(1 Jun)	**LUL**	**LFP**	0.020	10	20	-10	16	271
	GOT	**NCA**	0.052	26	5.1	21	4.7	18
	GOT	**LFP**	0.017	8.5	10	-1.8	9.9	122
Fall	**LUL**	**NCA**	0.31	1.5	1.0	0.53	-0.26	-100
(1 Sep)	**LUL**	**LFP**	0.016	7.7	15	-7.6	11	342
	GOT	**NCA**	0.013	6.6	2.7	3.8	2.2	37
	GOT	**LFP**	0.012	6.0	12	-6.4	11	256

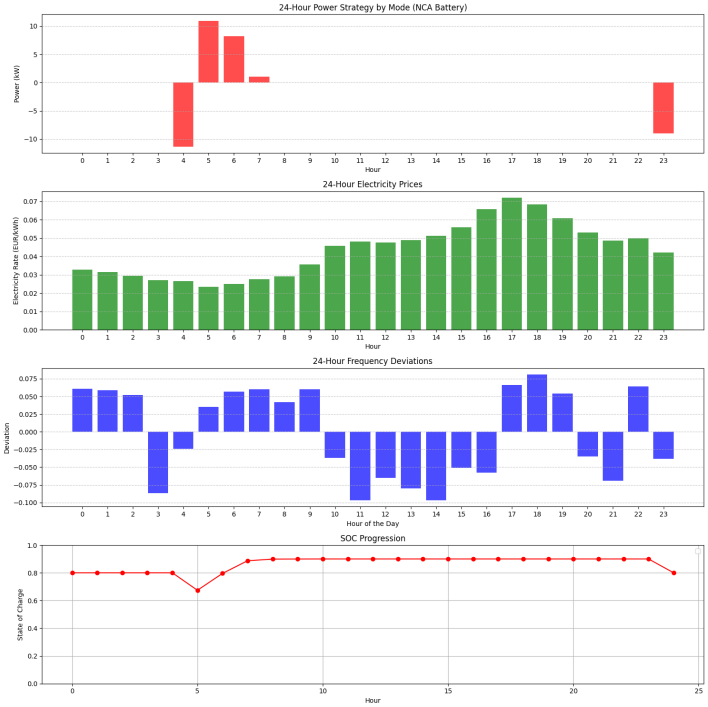

(a) NCA – LUL

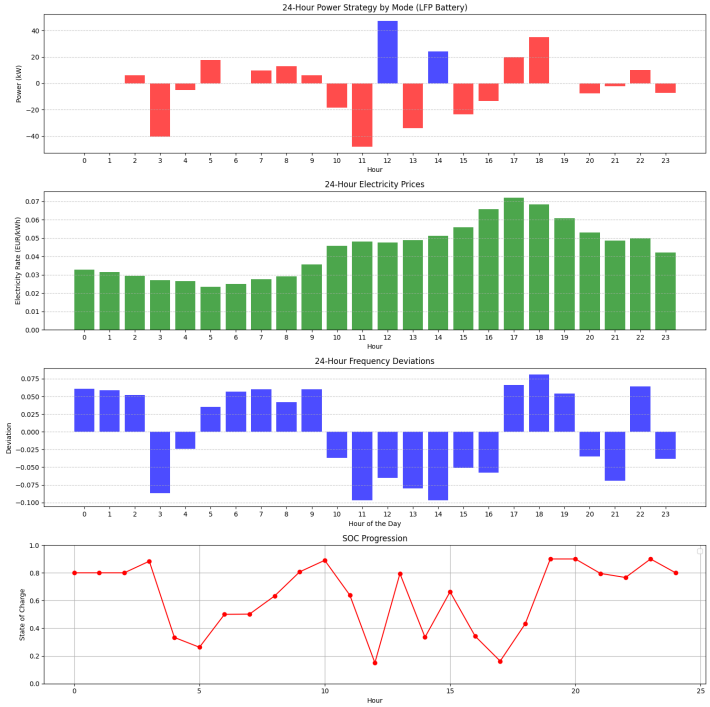

(b) LFP – LUL

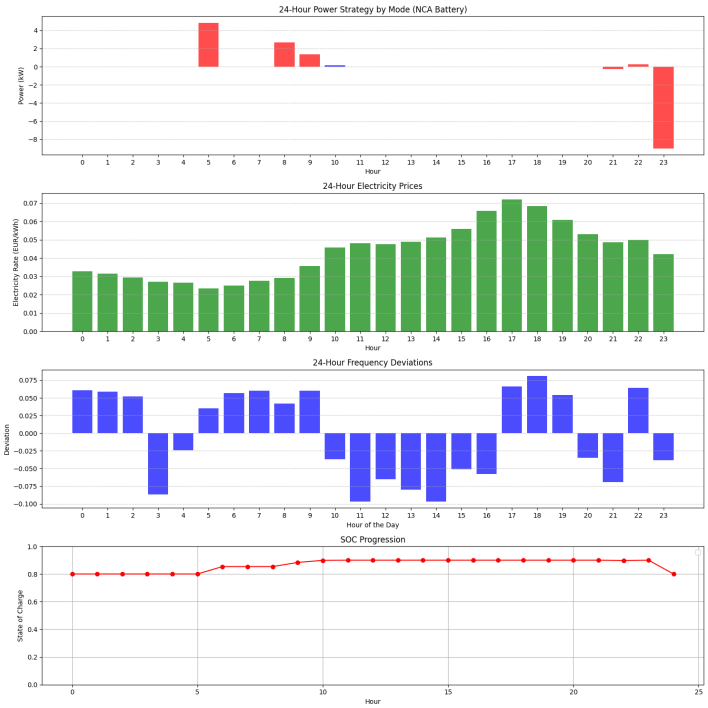

(c) NCA – GOT

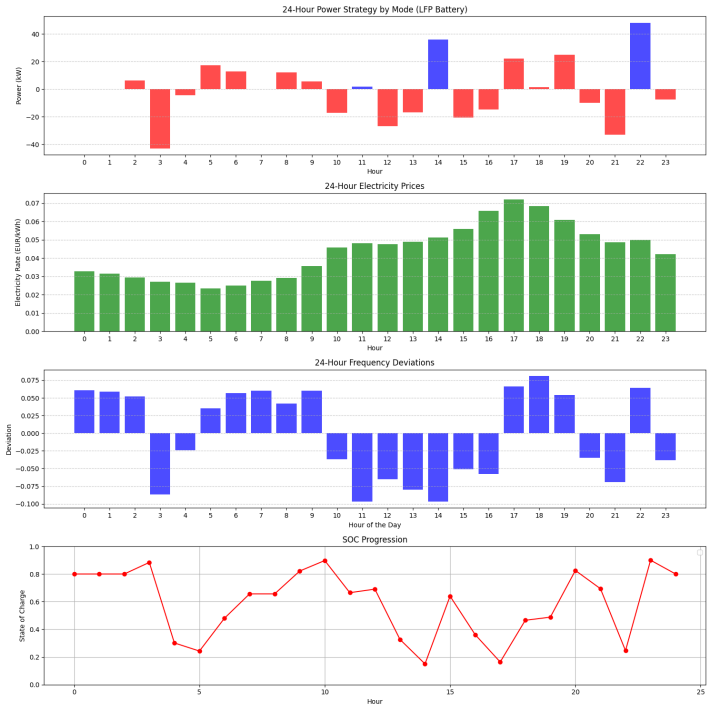

(d) LFP – GOT

Figure 4.16: Result for day in winter using MPC and Use Case 1.

The color map summarizing the daily simulations for Use Case 1 using GA is shown below, see Figure 4.17.

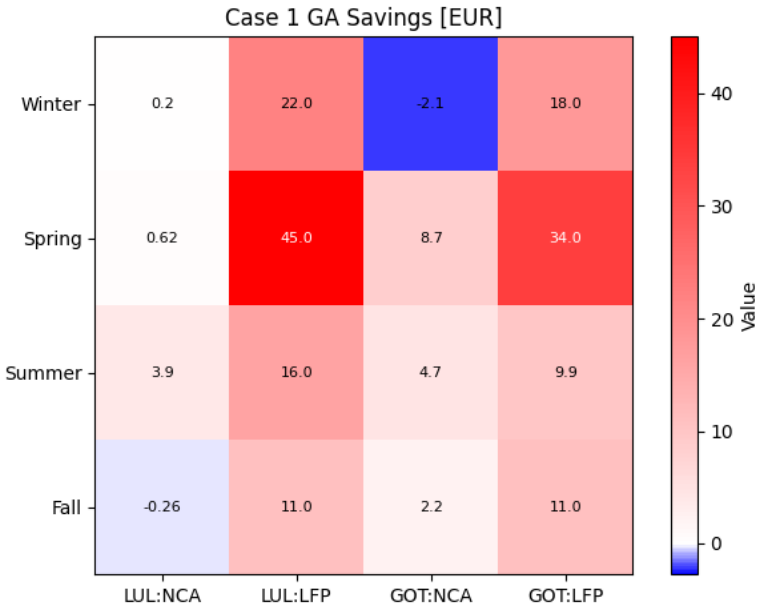

Figure 4.17: Color map summarizing the daily simulations done with GA, for Use Case 1.

4.2.3 Case study 2 for limited degradation

Below the collection of results for Use Case 2 are presented. Similar to the results for Use Case 1, there is one row per combination of season, location, and battery chemistry.

Result using MPC

Table 4.5: Battery Degradation and Cost of Daily Usage With degradation limit equal to prim usage deg (MPC)

Season	Location	Battery	Daily aging [%]	Degradation cost [EUR]	Total Revenue [EUR]	Total secu Cost [EUR]	Total prim Cost [EUR]	Savings [EUR]	Savings [%]	Solver fail
Winter	**LUL**	**NCA**	4.4e-04	0.22	0.0018	0.22	0.22	9.9e-04	0.45	
(1 Jan)	**LUL**	**LFP**	0.024	12	5.3	6.9	12	4.8	41	
	GOT	**NCA**	0.0054	2.7	8.3e-07	2.7	2.7	4.5e-04	0.017	20
	GOT	**LFP**	0.024	12	4.8	7.0	12	4.7	40	
Spring	**LUL**	**NCA**	0.015	7.5	2.0	5.5	8.1	2.5	31	
(1 Apr)	**LUL**	**LFP**	0.021	11	25	-14	11	25	220	
	GOT	**NCA**	0.059	30	-0.61	30	33	2.7	8.3	10
	GOT	**LFP**	0.023	12	8.4	3.4	12	9.0	73	
Summer	**LUL**	**NCA**	0.088	44	0.40	43	45	2.0	4.3	12:1
(1 Jun)	**LUL**	**LFP**	0.026	13	3.7	9.4	14	4.5	32	
	GOT	**NCA**	0.019	95	2.5	93	97	4.3	4.4	
	GOT	**LFP**	0.036	18	1.2	17	21	4.0	19	
Fall	**LUL**	**NCA**	0.011	5.5	4.9e-07	5.5	5.5	0.0032	0.057	12
(1 Sep)	**LUL**	**LFP**	0.026	13	2.7	10	12	1.4	12	
	GOT	**NCA**	0.081	40	-0.062	40	42	2.1	4.8	2
	GOT	**LFP**	0.031	15	6.1	9.1	14	5.0	35	

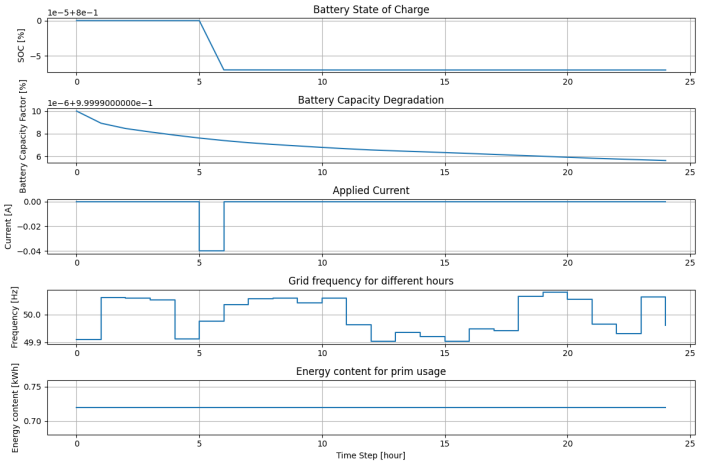

(a) Use Case 2: NCA – LUL

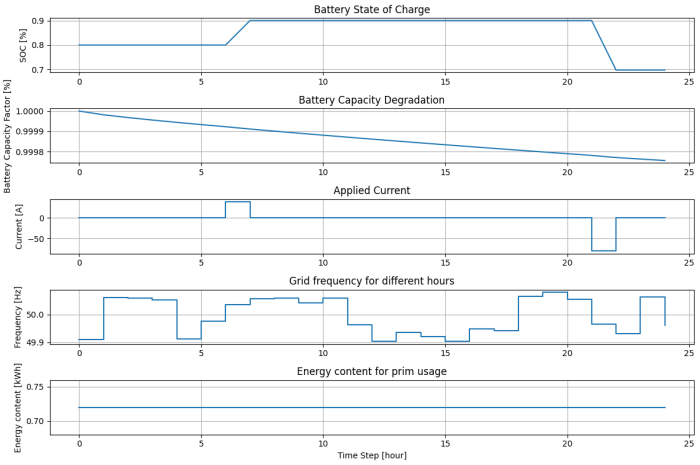

(b) Use Case 2: LFP – LUL

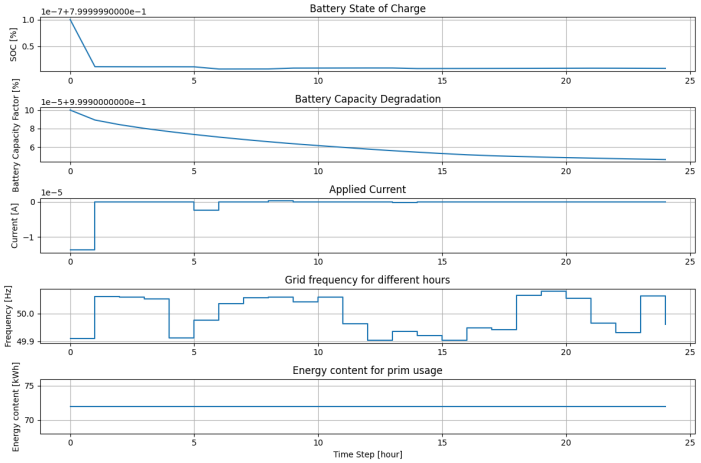

(c) Use Case 2: NCA – GOT

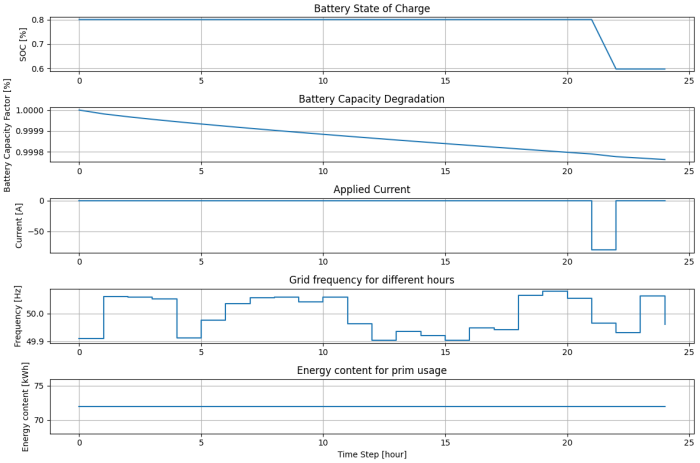

(d) Use Case 2: LFP – GOT

Figure 4.18: Results for a winter day using MPC and Use Case 1. The x-axis in all subfigures represents time, while the y-axes vary: the top graph shows the state of charge (SOC), the second shows battery capacity, the middle graph presents current, the second-to-last shows grid frequency, and the last graph shows battery energy content.

The color map summarizing the daily simulations for Use Case 2 using MPC is shown below, see Figure 4.19.

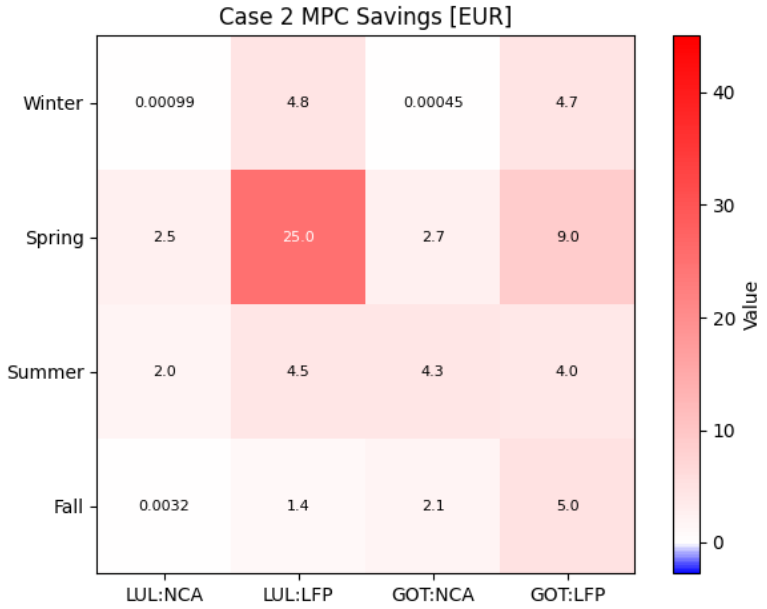

Figure 4.19: Color map summarizing the daily simulations done with MPC, for Use Case 2.

Result using GA

Table 4.6 shows the results from when the daily aging limit is set equal to that of the primary usage.

Table 4.6: Battery Degradation and Cost of Daily Usage With degradation limit equal to prim usage deg (GA)

Season	Location	Battery	Daily aging[%]	Degradation cost[EUR]	Total Revenue[EUR]	Total Cost[EUR]	Savings [EUR]	Savings %
Winter	**LUL**	**NCA**	0.0011	5.4	5.5	-0.11	0.33	148
(1 Jan)	**LUL**	**LFP**	0.023	12	22	-11	22	192
	GOT	**NCA**	0.014	6.9	1.5	5.4	-2.7	-102
	GOT	**LFP**	0.023	12	4.6	7.1	4.5	39
Spring	**LUL**	**NCA**	0.023	12	6.7	5.1	0.033	0.66
(1 Apr)	**LUL**	**LFP**	0.0078	3.9	12	-7.8	12	299
	GOT	**NCA**	0.029	14	6.2	8.6	6.5	44
	GOT	**LFP**	0.0098	4.9	7.9	-3.0	7.9	160
Summer	**LUL**	**NCA**	0.040	20	4.3	16	2.6	15
(1 Jun)	**LUL**	**LFP**	0.010	5.0	1.5	3.5	2.4	40
	GOT	**NCA**	0.050	25	3.6	21	4.4	17
	GOT	**LFP**	0.010	5.2	8.5	-3.3	11	141
Fall	**LUL**	**NCA**	0.0030	1.5	0.84	0.68	-0.42	-159
(1 Sep)	**LUL**	**LFP**	0.0068	3.4	0.59	2.8	0.31	9.8
	GOT	**NCA**	0.013	6.2	1.3	4.9	1.2	19
	GOT	**LFP**	0.0076	3.8	3.4	0.44	3.7	89

Figure 4.20 shows the result of a the first of January day GA optimization in winter under limited degradation.

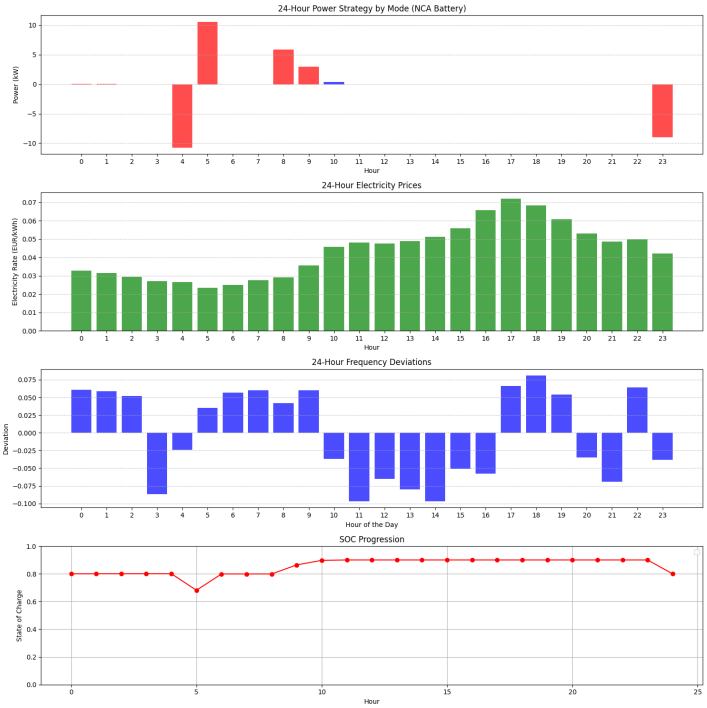

(a) NCA – LUL

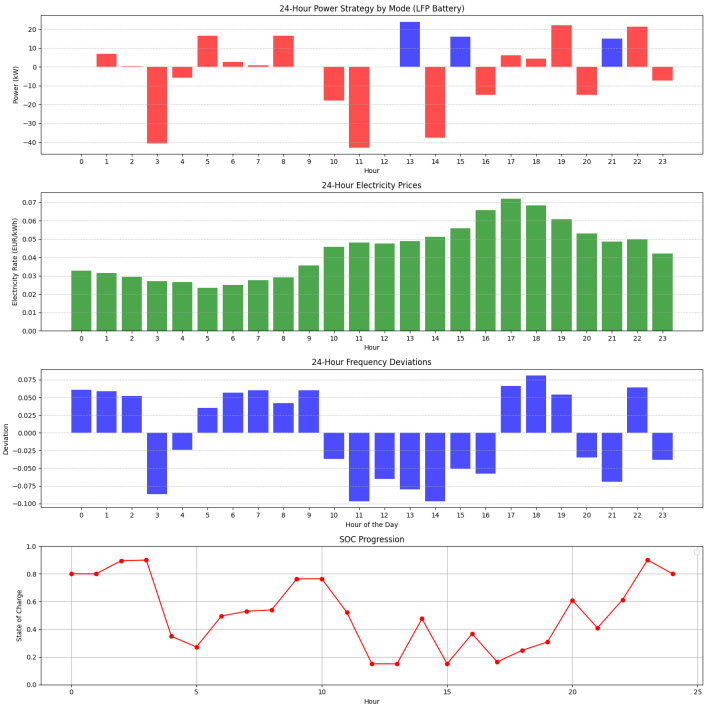

(b) LFP – LUL

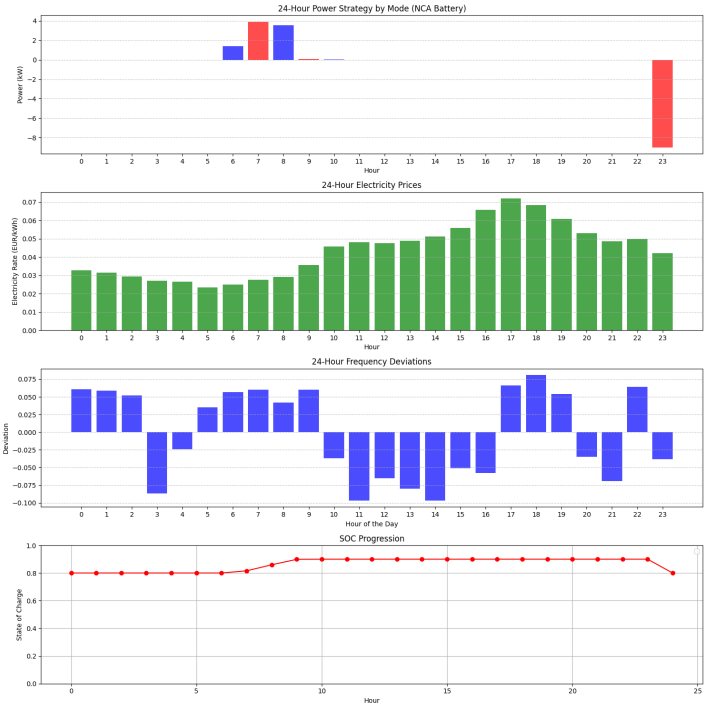

(c) NCA – GOT

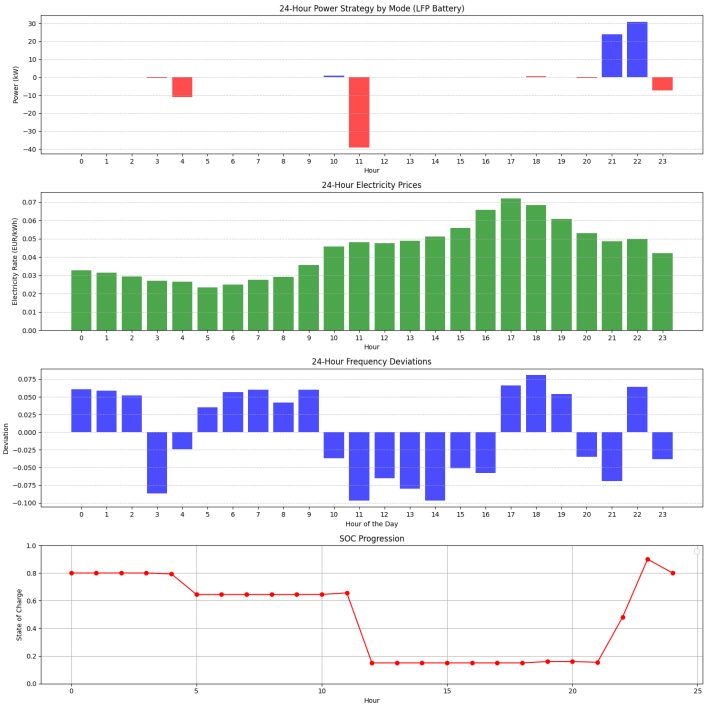

(d) LFP – GOT

Figure 4.20: Result for day in winter using MPC and Use Case 2

The color map summarizing the daily simulations for Use Case 2 using GA is shown below, see Figure 4.21.

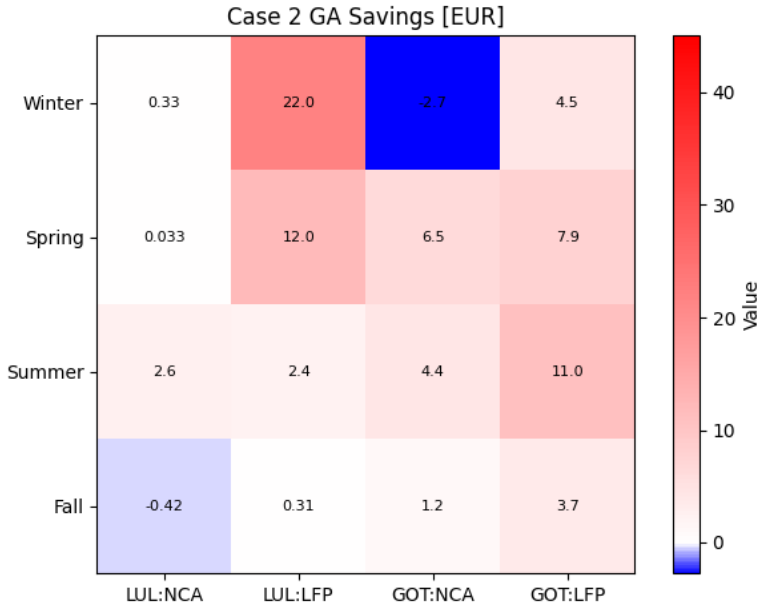

Figure 4.21: Color map summarizing the daily simulations done with GA, for Use Case 2.

4.3 Yearly simulations using MPC

Having data for daily simulations using both MPC and GA, the remaining data to be presented is for the yearly simulations conducted using only MPC.

LFP Luleå

Case 1 for yearly simulation

Table 4.7: Results for 1 year runs using LFP in Luleå ($t_{start} = 0$), $T_{war} = 1$ year

B2G approch	Degradation factor	Yearly aging	Degradation cost	Total Revenue	Total secu Cost	Total prim Cost	Savings [EUR]	Savings percentage
Unlimited	1	0.029	1400	4900	-3500	2000	5400	280
	$5 \cdot [1.39]$	0.17	8600	6100	2500	5900	3400	58
	$5 \cdot [1.45]$	0.17	8400	4900	3500	6200	2700	44
	$5 \cdot [1.45, 1.65]$	0.17	8300	4800	3600	6200	2700	43
Limited	1	0.027	1300	4400	-3100	2000	5100	260
	$5 \cdot [1.39]$	0.13	6500	1800	4800	5900	1200	20
	$5 \cdot [1.45]$	0.14	6900	2200	4700	6200	1500	24
	$5 \cdot [1.45, 1.65]$	0.14	6900	2100	4700	6200	1500	24

The savings data from Table 4.7 can be plotted against the scaling factor which gives Figure 4.22

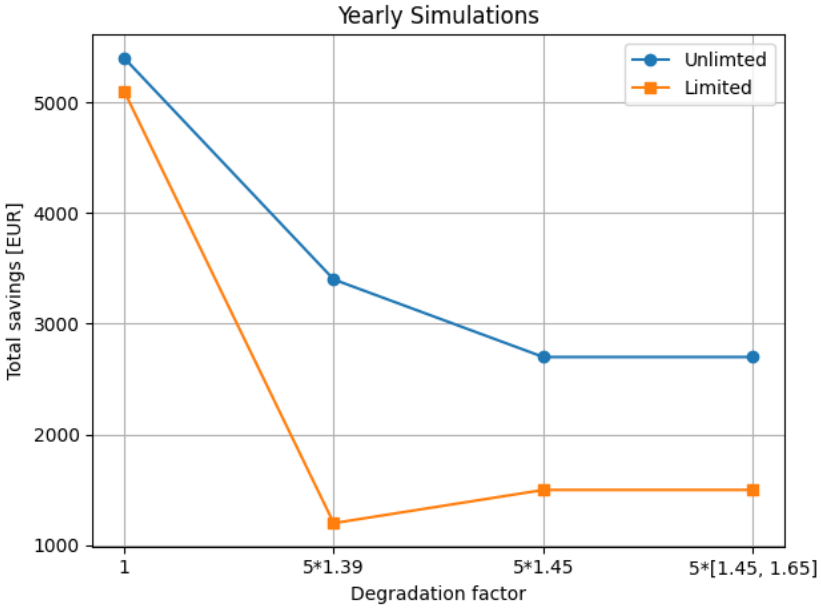

Figure 4.22: Savings in Euros for the yearly data as a function of scaling factor.

5
Discussion

Based on the results obtained in this thesis, several conclusions may be drawn. To reach these conclusions, the data must be carefully analyzed, and any observed patterns and/or differences discussed. These discussions and analyzes will be presented in this chapter and serve as the foundation for this thesis's conclusions. The chapter begins by analyzing the similarities found between this studies degradation models and the ones implemented in Cassandra.

5.1 Degradation models

In the previous results section, results demonstrating the alignment between Volvo's degradation software, Cassandra, and this thesis's degradation models were presented. By comparing the two, it is apparent that the nature of the degradation and the final capacities are somewhat similar. One major difference is that, while the final capacity using Cassandra for NCA is similar for both Gothenburg and Luleå, this is not true for this thesis's degradation models. The opposite is true when analyzing the degradation results for LFP. Here the Cassandra software resulted in a large absolute and relative difference between Gothenburg and Luleå. The situation with the most similarities is NCA in Gothenburg. Here, both Cassandra and the Python script based on the thesis's degradation models resulted in a final degradation of roughly 20%.

Although the degradation models used in this thesis do not perfectly align with the Cassandra software, the similarities ensure that conducted simulations will produce close to realistic numbers. This statement is obviously only true for a working code and under the assumption that the Cassandra software is accurate. Furthermore, this study treats the degradation models as input parameters and are therefore not central to the study itself. For future work and applications of the developed simulation tools, the degradation models should always be changed to suit the special scenario being analyzed. It would therefore be unnecessary to put too much focus on the accuracy or performance of the degradation models instead of the performance and reliability of the simulation code itself.

5.2 MPC results

In the following paragraphs, the results obtained using the MPC code will be analyzed and discussed. To begin this section, the MPC verification is examined.

Verification

As seen in Figures 4.11 - 4.12 both the simulations conducted for the code verification properly include the primary usage for a summer day in Gothenburg. Furthermore, in accordance with the trivial solutions presented in the method section, one simulation is frequently charging and discharging while the other one displays zero current for the majority of the time. Accurately implementing the primary usage and closely following the trivial solutions for the remaining hours clearly proves that the MPC code works for simple scenarios.

Being satisfied with the "easy case" verifications for MPC, more realistic simulations were performed. The first data set tested using MPC represents the daily scenario with only primary usage implemented. With exclusively primary usage, it is apparent that degradation is the highest during summer, reaching a value of 0.19 % and lowest during winter, see Table 4.1. This behavior is expected due to the absence of primary usage and colder temperatures during the winter season. Analyzing the total cost follows the same trend where during the summer cost goes up towards 100 Euros, while winter only ever reaches 12 Euros. Knowing the results for strictly primary usage makes it easier to distinguish advantages and disadvantages when applying B2G and attending the FCR-N market as done in Use Case 1 and 2. In the following, the daily simulations for Use Case 1 and 2 will be properly discussed.

Use Case 1

Table 4.3 presents the results from implementing Use Case 1. Containing a lot of values, perhaps the most interesting and important set of data is the column second from the right, showing savings in euros. This column is simply the result of taking the secondary usage cost and subtracting the primary usage cost. The savings are positive for all 16 combinations simulated. This shows that independently of battery type, season and/or location, the MPC code always saves the boat owner money.

It is important to keep in mind that the savings are given in relation to the primary cost. Hence a positive saving does not immediately imply that money is being earned; rather, this implies that money is being saved by a reduction of the total cost. The savings can be converted into relative savings by dividing each absolute saving with its corresponding primary cost. This is shown in the right edge column, and it reveals that the largest relative saving is obtained for a LFP battery in Luleå during spring. For this scenario the code manages to save the user close to 200 %. Being larger than 100 % this saving actually implies that money is being earned. Though this indicates huge potential, the value of 200 % is much larger than the remaining results obtained, where none of the other passes the 100 % limit.

Use Case 2

For Use Case 2 the results are all presented in Table 4.5. Though similar to Table 4.5 one additional column is added. This column presents the number of iterations that could not be solved by the first MPC solver. For all these scenarios, except for the combination with a NCA battery in Luleå during summer, only one number is given in this extra column. This means that the unsuccessful iterations were solved by the second solver instead of the first. The difference between solver 1, 2 and 3 is that solver 2 has a higher relative unit less tolerance of 10^{-9} compared to solver 1 having a tolerance of 10^{-11}. Solver 3 has an even higher tolerance of 10^{-7} making it less accurate. Having two numbers in the added column, as for the NCA battery in Luleå during summer, means that both solver 2 and 3 were needed to get out any savings. The first of the two numbers represents the number of iterations solved by solver 2 and the second number represents the number of iterations solved by solver 3.

The fact that not every iteration is solved by the first solver proves that Use Case 2 is more computationally heavy compared to Use Case 1. This is reasonable since the only difference between the two cases is that Case 2 has an additional constraint, making it more strict. Furthermore, having iterations being solved by solvers other than the first one will, due to the increased tolerance, result in solutions further from the optimal one. Since the optimal solution is the one where most money is saved, drifting away from this solution means that less money is being saved. With this in mind, it is satisfying to see that the MPC code still manages to save money for the more troublesome scenarios. The most profitable combination is the same as in Use Case 1, this time resulting in a saving of 220 %. Use Case 1 and 2 not only have their largest savings for the same combinations but they also have very similar savings profiles overall.

Continuing to analyze the savings, it becomes apparent that neither Use Case 1 nor 2 always results in higher savings than the other. The absolute and relative savings are larger for 11 combinations using use Case 1 and 5 using Use Case 2. This is highly unexpected when thinking about the difference between Use Case 1 and 2. The reason for this to be unexpected is most easily explained by comparing the solution domain/pool for Use Case 1 and Use Case 2. Implementing the additional constraint for Use Case 2 only affects the solution domain by making it slightly smaller. This is because solutions that where allowed in Use Case 1 now might have to be discarded to to their high degradation. A representation of the solution domain for Case 1 and 2 is represent in Figure 5.1.
If the most optimal solutions lies within the solution domain for Use Case 1 but not for Use Case 2, this would result in Case 2 giving out a less optimal solution, hence a lower saving. This can never happen the other way around, since all the solutions found in the solution domain for Use Case 2, lies within the solution pool for Case 1. Knowing this, it is very odd to observe that Case 2 sometimes results in higher savings than Case 1. The reason why this happens is still unclear; however, one guess could be that limiting the solution domain takes the solver closer to the correct solution faster and might therefore converge faster and more closely to the

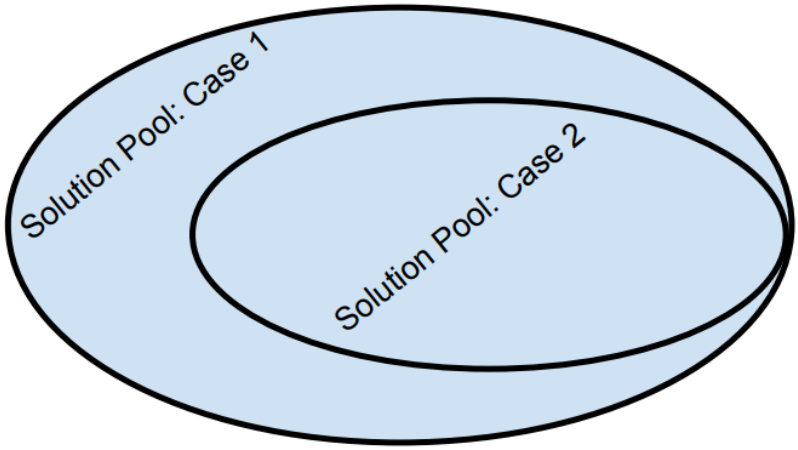

Figure 5.1: Representation of the solution pool for Use Case 1 and 2.

exact optimal solution. This theory, on the other hand, fails to explain why difference can be relatively large. Therefore, in order to properly find the origin of this phenomenon, a deeper analysis must be conducted.

Having distinguished the differences for Use Case 1 and 2, using the MPC code, it can be of value to investigate how savings change with other parameters. Comparing the two battery chemistries, a larger difference can be distinguished, namely the fact that LFP generally results in greater savings, with the only exception being in Luleå, during summer for Case 1. For example, no daily simulation using LFP has a saving smaller than 14 %, while only one simulation using NCA gets past this limit. Even the only exception disappears when looking at relative savings, for which LFP always gives the highest savings. This trend can be explained by the low cycling aging for LFP, illustrated in Figure 4.2. Having low cycling aging enables more frequent charging and discharging without increasing the overall degradation too much. For NCA, on the other hand, the largest degradation contributor is the cycling aging. Hence, increasing the charging and discharging slightly has a much larger effect on the NCA batteries compared to LFP batteries. This, together with the fact that the compensation for attending the FCR-N market is the same for both chemistries, helps explain why the savings found are larger for LFP than for NCA.

The two locations Gothenburg and Luleå should also be compared. Doing so it becomes apparent that each of them are more profitable than its counterpart for different scenarios. Gothenburg give a larger absolute and relative saving for each simulation made for fall. The opposite is true during winter even though the margin here is small for a couple of scenarios. For spring and Summer some combinations are more profitable in Luleå and some in Gothenburg. The reason to why Gothenburg is more profitable during fall than Luleå is probably due to the difference in primary usage. Some primary usage is applied in Gothenburg but not for Luleå. Since the degradation limit in Case 2 is set equal to the degradation obtained allowing only primary usage, a profile like Luleå in fall, which contains no primary

usage, results in almost no allowable degradation, hence leaves very little room for generating revenue by attending the FCR-N market.

5.3 GA results

When using GA, Case 1 and Case 2 showed clear differences in economic benefits and battery aging. In Case 1, revenue was quite high; most total revenues were between 5 and 25 EUR per day. But at the same time, the degradation cost was also high, mostly between 5 and 15 EUR. It meant we could earn more, but the battery aged faster. For example, the aging of NCA in winter at Gothenburg increased from 0.0000535 % to 0.00014 %, mainly because participating in FCR caused more frequent charging and discharging. Case 1 was suitable for maximizing short-term profits; however, this case results in a shorter battery life. In some conditions, this case achieved very high revenue. In Case 2, most degradation costs stayed below 5 EUR, and most revenue was below 7 EUR. This meant we could still make a profit, but also better protect the battery. In many cases, the aging rate only increased slightly, such as for the NCA battery in Gothenburg during summer (from 0.00049 % to 0.000497 %). In some cases, the aging was even lower than that of the primary usage, like the NCA battery in Gothenburg during spring (from 0.000295 % to 0.000289 %). This showed that Case 2 could balance revenue and battery aging effectively. In total, 12 out of 16 configurations achieved more than 14% saving rate, and 5 configurations exceeded 100 %. The choice of Case 1 or Case 2 depended on whether the priority was immediate gain or long-term sustainability. If the battery was under warranty or sensitive to aging, Case 2 was the better choice. If the goal was a quick return on investment, Case 1 might be better.

Battery type selection had a strong impact. LFP batteries performed much better than NCA in all seasons and locations. LFP showed lower aging cost, higher net benefit, and positive saving rates, especially in spring and summer. It meant LFP was more suitable for regular grid service. In contrast, NCA batteries performed poorly, due to their degradation being highly dominated by cycling aging. Even minor charging actions caused noticeable degradation, leading to higher aging costs and lower or negative savings. This made NCA batteries less suitable for grid services, especially in winter and fall.

Geographical location and seasonal factors influenced results across both cases. Location and season influenced the electricity price and primary usage. In the same season, two locations performed quite differently. For example, in summer at Gothenburg LFP saved 141%, while at Luleå, the saving rate was only 14.53%. Spring and autumn were the most favorable seasons. For example: LFP at Luleå in spring: 298.6%; LFP at Gothenburg in spring: 159.5%. In summer, although usage time was high and optimization windows were limited, the model still achieved good revenue in several cases.

Although GA worked effectively in most cases, it could not always guarantee a good result, for example, in fall for Luleå of NCA a negative savings was obtained. There

were several reasons behind this. First, the optimization problem involved multiple constraints, such as target SoC at the end of the charging window and daily aging limit. These constraints were implemented as penalty terms in the fitness function. The algorithm might have focused more on reducing the penalties rather than minimizing the actual operational cost. Second, GA was a heuristic method. It searched based on random population and evolution rules. Although GA provided a way to explore complex search spaces, its performance was still affected by the design of the cost function and the way constraints were handled. However, this negative optimization result also had practical value, it helped to determine conditions when the batteries should not be used for the grid service.

In conclusion, the LFP battery was more suitable for FCR service due to its aging behavior. Location and seasonal factors influenced performance across both cases. Geographical location and seasonal factors had a significant influence on the results. Case 1 was suitable when maximizing short-term revenue was the goal, and battery aging was acceptable. Case 2 was suitable when battery lifetime needed protection, as it balanced the revenue with degradation.

Comparison of MPC and GA

Having analyzed the results for both the MPC and GA approaches individually, the next step was to compare the results. Analyzing the scenarios for which only primary usage was allowed can be used to assess how well the codes align and will therefore be the starting point of this comparison.

Focusing on January 1st in Tables 4.1 and 4.2 clearly shows how the MPC and GA codes produce the same results. For spring, this statement is no longer true. For spring, summer, and fall, the only parameter being the same is electricity cost. The remaining parameters are all larger for when MPC has been used. Factors contributing to this difference will be discussed later in this chapter.

The numbers start to differ even more when analyzing the results produced by MPC and GA for Use Case 1 and 2. While the numbers are largely different, see the highest relative savings for Use Case 1 below, the total trend and relation between different combinations are largely the same. Analyzing only Use Case 1, an interesting observation can be made. Although the GA code results in the highest relative saving of nearly 1200 %, compared to the MPCs highest relative saving of 200 %, the GA code is also the only approach of the two that ever results in negative savings. Negative savings also occur when using the GA code for Use Case 2. This indicates that the GA solver is somehow less reliable compared to the MPC code. However, although it is less reliable, the data produced in this study indicates that the GA code results in larger overall savings compared to the MPC code. The average savings for using MPC and GA for both Use Case 1 and 2 are presented in Table 5.1 below.

Table 5.1: Average absolute saving for Use Case 1 and 2, using MPC and GA.

	Case 1 (MPC)	Case 1 (GA)	Case 2 (MPC)	Case 2 (GA)
Average Savings	6.14	11.5	4.5	4.77

Based on the cost function, it is known that savings can be achieved in one of two ways. Firstly, revenue can be increased, and secondly, degradation cost can be decreased. Both these changes result in an increase in the total savings. Up until this point, only savings have been compared for the different scenarios, use cases, and solvers. Therefore, it is currently impossible to draw any conclusions about whether certain scenarios focus more on increasing revenue or lowering degradation costs. To address this, additional plots considering both these contributions will be made. The two contributions will be compared to the reference case, which only allows for primary usage, and the difference in revenue and degradation cost is what will be analyzed.

In Figure 5.2 the difference in revenue and degradation cost, compared to the reference case, which only allows for primary usage, is illustrated. The green dots represent the optimal solutions found using GA while the blue dots are representing the optimal solutions found using MPC. The included red line marks the boundary separating the area where savings are positive (above the curve) from where savings are negative (below the curve). The average values are also represented in Figure 5.2 as squares, where the red is for GA and the yellow is for MPC.

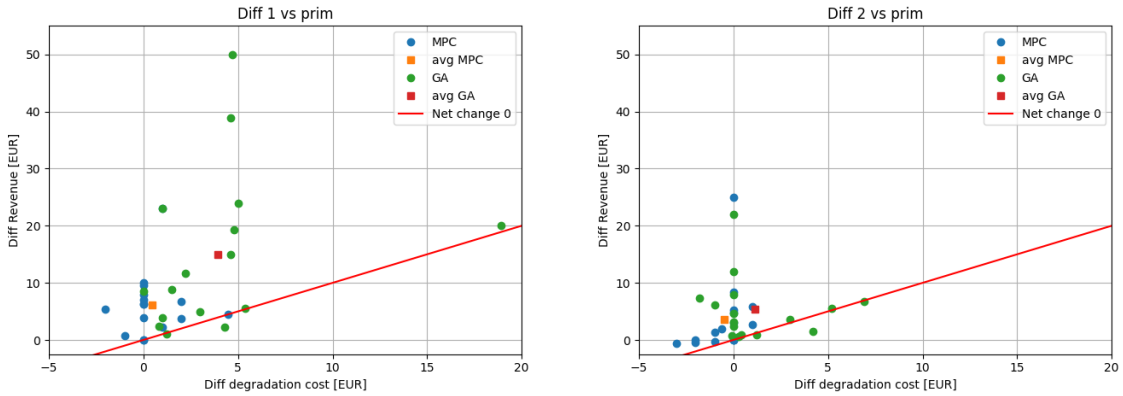

(a) Difference in revenue and degradation cost for both MPC and GA when applying Use Case 1.

(b) Difference in revenue and degradation cost for both MPC and GA when applying Use Case 1.

Figure 5.2: The difference in revenue and difference in degradation cost for each daily simulation using both MPC and GA.

Analyzing Figure 5.2, starting with Use Case 1, it is clear that GA finds solutions with much higher revenue, but also much higher degradation cost, compared to the MPC. As seen in the color maps 4.15 - 4.21, in the result section, also Figure 5.2a successfully illustrates the occurrence of negative savings. These are the dots found below the red line. Comparing Figure 5.2a with Figure 5.2b it can be seen that the

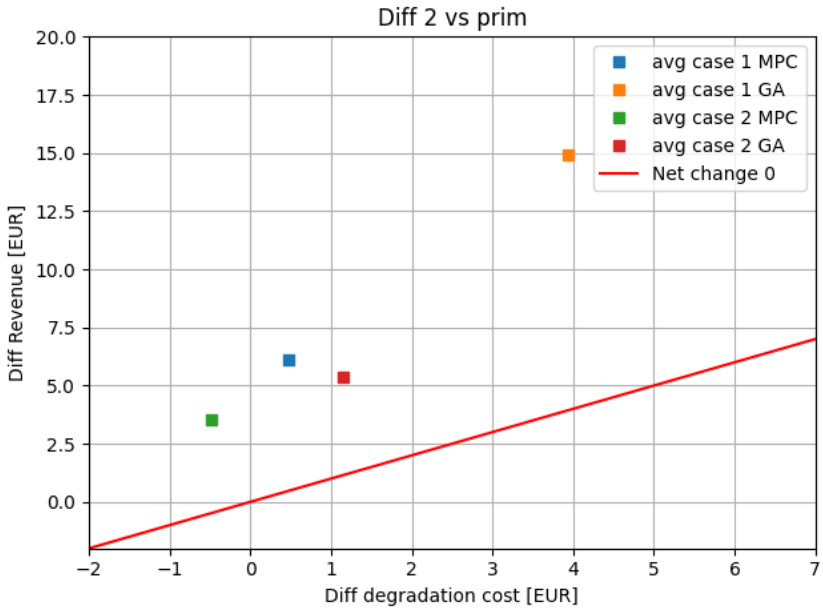

Figure 5.3: The average for each combination of Use case and solver algorithm.

effect of implementing the additional degradation constraint found for Case 2 has a much larger effect on the GA than the MPC. This is what to except knowing that the MPC never reaches very high degradation costs even for implementing Use Case 1. When doing a more general comparison between Use Case 1 and 2 it is logical to compare the average values depicted as squares. In order to do so all other dots can be removed and one obtains Figure 5.3.

It is clear that the most revenue is obtained using GA as a solver and implementing Use Case 1. On the other hand, it is the same combination that on average results in the highest degradation cost. Some further observations that can be made are that applying MC as a solver and implementing Use Case 2 the degradation cost has assumed a negative value. This corresponds to lower degradation than for only primary usage. This is is what to expect from Use Case 2, since the additional short term constraint is set to limit the degradation to that of the primary usage. The degradation for Use Case 2 should therefore never be higher than the degradation for primary usage. It is therefore more unexpected to see that the GA for Use Case 2 actually breaks this limit by having a positive degradation cost difference. This can be explained by the soft constraints used for the GA. Lastly, it can be mentioned that if the average revenue is subtracted with the difference in degradation cost, each of the averages in Table 5.1 are recovered.

Although differences can be found for the MPC and GA, it is both difficult and somewhat unjustified to reach conclusions based on these differences. This is based on the fact that the MPC code and GA code used in this thesis have subtle, yet vital differences. These differences make the codes non-equivalent in their structure and can therefore not be compared directly without obtaining some slight differences. These differences are explained in the following subsection.

Structure differences between MPC and GA

The comparison between MPC and GA can not really be done one to one, simply because the constructed codes have subtle differences that will affect the results obtained.

The first difference between the MPC and GA is that the GA always assumes the simulation start to be the first hour of 2024. Implementing B2G at a later time is done by specifying that only primary usage is allowed up until the start time of B2G. All primary usage conducted before the B2G start contributes to increasing the current throughput. Hence, a larger current throughput is used for any simulations done later than the first primary usage occurrence. Higher current throughput lowers the degradation derivative, hence resulting in less degradation for later simulations that use a larger current throughput as input value.

For the MPC code the simulation start can be changed, depending on simulation specification. Therefore, in producing the results for Use Case 1 and Use Case 2 the simulation start was set to the same day. By doing so the initial current throughput was always kept equal to the default value given in Table 3.7. The simulation start time also differs within the days between the MPC and GA code. The MPC starts at midnight or the first departure hour, while the GA starts at either midnight or the first docking hour. This difference in start time results in different data sets being used for the optimization. Another difference between the two codes is that the MPC code uses a receding horizon approach of different lengths, whereas the GA code has a fixed horizon of 24 hours. Exploiting different horizons results in different data sets being used. Both these last differences only change which data sets are being used This should not result in any global difference in profitability between the MPC and GA, however it will slightly change what the optimal solution is for the different scenarios.

To continue, the limitation applied in Use Case 2 is equal to the primary usage for a horizon of 24 hours. Therefore, it should only limit the upcoming 24 hours; however, this implementation was not done for the MPC code. Instead, it was applied on the MPC horizon regrdless of its length. This results in too strict degradation limits for horizons with a length longer than 24 hours and too easy for those shorter than 24 hours. The total effect should therefore be roughly correct; however, this is something that potentially could be corrected in future work.

While MPC only applies the first control sequence and iterates forward one hour, the GA code solves one optimization problem each day and applies the found solution directly. This essentially means that each day is treated separately when using the GA. Finally, it should be mentioned again that the battery specifications implemented in the MPC and GA codes are slightly different and will therefore contribute to the overall difference between the two.

All the previous differences add up to changing the outcome between the GA and MPC. These differences make it difficult to reach accurate and correct conclusions.

It is also difficult to reach accurate conclusions based on sparse data, which all are based on input parameters with a varying nature.

5.4 Yearly simulations using MPC

In the final part of the result section, the results for longer simulations, using MPC, are presented. The data, in Table 4.7 indicates that a lower degradation factor results in a higher absolute saving. This is trivial since all the degradation factor does is scale the amount of degradation obtained for any given usage profile. The savings, expressed as percentage, do not explicitly decrease for a higher degradation factor. However, this follows from the fact that the primary cost, which acts as the denominator when calculating the percentage, also increases as the degradation factor grows.

More interesting than comparing the results for different degradation factors is the difference between the approaches used in Use Case 1 and 2. Namely, the difference between having unlimited degradation for all iterations where secondary usage is allowed versus the case where the degradation is limited for its next 24 hours. Based on the numbers presented in Table 4.7 one can see that the savings are always higher for the unlimited degradation approach (Use Case 1). Having no scaling gives a relative saving of 280 % for unlimited hourly degradation, while it goes down slightly to 260 % for the limited hourly degradation. Both of these are above the 100 % limit, which means that both approaches not only save money but actually earn money for the boat user.

The difference between the two approaches and why the short term limited degradation approach (Use Case 2) is slightly less cost effective can be explained by the nondynamic nature of the limited approach. The problem with limiting degradation over the next 24 hours is that some optimal solutions might have a lower degradation than that of the primary usage case. Having less degradation for these intervals should create the opportunity of allowing higher degradation for other iterations and/or intervals. However, this dynamic change in hourly degradation limit is not implemented in the MPC code used in this thesis. The code in question is always forcing the degradation to be less than that of the fixed degradation limit. The surplus of allowed degradation will therefore never be exploited; instead, it will accumulate and result in too high capacity at the end of the warranty period.

Even if a dynamic correction of the allowed degradation were to be implemented in Use Case 2, Use Case 1 would still result in more savings for the simulations conducted. This comes from the fact that neither Use Case 1 nor Use Case 2 results in a final degradation of 0.2, see Table 4.7. The reason why this observation directly indicates that Use Case 1 would have been more profitable than Use Case 2 is because of the solution domains for the two cases. This was described more in detail in the MPC part of subsection 4.2.2. Having the larger solution domain, such as for Use Case 1, should always result in a better or as good solution as Use Case 2 with a smaller solution domain. This is because Use Case 1 always should be able

to find the best solution for Use Case 2 however, it could also potentially find an even better solution in the domain part that is not reached with Use Case 2. Using this argument and analyzing a longer time interval, see Table 4.7, it becomes clear that Use Case 1 not only produces the most savings short term but also long term. This is true all the way up until the utilized MPC code sends out that no more B2G can be applied. This output is obtained when the code calculates that the obtained EOL, allowing for only primary usage, is the same length as the warranty time. This output is never obtained in the simulations conducted in this thesis. This is easily seen by knowing that the degradation limit is set to 0.2 and the maximum degradation obtained in Table 4.7 only ever reaches 0.17. Having an end degradation lower than that of the degradation limit implies that the breaking point, where Use Case 1 goes from being unlimited to limited, never is reached.

Never having this transition of the degradation limit results in Use Case 1 being able to always search for the optimal solution in the larger solution domain. If the breaking point were reached in Use Case 1 the solution domain would shrink and the maximum degradation allowed would be the same as that of primary usage. This essentially means that at this breaking point, Use Case 1 would be converted into Use Case 2 until the EOL. This last statement is not entirely true since the code might find a solution where the degradation becomes lower than that of the primary usage. Therefore, during the next iteration, the code may determine that the expected EOL is longer than the warranty period and would therefore let the solution pool expand to its nominal size again.

In this specific scenario, where the additional degradation limit in Use Case 2 is set to be exactly the same as that of the primary usage, one quickly realizes that Use Case 2 would never gain savings on Use Case 1 even after the breaking point. However, this would change if the additional constraint, in Use Case 2, allowed for more degradation than that of degradation from only primary usage. Then after the breaking point for Use Case 1 the allowed degradation would indeed be lower than that for Use Case 2. This dynamic and comparison between the two cases are illustrated in Figure 5.4 below. In Figure 5.4 the lower graph represent the hypothetical scenario of using Use Case 1 while the top graph represent Use Case 2. For Use Case 1, high degradation is allowed in the beginning, however after some time the break point is reached and no additional degradation is longer allowed. From here on forward the degradation limit is that of the primary usage. For Use Case 2, the degradation is less in the beginning compared to Use Case 1 however, that decrease in early degradation results in the possibility to degrading the battery for a longer time. Desirably for the remaining part of the battery life time.

From the above graph it also becomes clear why the additional degradation constraint in Use Case 2 has to allow for more degradation than the primary usage level. Having the primary usage degradation as the limit essentially results in the exact same early profile as in Figure 5.4. However, having a limit equal to that of the primary usage would result in the top graph, representing Use Case 2, to have almost exactly the same derivative as that of the lower graph, representing Use Case 1. Having the same derivative after the breaking point implies that the final degra-

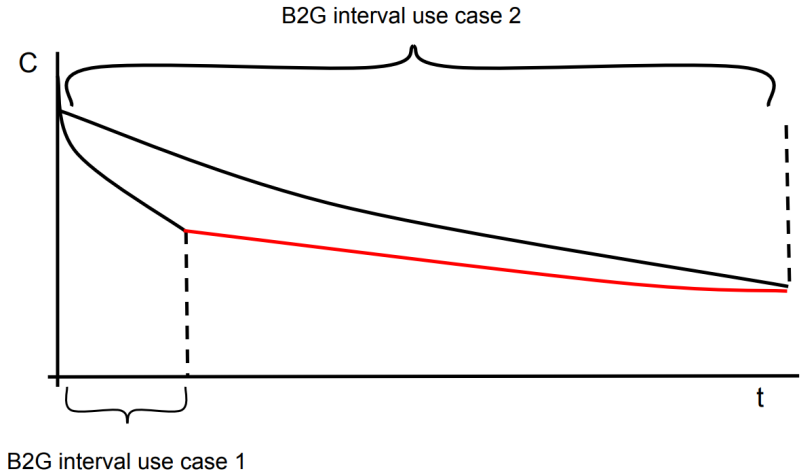

Figure 5.4: An illustration of Use Case 1 and Use Case 2, for when the additional short term constraint is higher than that of the primary usage close to the EOL.

dation of Use Case 2 never reaches that of Use Case 1, which at the EOL should be the same as the degradation limit. This means that Use Case 2 could allow for more degradation and in doing so, expand the solution domain, which, as we know from previous sections, can improve the profitability.

Instead of having the degradation limit to be the same as for only primary usage, the limit should be given a value calculated based on the warranty time and degradation limit. This would result in the degradation being limited throughout the battery lifetime. However, compared to Use Case 1, which is limited by primary usage after the breaking point, the degradation limit should be slightly higher for Use Case 2. This would enable Use Case 2 to achieve greater savings compared to Use Case 1 toward the end of the battery lifetime. Converting Use Case 2 and its additional constraint in this way is only possible if the total primary usage degradation is lower than the total degradation limit.

6
Conclusion

This thesis focused on the optimal charging strategy of boat batteries under the Boat-to-Grid (B2G). The goal was to meet the primary usage power demand of the boat while maximizing revenue and ensuring battery lifetime. To achieve this, two different optimization models were developed. These models took into account several key factors, including battery chemistry, electricity price, usage behavior, environmental conditions, and the characteristics of grid services.

In terms of methodology, the system boundaries were first defined. Two typical battery chemistries, LFP and NCA, were selected as study cases. Based on their characteristics, suitable SoC operating ranges and degradation models were chosen and validated. Two geographical locations, Gothenburg and Luleå, were chosen, and seasonal daily usage profiles were designed to simulate typical boat operation patterns. The requirements and regulations for participating in grid services in Sweden were also studied. Two optimization frameworks were implemented: the first is based on Model Predictive Control (MPC), using IPOPT as the solver and battery current as the control variable to maximize daily revenue under constraints; the second is based on a Genetic Algorithm (GA), using the DEAP library, with charging/discharging power as the variable to minimize daily cost.

The results showed that the optimization tools were able to generate effective charging and discharging strategies under various usage scenarios. It enabled profit generation while keeping battery degradation within acceptable limits. Even when aging was strictly limited, the battery could still participate in grid services and provide economic value. This showed that B2G strategies could be both practical and profitable, as long as the appropriate aging control methods were implemented. The tool achieved a good balance between maximizing revenue and preserving battery health, making it valuable for real-world marine applications. This study also succeeds in proving that not only can revenue be increased with an optimizer, but degradation can also be reduced. This is clearly seen in Figure 5.3 where the green square representing Use Case 2 and MPC lowers the degradation to a level lower than for only primary usage. Finally, this thesis has provided results indicating that both MPC and GA can be used to optimize the current profile for B2G applications.

7
Future Work

Although this study has achieved multiple results, the thesis leaves room for plenty of future work. First, the usage profiles used are manually designed and may not fully reflect real boat operating conditions. Incorporating real world operation data can be used to improve the accuracy of usage profiles, hence improving the final B2G results.

Second, the degradation models used in this study are based on literature roughly ten years old. Developing more accurate and modern degradation models is essential to accurately represent the degradation of newer batteries.

Third, this study only considered LFP and NCA chemistries. Including additional battery chemistries would expand the understanding of which battery chemistries that have have the greatest potential for B2G applications.

Fourth, in the current model, frequency deviation is assumed to be known in advance, which is a simplification. In reality, frequency deviation is instantaneous and unpredictable. Future work should consider adding predictions based on statistics to improve the decision making of when it is reasonable to apply B2G. This would take the simulation tools one step closer to being a working online tool that can be used in reel boats.

Fifth, in addition to frequency containment reserve, other grid services with different characteristics and requirements can be explored to evaluate their suitability and profitability for marine B2G applications. In addition, some other locations should be tested to better understand for what climates and energy markets B2G is most suitable.

In future projects, it could be interesting to try different algorithms and solvers. One optimization method that should be investigated is reinforcement learning, which might be able to solve for more complex environments and improve solver performance.

Finally, perhaps the most important change to enforce in future works is to minimize or eliminate the differences between the two utilized codes. This includes implementing a receding horizon for GA and changing the simulation start time. It also includes having the same specifics for the battery cells and the same horizon length.

More specific scenarios that could add value to this investigation would be to replace the degradation limit used for Use case 2. Instead of defining the limit based on primary usage, it should rather be calculated based on the warranty period itself. Such a limit could potentially be calculated based on Equation (7.1).

$$deg_t^h = k \cdot h \cdot \frac{deg^{lim}}{t_{war}} \tag{7.1}$$

The h represents the length of the current receding horizon, while deg^{lim} and t_{war} represent the overall degradation limit and the warranty period respectively. As a consequence, the fraction represents the highest allowed degradation, ensuring an EOL longer than that of the warranty period. The last parameter k is a season dependent constant, allowing for different degradation limits for each season. This could be implemented for applications that require higher degradation during certain seasons. The only requirement for k should be that the average value of k is 1. An average value greater than one would result in an excessively high degradation allowance, while an average value that is too low would lead to an too low degradation allowance.

Implementing this limit would eliminate the risk of the battery being over exploited in the beginning of its lifetime. Moreover, this ensures a more continues revenue stream, while keeping the battery performance higher. The second part is something that does not really affect the total calculations, however a rapid performance decline might concern costumers. If the imposed limit turns out to be unreachable the code should set the new degradation limit to that of the primary usage, just as in Use case 2 in this study. This ensures that the primary usage always works as a solution and should therefore prevent the solver from ever failing.

Bibliography

[1] IMO, "2023 imo strategy on reduction of ghg emissions from ships." https://www.imo.org/en/OurWork/Environment/Pages/2023-IMO-Strategy-on-Reduction-of-GHG-Emissions-from-Ships.aspx, 2023. [Accessed: May 2, 2025].

[2] MarketsandMarkets, "Electric ships market by type, system, mode of operation, power, range, ship type and region – global forecast to 2030." https://www.marketsandmarkets.com/Market-Reports/electric-ships-market-167955093.html, 2023. [Accessed: May 15, 2025].

[3] International Energy Agency, "Renewable integration – analysis." https://www.iea.org/energy-system/electricity/renewable-integration, 2024. [Accessed: May 15, 2025].

[4] D.-I. Stroe, M. Swierczynski, A.-I. Stroe, R. Teodorescu, R. Laerke, and P. Kjaer, "Degradation behaviour of lithium-ion batteries based on field measured frequency regulation mission profile," in *2015 IEEE Energy Conversion Congress and Exposition (ECCE)*, pp. 14–21, IEEE, 2015.

[5] M. Romare and L. Dahllöf, "The life cycle energy consumption and greenhouse gas emissions from lithium-ion batteries," Tech. Rep. C 243, Swedish Energy Agency (Energimyndigheten), 2017. [Accessed: May 28, 2025].

[6] R. B. Roy, S. Alahakoon, and S. Jayasinghe, "Microgrid and fleet to grid operation of a hybrid electric ferry," in *2021 Australasian Universities Power Engineering Conference (AUPEC)*, pp. 1–6, 2021.

[7] R. B. Roy, S. Alahakoon, P. J. V. Rensburg, and S. J. Arachchillage, "Impact analysis on distribution network due to coordinated electric ferry charging," *IET Energy Systems Integration*, Aug. 2024. First published: 28 August 2024.

[8] G. Pintér, A. Vincze, N. Baranyai, and H. Zsiborács, "Boat-to-grid electrical energy storage potentials around the largest lake in central europe," *Applied Sciences*, vol. 11, no. 16, p. 7178, 2021.

[9] E. K. Johansson and S. Petersson, "Exploring future boat-to-grid revenue streams, battery health and capacity in sweden," master's thesis, KTH Royal Institute of Technology, 2024.

[10] J. Wang, P. Liu, J. Hicks-Garner, E. Sherman, S. Soukiazian, M. Verbrugge, H. Tataria, J. Musser, and P. Finamore, "Cycle-life model for graphite-lifepo4 cells," *Journal of power sources*, vol. 196, no. 8, pp. 3942–3948, 2011.

[11] D. Wang, J. Coignard, T. Zeng, C. Zhang, and S. Saxena, "Quantifying electric vehicle battery degradation from driving vs. vehicle-to-grid services," *Journal of Power Sources*, vol. 332, pp. 193–203, 2016.

[12] S. Han, S. Han, and K. Sezaki, "Economic assessment on v2g frequency regulation regarding the battery degradation," in *2012 IEEE PES Innovative Smart Grid Technologies (ISGT)*, pp. 1–8, 2012.

[13] G. Plett, "Chapter 1 - battery boot camp," in *Battery Management Systems, Volume I: Battery Modeling*, pp. 1–28, Artech House, first edition ed., 2015.

[14] T. F. Fuller and J. N. Harb, *Electrochemical engineering*. Hoboken, N.J: Wiley, 1st edition ed., 2018 - 2018.

[15] T. F. Fuller and J. N. Harb, "Cell potential and thermodynamics," in *Electrochemical Engineering*, pp. 1–1, United States: John Wiley & Sons, 2018.

[16] J. N. Harb and T. F. Fuller, "Appendix a: Electrochemical reactions and standard potentials," in *Electrochemical Engineering*, United States: John Wiley & Sons, Incorporated, 2018.

[17] M. A. Syed, M. Salehabadi, and M. Obrovac, "High energy density large particle lifepo4," *Chemistry of Materials*, vol. 36, no. 2, pp. 803–814, 2024.

[18] J. Li, J. Fleetwood, W. B. Hawley, and W. Kays, "From materials to cell: state-of-the-art and prospective technologies for lithium-ion battery electrode processing," *Chemical Reviews*, vol. 122, no. 1, pp. 903–956, 2021.

[19] M. Li, J. Lu, Z. Chen, and K. Amine, "30 years of lithium-ion batteries," *Advanced materials*, vol. 30, no. 33, p. 1800561, 2018.

[20] B. Ramasubramanian, S. Sundarrajan, V. Chellappan, M. Reddy, S. Ramakrishna, and K. Zaghib, "Recent development in carbon-lifepo4 cathodes for lithium-ion batteries: a mini review," *Batteries*, vol. 8, no. 10, p. 133, 2022.

[21] J. T. Warner, "Chapter 7 - lithium-ion and other cell chemistries," in *The Handbook of Lithium-Ion Battery Pack Design (Second Edition)* (J. T. Warner, ed.), pp. 125–158, Elsevier, second edition ed., 2024.

[22] F. El Kouihen, Z. Kharbouch, and A. Faik, "advancements in synthesis methods for nickel-rich nca cathode materials: optimizing synthesis conditions and their impact on electrochemical performances for next-generation lithium batteries," *Journal of The Electrochemical Society*, vol. 170, no. 10, p. 100520, 2023.

[23] C. M. Julien and A. Mauger, "Nca, ncm811, and the route to ni-richer lithium-ion batteries," *Energies*, vol. 13, no. 23, p. 6363, 2020.

[24] A. Maheshwari, "Modelling, aging and optimal operation of lithium-ion batteries," 2018.

[25] M. Swierczynski, D.-I. Stroe, A.-I. Stan, R. Teodorescu, and S. K. Kær, "Lifetime estimation of the nanophosphate $LiFePO_4$/C battery chemistry used in fully electric vehicles," *IEEE Transactions on Industry Applications*, vol. 51, no. 4, pp. 3453–3461, 2015.

[26] I. Baghdadi, O. Briat, J.-Y. Delétage, P. Gyan, and J.-M. Vinassa, "Lithium battery aging model based on dakin's degradation approach," *Journal of Power Sources*, vol. 325, pp. 273–285, 2016.

[27] M. Petit, E. Prada, and V. Sauvant-Moynot, "Development of an empirical aging model for li-ion batteries and application to assess the impact of vehicle-to-grid strategies on battery lifetime," *Applied Energy*, vol. 172, pp. 398–407, 2016.

[28] S. Dhundhara, M. Sharma, F. Guéniat, and Y. Arya, "Chapter 1 - overview of the renewable-dominated power systems and their frequency regulation issues,"

in *Advanced Frequency Regulation Strategies in Renewable-Dominated Power Systems* (S. Dhundhara, Y. Arya, and R. C. Bansal, eds.), pp. 1–19, Academic Press, 2024.

[29] A. D. Bank, *Handbook on Battery Energy Storage System*. Asian Development Bank, 2018.

[30] Svenska kraftnät, "Frequency stability." https://www.svk.se/en/stakeholders-portal/electricity-market/system-services/frequency-stability/, n.d. [Accessed: May 10, 2025].

[31] P. Kundur, J. Paserba, V. Ajjarapu, G. Andersson, A. Bose, C. Canizares, N. Hatziargyriou, D. Hill, A. Stankovic, C. Taylor, *et al.*, "Definition and classification of power system stability ieee/cigre joint task force on stability terms and definitions," *IEEE transactions on Power Systems*, vol. 19, no. 3, pp. 1387–1401, 2004.

[32] C. Zhao, S. Hashemi, P. B. Andersen, and C. Træholt, "Data-driven state of health modeling of battery energy storage systems providing grid services," in *2021 11th International Conference on Power, Energy and Electrical Engineering (CPEEE)*, pp. 43–49, 2021.

[33] C. Zhao, P. B. Andersen, C. Træholt, and S. Hashemi, "Grid-connected battery energy storage system: a review on application and integration," *Renewable and Sustainable Energy Reviews*, vol. 182, p. 113400, 2023.

[34] Fingrid, "Frequency quality analysis 2022." https://www.fingrid.fi/globalassets/dokumentit/fi/kantaverkko/suomen-sahkojarjestelma/frequency_quality_analysis_2022_public.pdf, 2023. [Accessed: May 11, 2025].

[35] Fingrid, "Part of the nordic power system." https://www.fingrid.fi/en/grid/development/part-of-the-nordic-power-system/, n.d. [Accessed: May 10, 2025].

[36] GridX, "What is a grid operator?." https://www.gridx.ai/knowledge/what-is-a-grid-operator, 2024. [Accessed: May 2, 2025].

[37] Svenska kraftnät, "Prequalification –provision of ancillary services." https://www.svk.se/en/stakeholders-portal/electricity-market/provision-of-ancillary-services/prequalification/, 2025. [Accessed: May 11, 2025].

[38] Svenska Kraftnät, "Fcr-n – frequency containment reserve for normal operation." https://www.svk.se/aktorsportalen/bidra-med-reserver/om-olika-reserver/fcr-n/, n.d. Accessed: 2025-05-11.

[39] Svenska kraftnät, "Is there a limit on the maximum fcr bid size?." https://www.svk.se/en/stakeholders-portal/electricity-market/provision-of-ancillary-services/questions-and-answers-about-reserves/fcr/is-there-a-limit-on-the-maximum-fcr-bid-size/, n.d. [Accessed: May 15, 2025].

[40] Fingrid, "Balancing energy and balancing capacity markets." https://www.fingrid.fi/en/electricity-market/reserves_and_balancing/balancing-energy-and-balancing-capacity-markets/, 2024. [Accessed: May 15, 2025].

[41] Svenska kraftnät, "Procurement and pricing of ancillary services." https://www.svk.se/en/stakeholders-portal/electricity-market/provision-of-ancillary-services/procurement-and-pricing-of-ancillary-services/, n.d. [Accessed: May 15, 2025].

[42] Fingrid, "The technical requirements and the prequalification process of frequency containment reserves (fcr)." https://www.fingrid.fi/globalassets/dokumentit/en/electricity-market/reserves/fcr-liite2---teknisten-vaatimusten-todentaminen-ja-hyvaksyttamisprosessi_en.pdf, 2023. [Accessed: May 16, 2025].

[43] E. F. Camacho and C. Bordons, "Introduction to model predictive control," in *Model Predictive control*, Advanced Textbooks in Control and Signal Processing, pp. 1–11, London: Springer London, 2007.

[44] CasADi, "Casadi." https://web.casadi.org/docs/#document-intro, 2023. [Accessed: May 19, 2025].

[45] J. H. Holland, *Adaptation in Natural and Artificial Systems*. Ann Arbor, MI: University of Michigan Press, 1975.

[46] F.-A. Fortin, F.-M. De Rainville, M.-A. Gardner, M. Parizeau, and C. Gagné, "Deap: Evolutionary algorithms made easy," *Journal of Machine Learning Research*, vol. 13, pp. 2171–2175, 2012.

[47] Fingrid, "Electricity Consumption and Production in Finland." https://data.fingrid.fi/en/datasets/206, 2024. [Accessed: May 16, 2025].

[48] Nordpool, "Day-ahead market." https://www.nordpoolgroup.com/en/the-power-market/Day-ahead-market, n.d. [Accessed: March 20, 2025].

[49] ENTSO-E, "Entso-e official website." https://www.entsoe.eu/, 2025. [Accessed: May 27, 2025].

[50] Swedish Meteorological and Hydrological Institute, "Smhi official website." https://www.smhi.se/, 2025. [Accessed: May 27, 2025].

[51] Fingrid, "Frequency containment reserve for normal operation, activated." https://data.fingrid.fi/en/datasets/123, n.d. [Accessed: May 16, 2025].

[52] Svenska kraftnät, "Fcr-mimer." https://mimer.svk.se/primaryregulation/primaryregulationindex, 2025. [Accessed: May 23, 2025].

A

Appendix A

A.1 GA

Use case 1

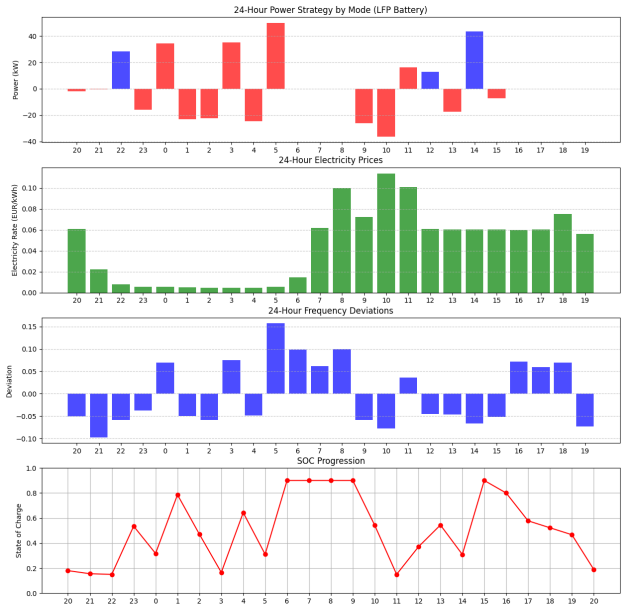

Figure A.1: Fall season optimization results using LFP battery in Gothenburg with high aging limit

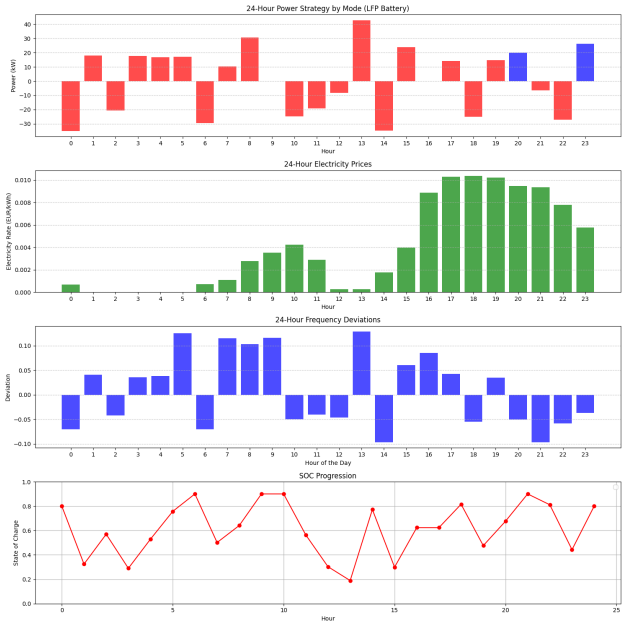

Figure A.2: Fall season optimization results using LFP battery in Luleå with high aging limit

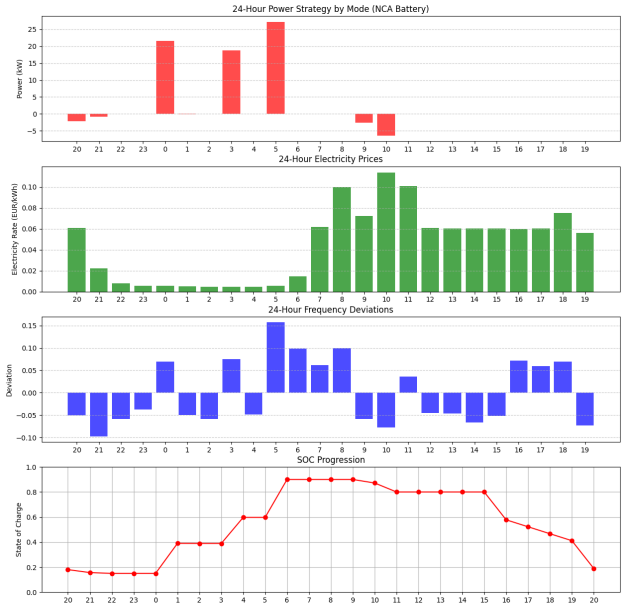

Figure A.3: Fall season optimization results using NCA battery in Gothenburg with high aging limit

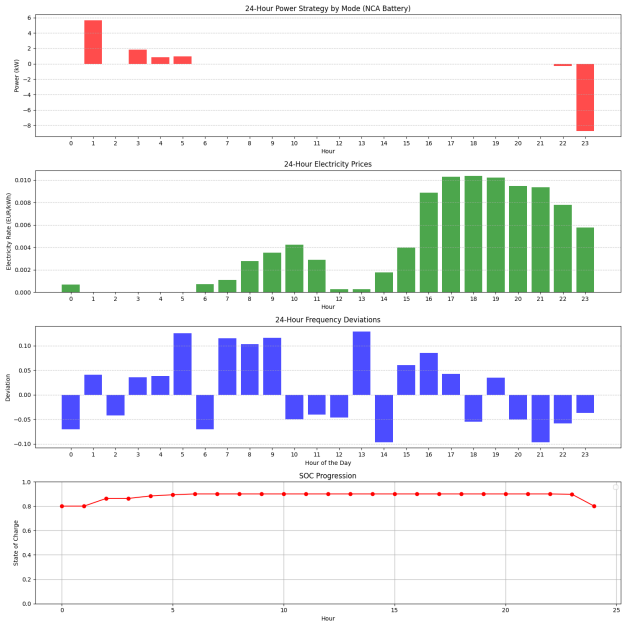

Figure A.4: Fall season optimization results using NCA battery in Luleå with high aging limit

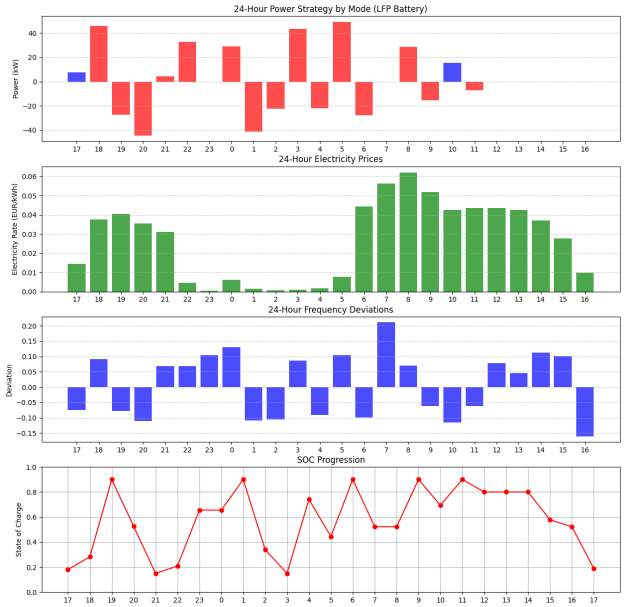

Figure A.5: Spring season optimization results using LFP battery in Gothenburg with high aging limit

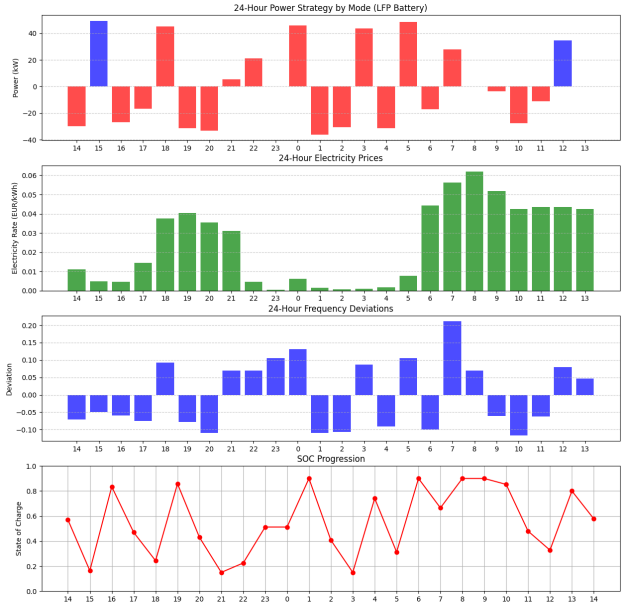

Figure A.6: Spring season optimization results using LFP battery in Luleå with high aging limit

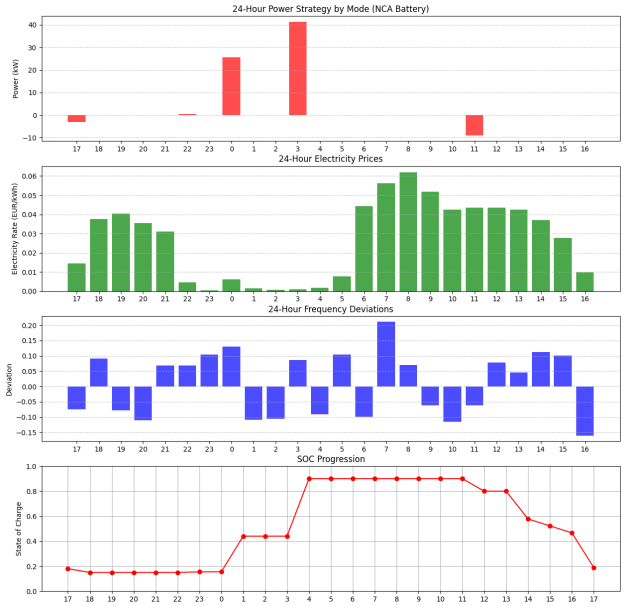

Figure A.7: Spring season optimization results using NCA battery in Gothenburg with high aging limit

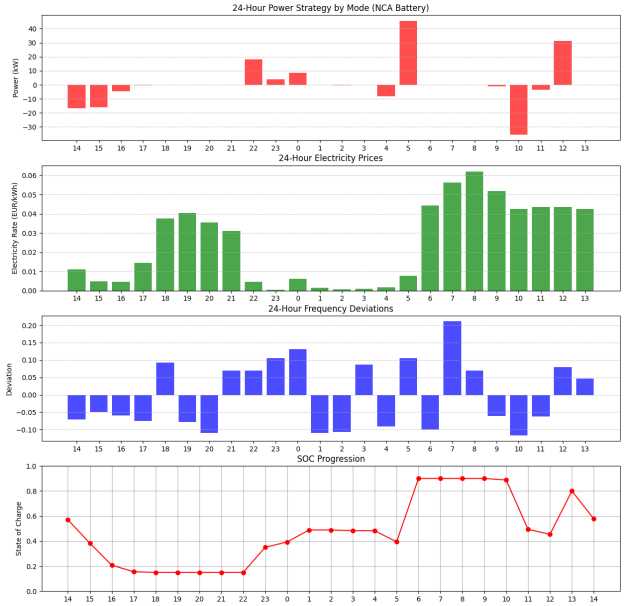

Figure A.8: Spring season optimization results using NCA battery in Luleå with high aging limit

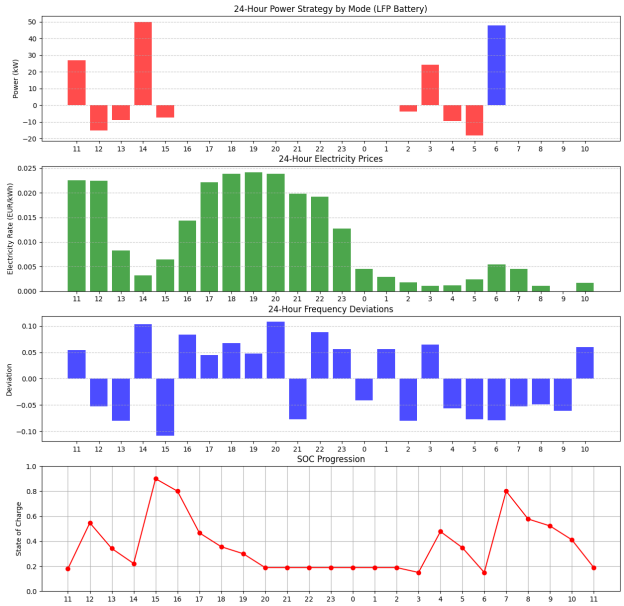

Figure A.9: Summer season optimization results using LFP battery in Gothenburg with high aging limit

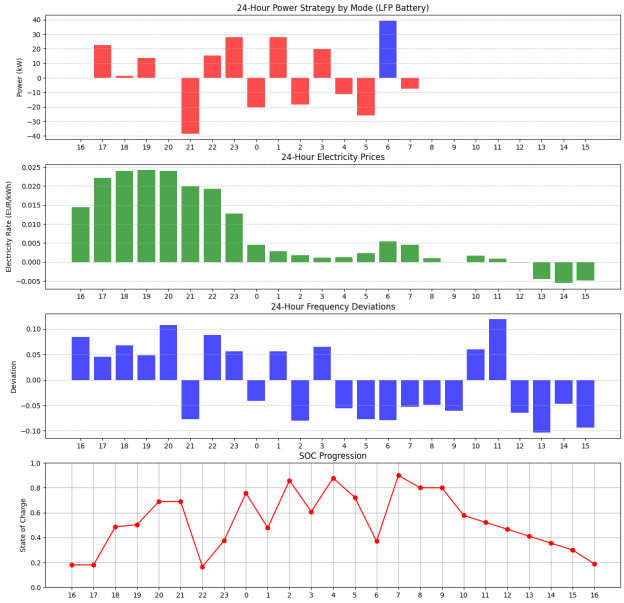

Figure A.10: Summer season optimization results using LFP battery in Luleå with high aging limit

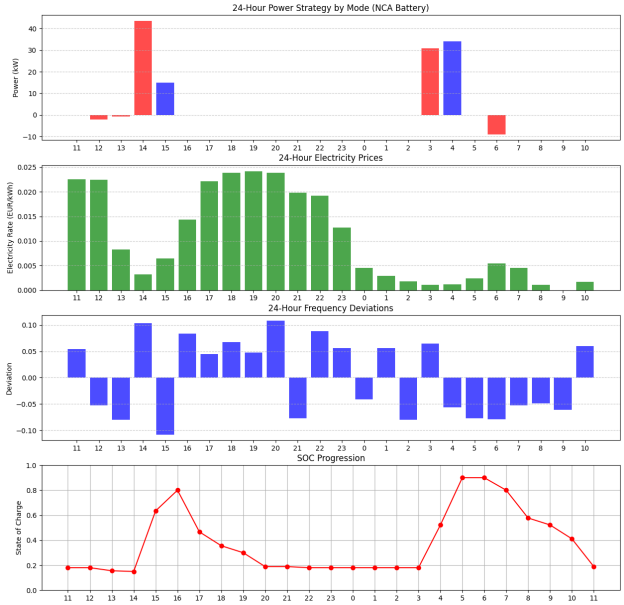

Figure A.11: Summer season optimization results using NCA battery in Gothenburg with high aging limit

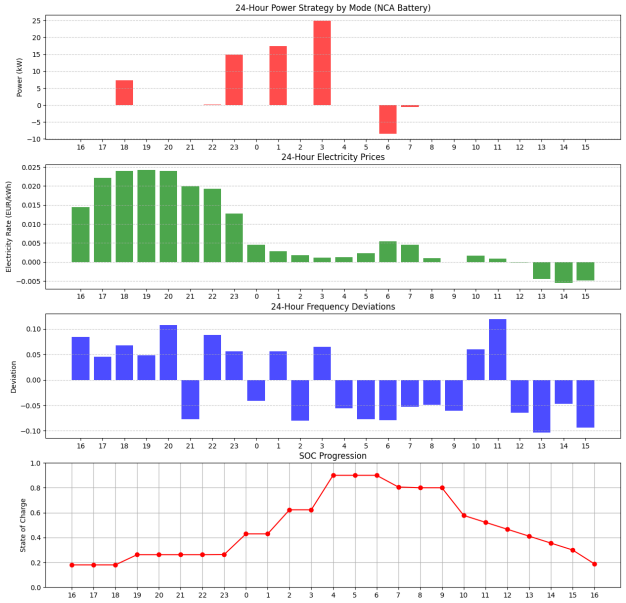

Figure A.12: Summer season optimization results using NCA battery in Luleå with high aging limit

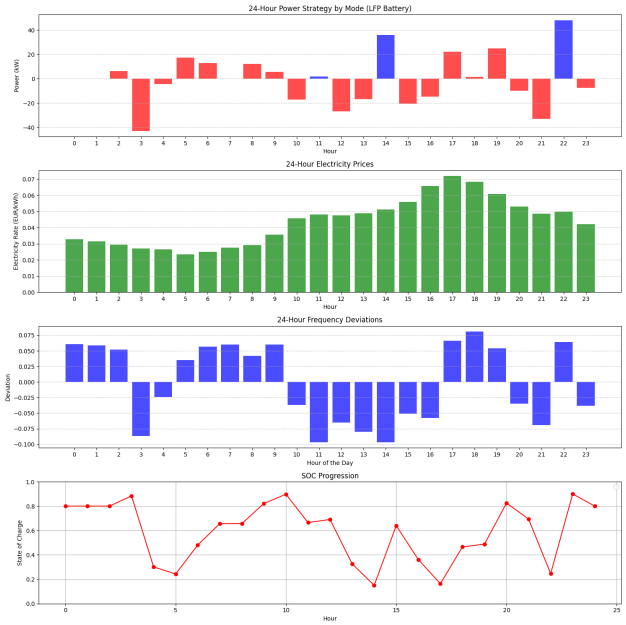

Figure A.13: Winter season optimization results using LFP battery in Gothenburg with high aging limit

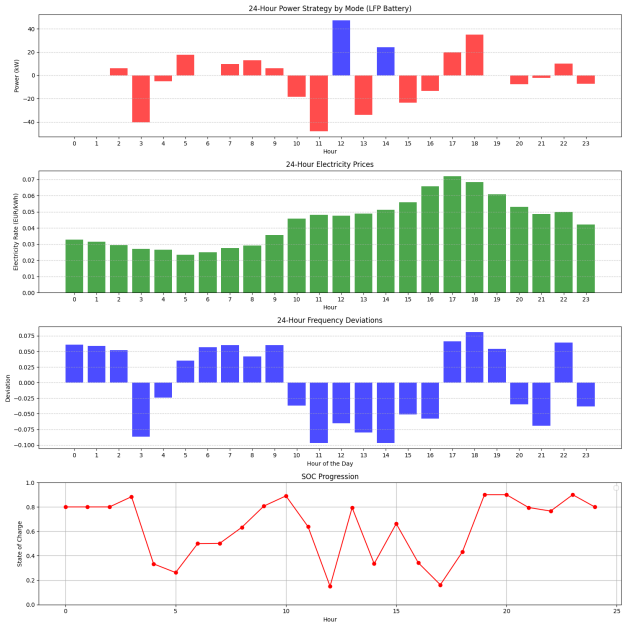

Figure A.14: Winter season optimization results using LFP battery in Luleå with high aging limit

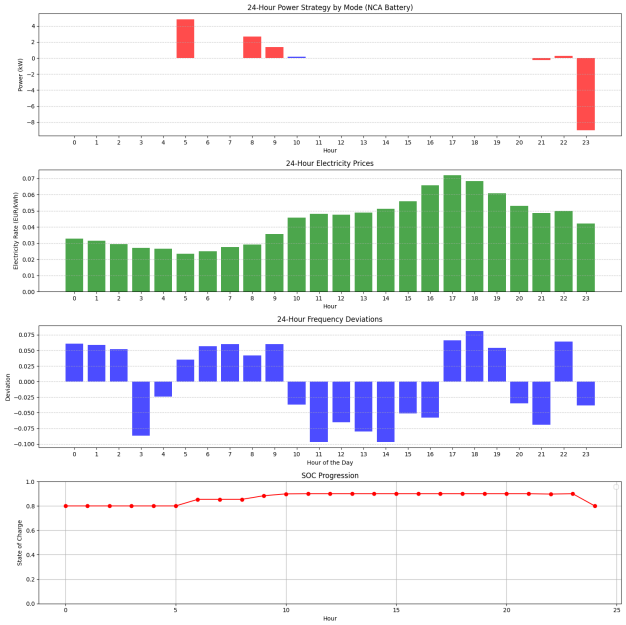

Figure A.15: Winter season optimization results using NCA battery in Gothenburg with high aging limit

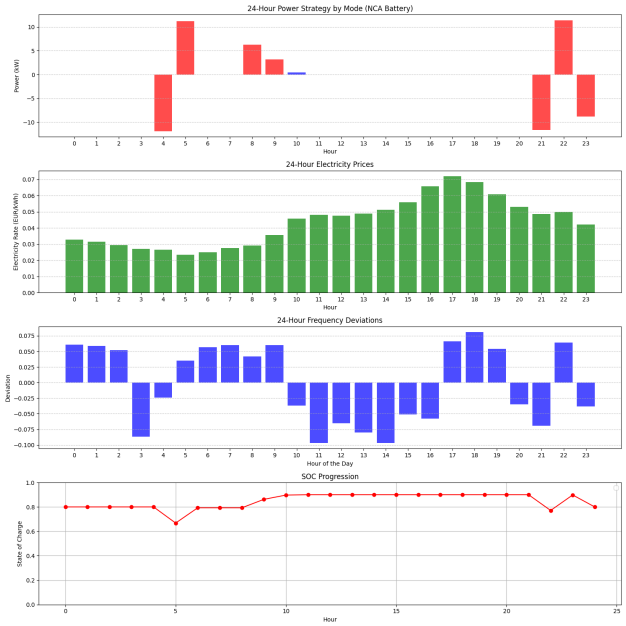

Figure A.16: Winter season optimization results using NCA battery in Luleå with high aging limit

Use case 2

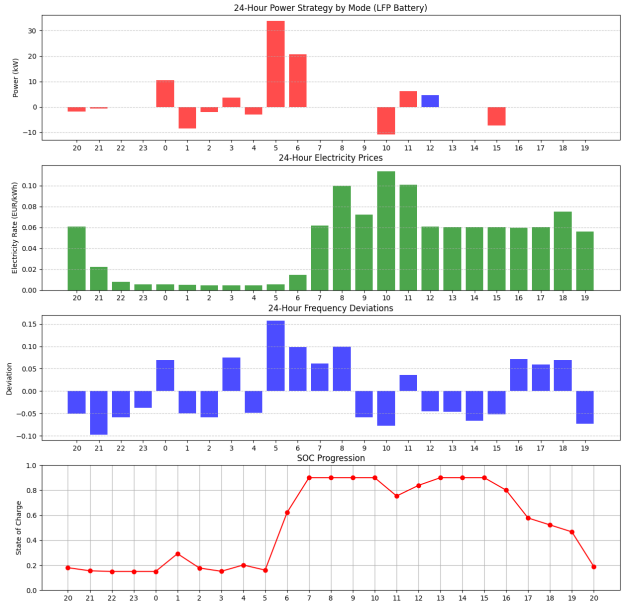

Figure A.17: Fall season optimization results using LFP battery in Gothenburg with primary usage aging limit

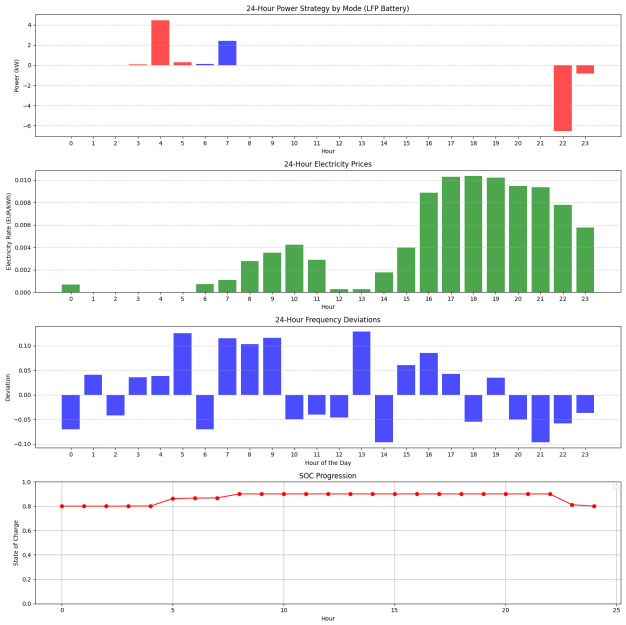

Figure A.18: Fall season optimization results using LFP battery in Luleå with primary usage aging

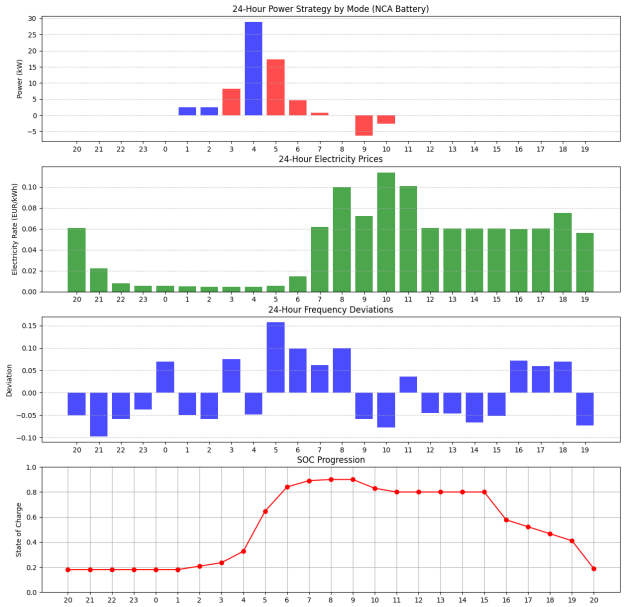

Figure A.19: Fall season optimization results using NCA battery in Gothenburg with primary usage aging limit

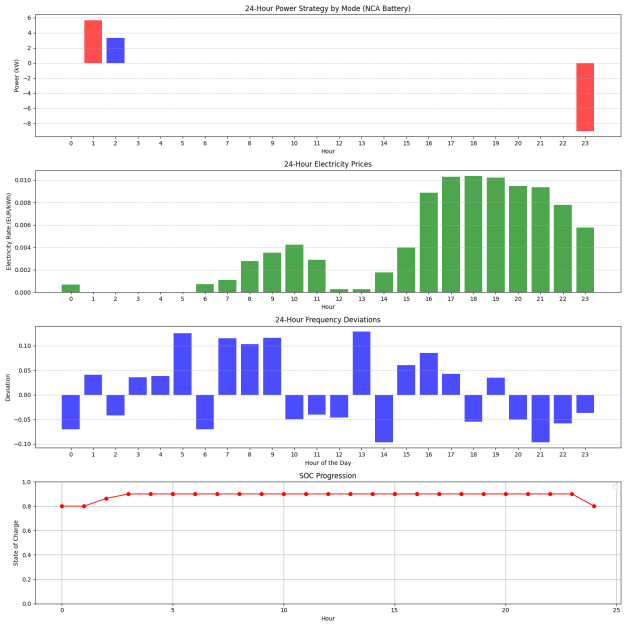

Figure A.20: Fall season optimization results using NCA battery in Luleå with primary usage aging limit

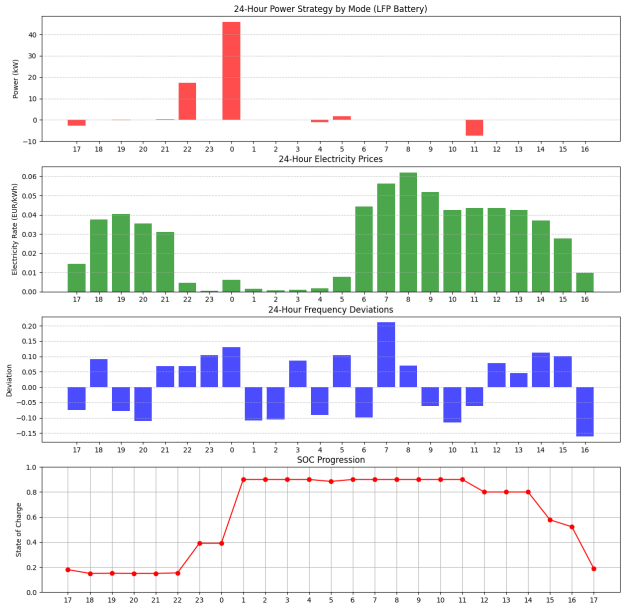

Figure A.21: Spring season optimization results using LFP battery in Gothenburg with primary usage aging limit

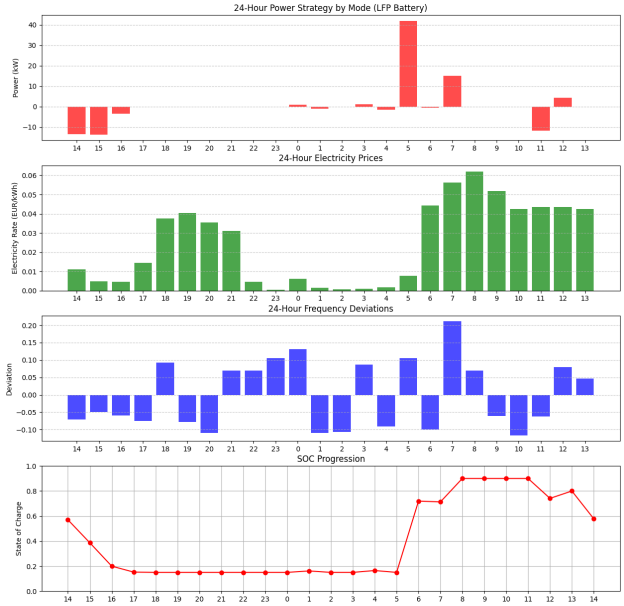

Figure A.22: Spring season optimization results using LFP battery in Luleå with primary usage aging limit

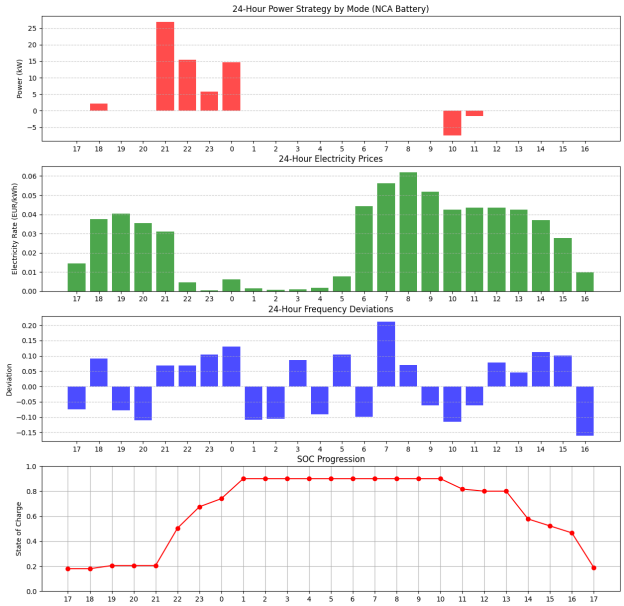

Figure A.23: Spring season optimization results using NCA battery in Gothenburg with primary usage aging limit

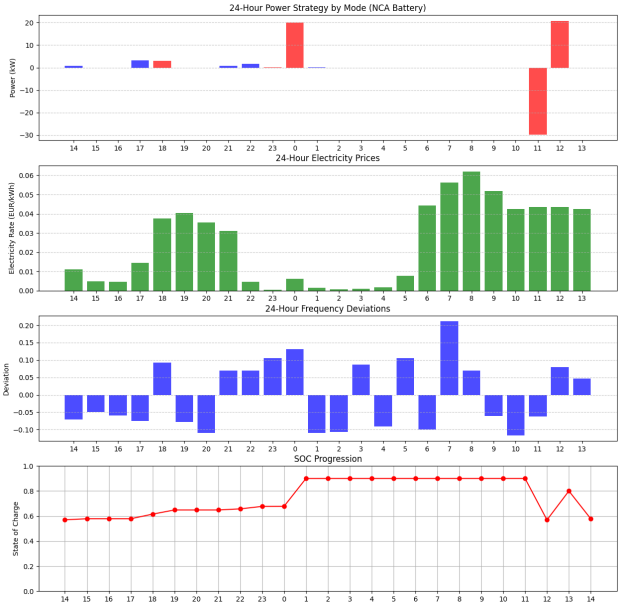

Figure A.24: Spring season optimization results using NCA battery in Luleå with primary usage aging limit

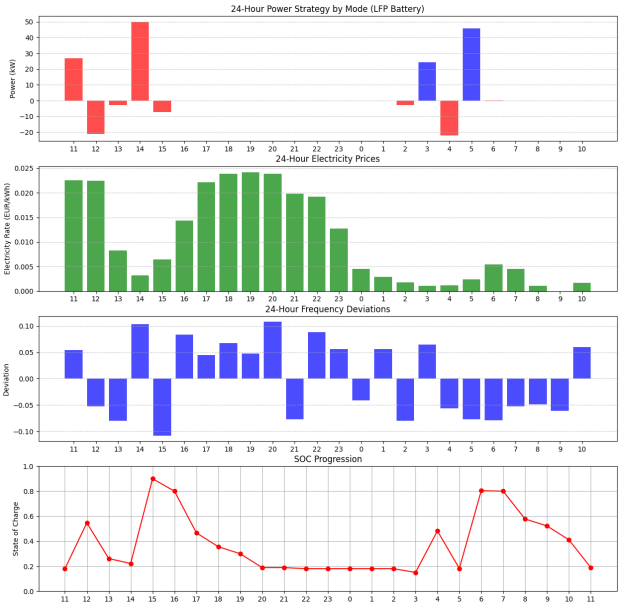

Figure A.25: Summer season optimization results using LFP battery in Gothenburg with primary usage aging limit

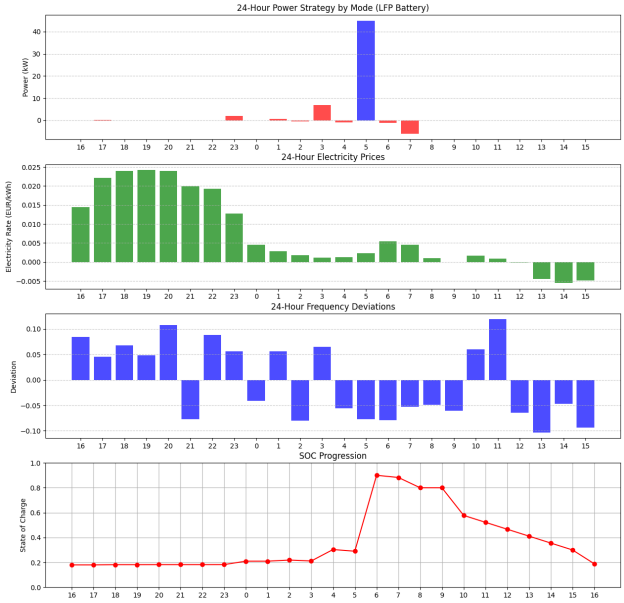

Figure A.26: Summer season optimization results using LFP battery in Luleå with primary usage aging limit

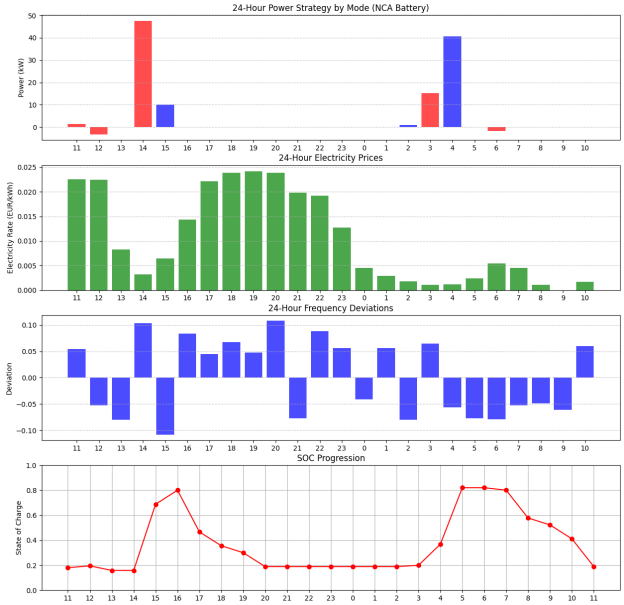

Figure A.27: Summer season optimization results using NCA battery in Gothenburg with primary usage aging limit

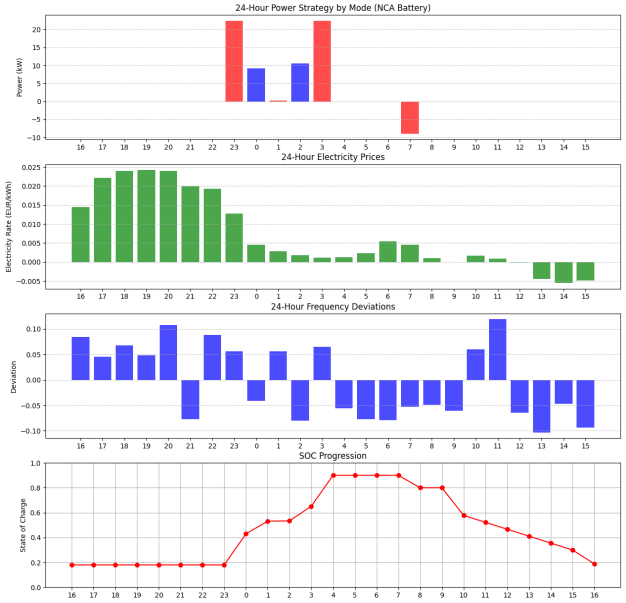

Figure A.28: Summer season optimization results using NCA battery in Luleå with primary usage aging limit

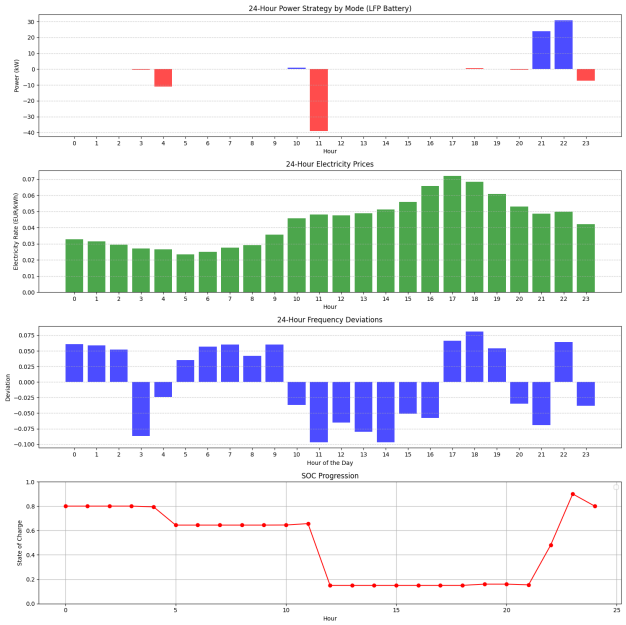

Figure A.29: Winter season optimization results using LFP battery in Gothenburg with primary usage aging limit

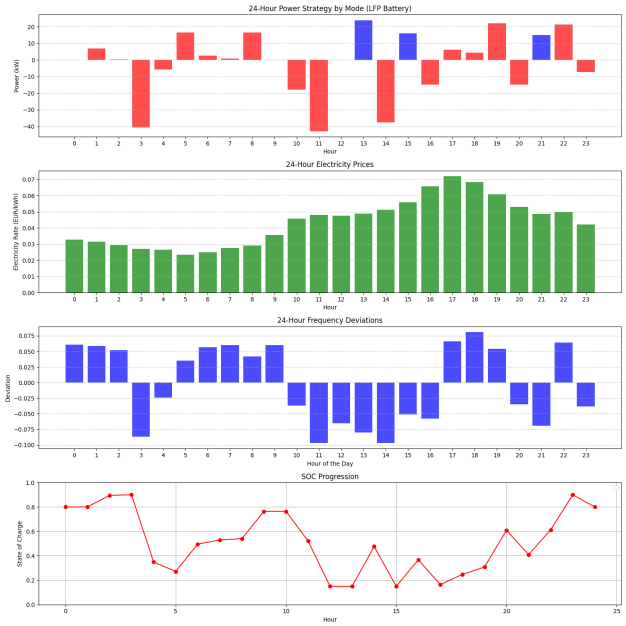

Figure A.30: Winter season optimization results using LFP battery in Luleå with primary usage aging limit

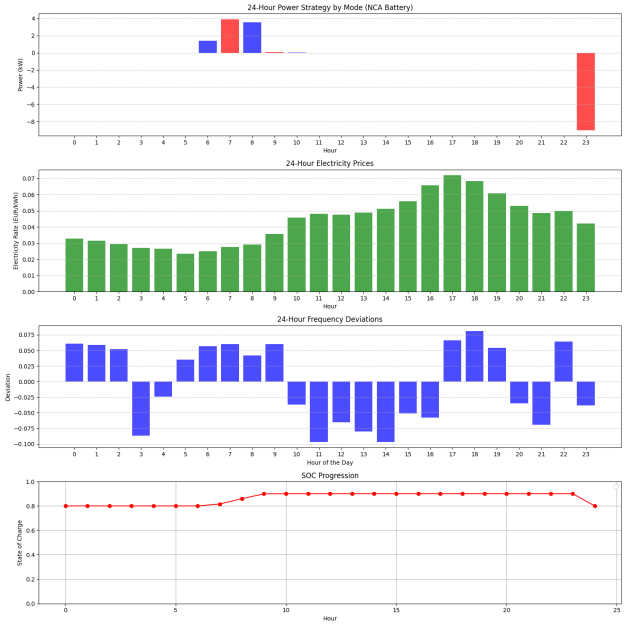

Figure A.31: Winter season optimization results using NCA battery in Gothenburg with primary usage aging limit

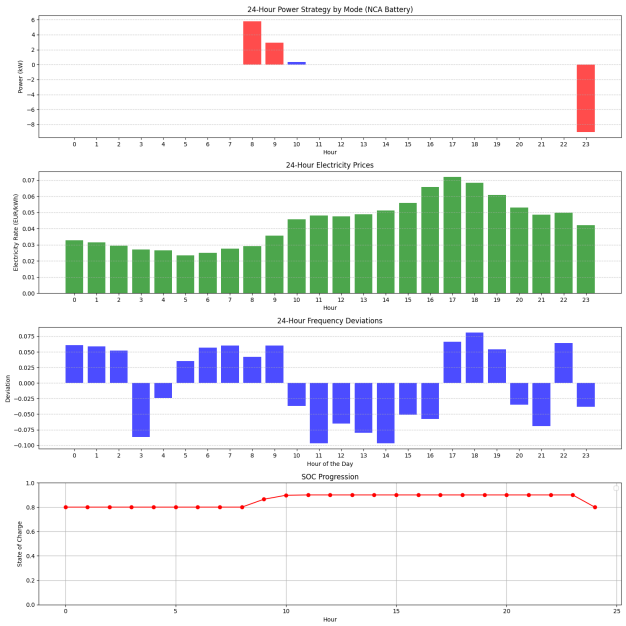

Figure A.32: Winter season optimization results using NCA battery in Luleå with primary usage aging limit

B

Appendix B

B.1 MPC

Daily runs

Use case 1

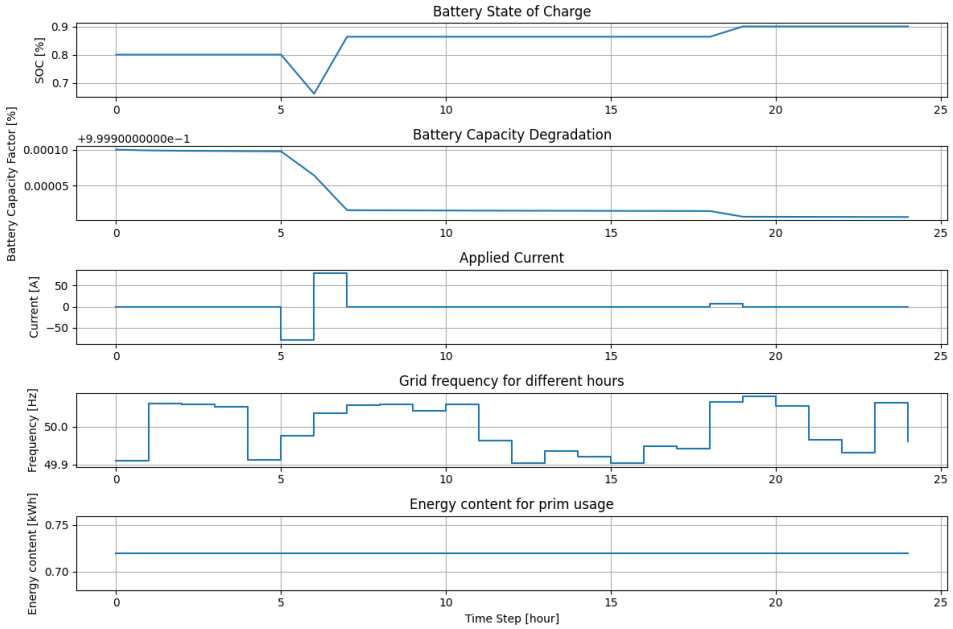

Figure B.1: NCA, LUL, 1 jan, unlimited

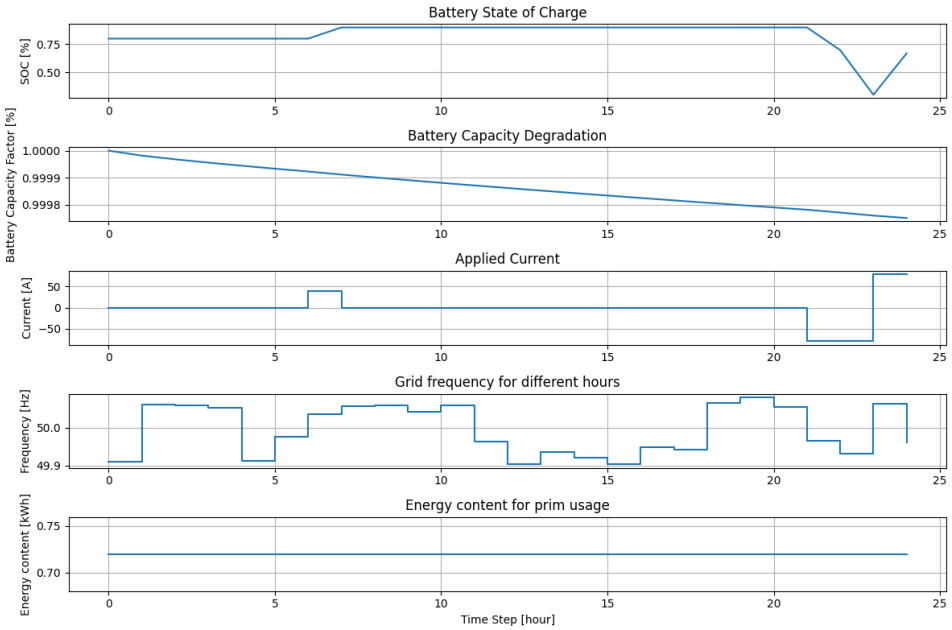

Figure B.2: LFP, LUL, 1 jan, unlimited

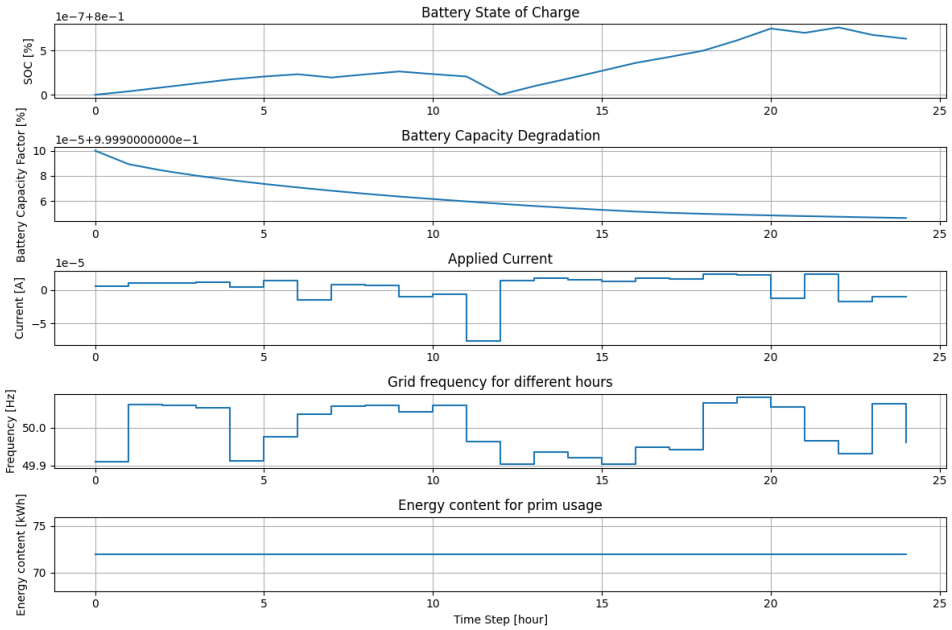

Figure B.3: NCA, GOT, 1 jan, unlimited

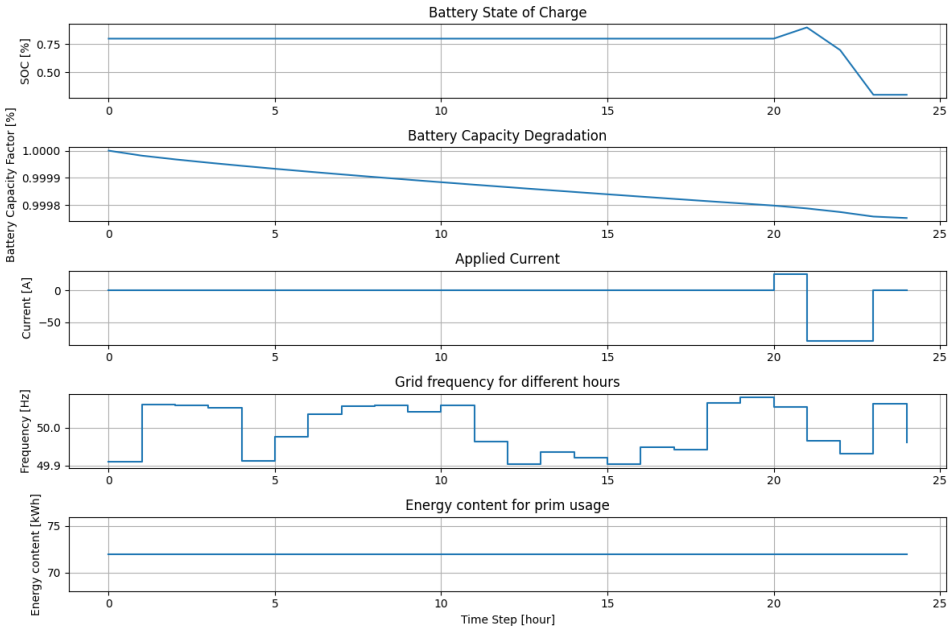

Figure B.4: LFP, GOT, 1 jan, unlimited

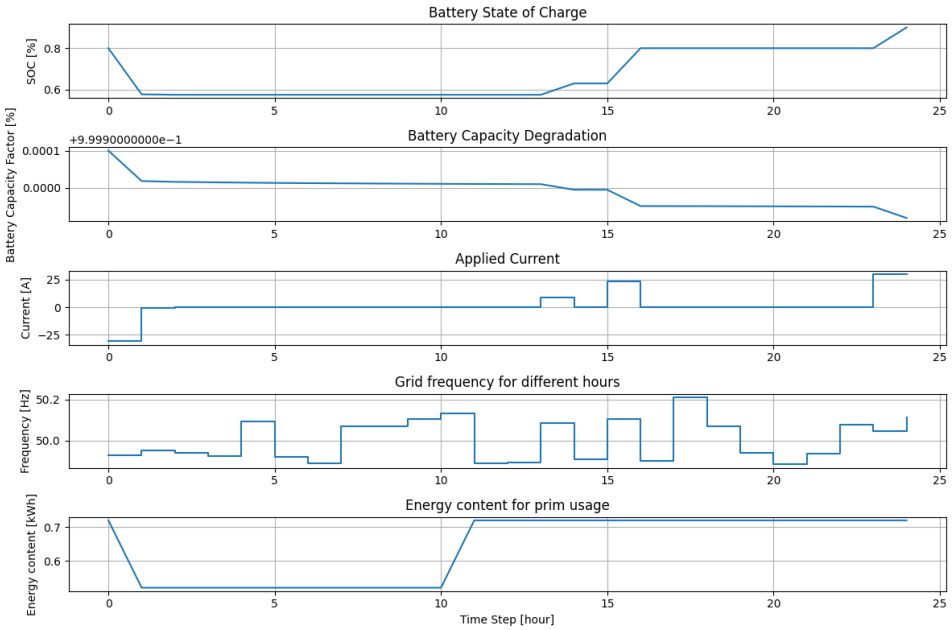

Figure B.5: NCA, LUL, 1 apr, unlimited

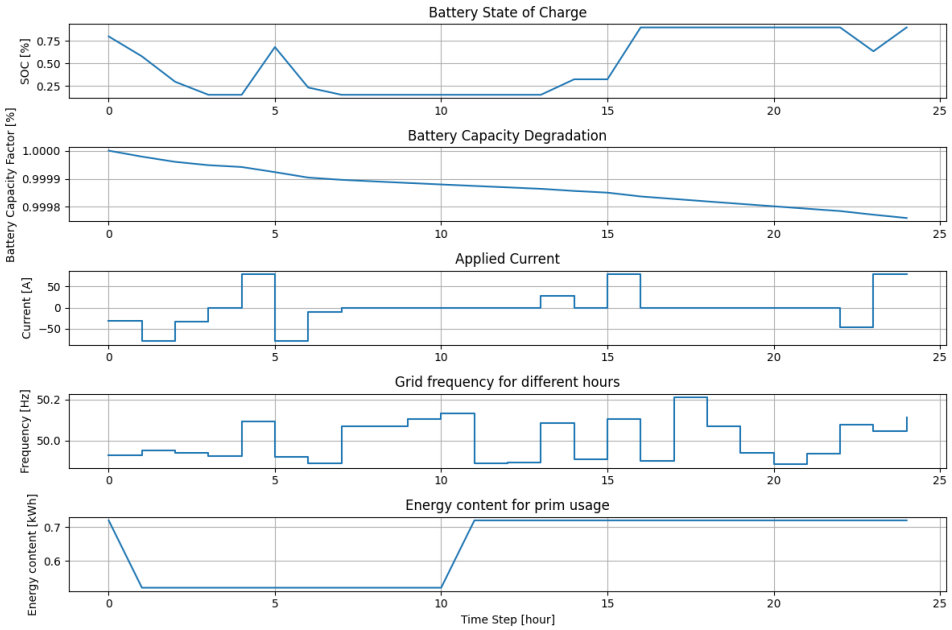

Figure B.6: LFP, LUL, 1 apr, unlimited

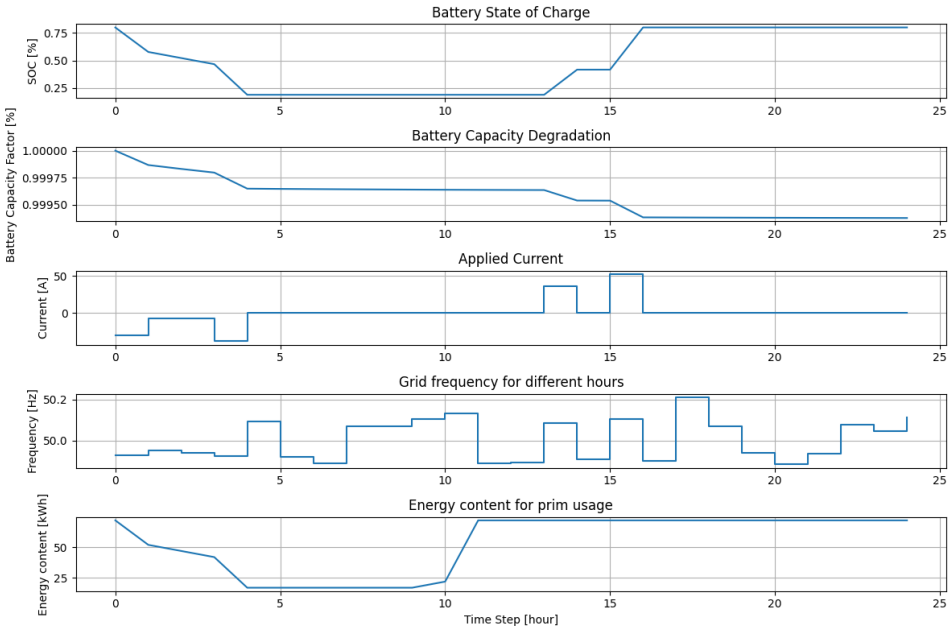

Figure B.7: NCA, GOT, 1 apr, unlimited

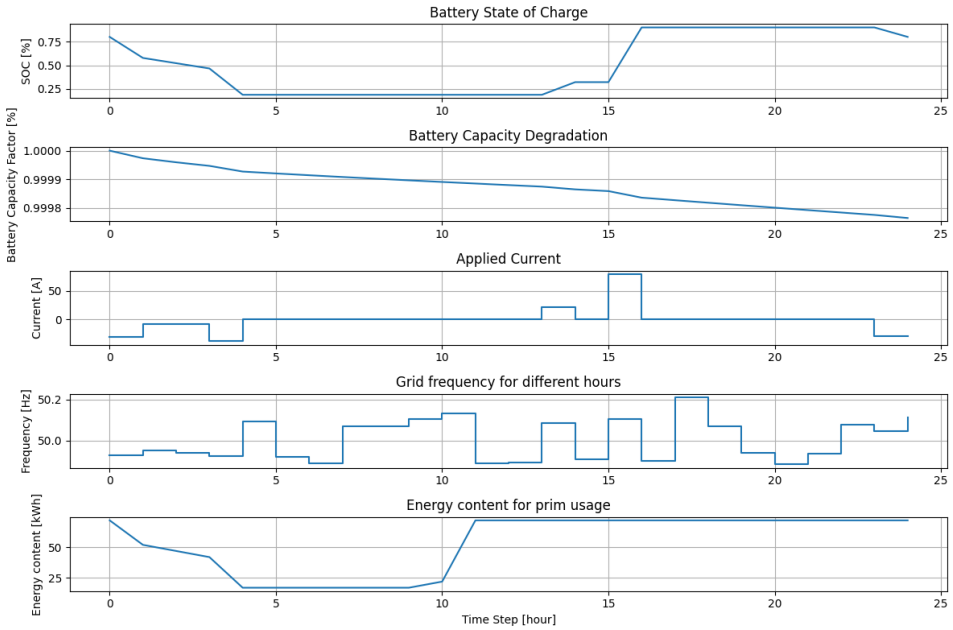

Figure B.8: LFP, GOT, 1 apr, unlimited

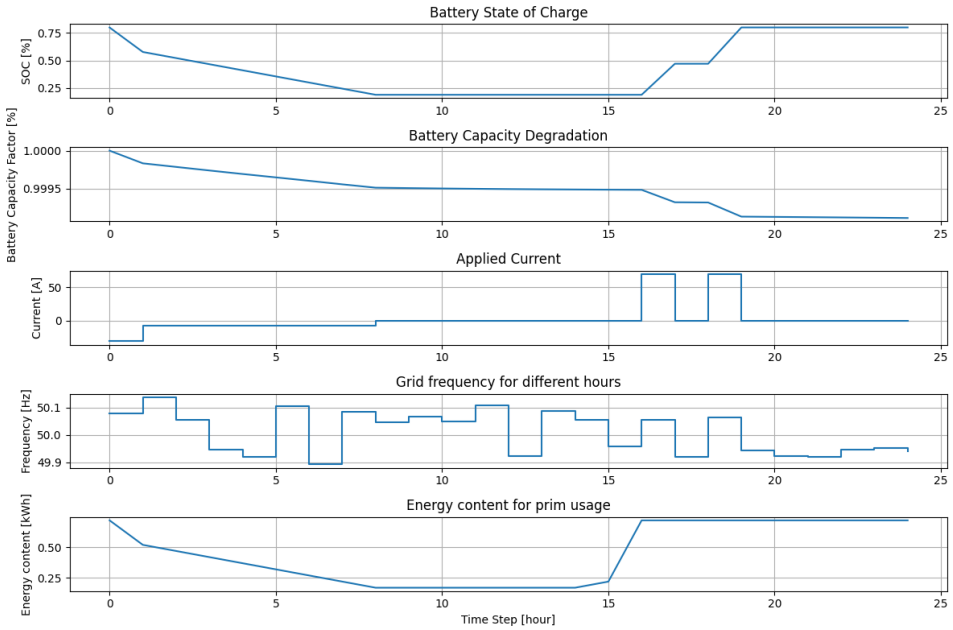

Figure B.9: NCA, LUL, 1 jun, unlimited

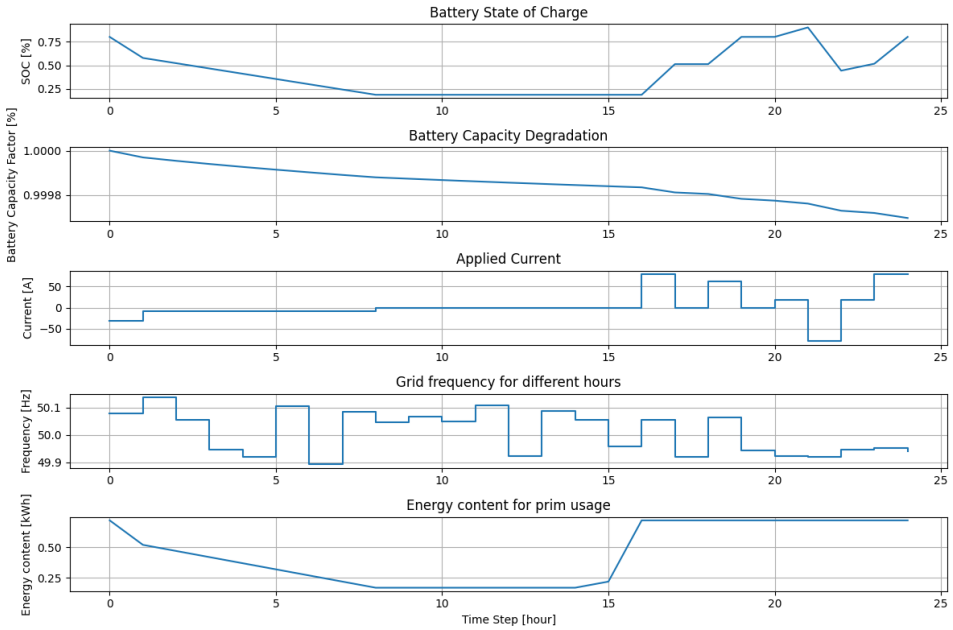

Figure B.10: LFP, LUL, 1 jun, unlimited

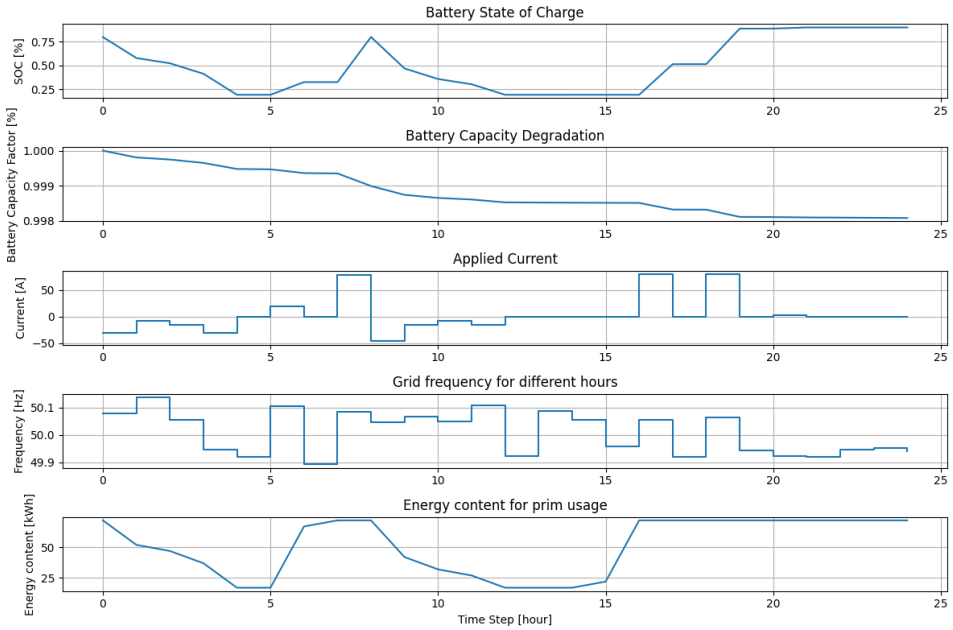

Figure B.11: NCA, GOT, 1 jun, unlimited

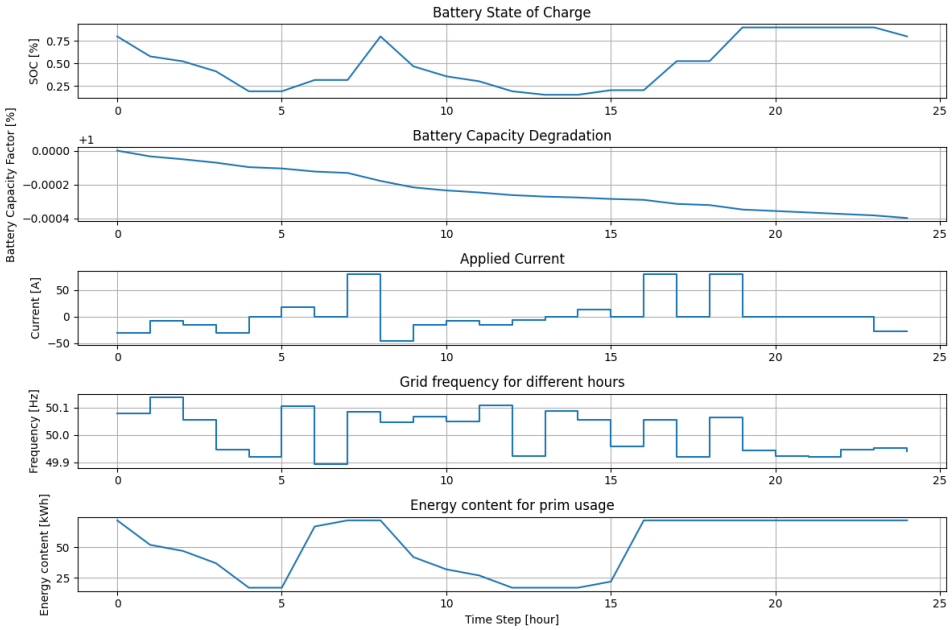

Figure B.12: LFP, GOT, 1 jun, unlimited

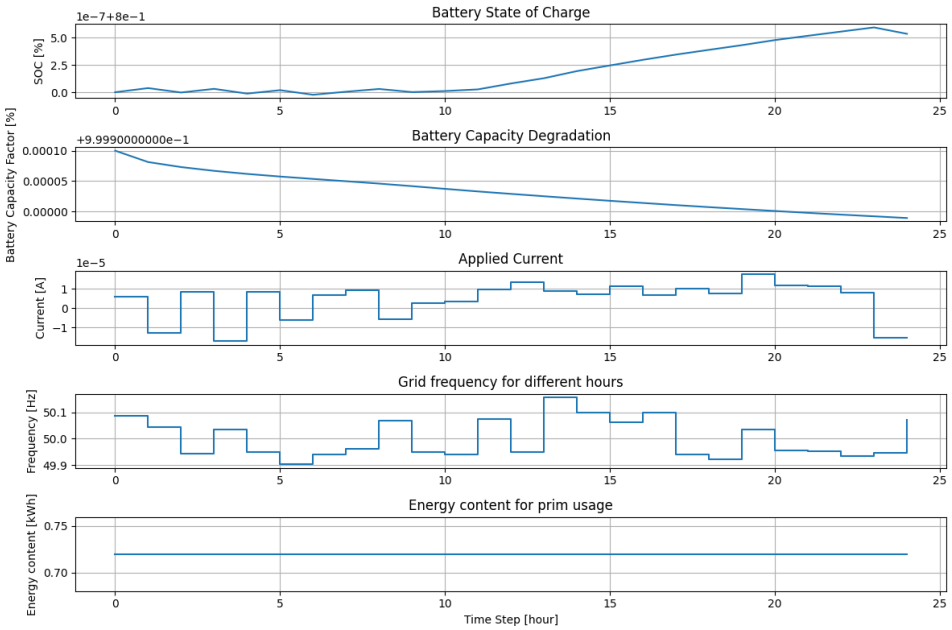

Figure B.13: NCA, LUL, 1 sept, unlimited

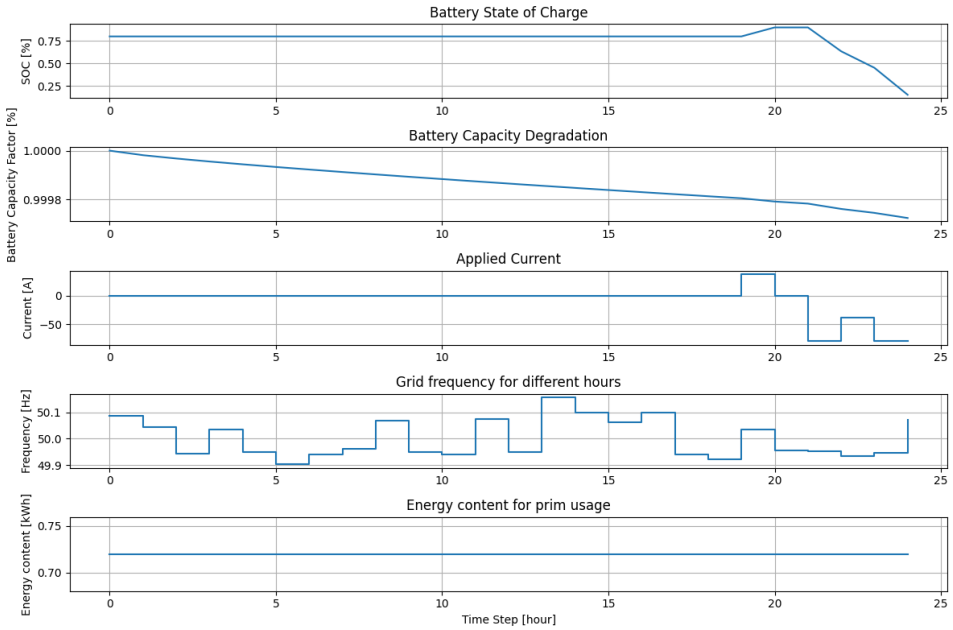

Figure B.14: LFP, LUL, 1 sept, unlimited

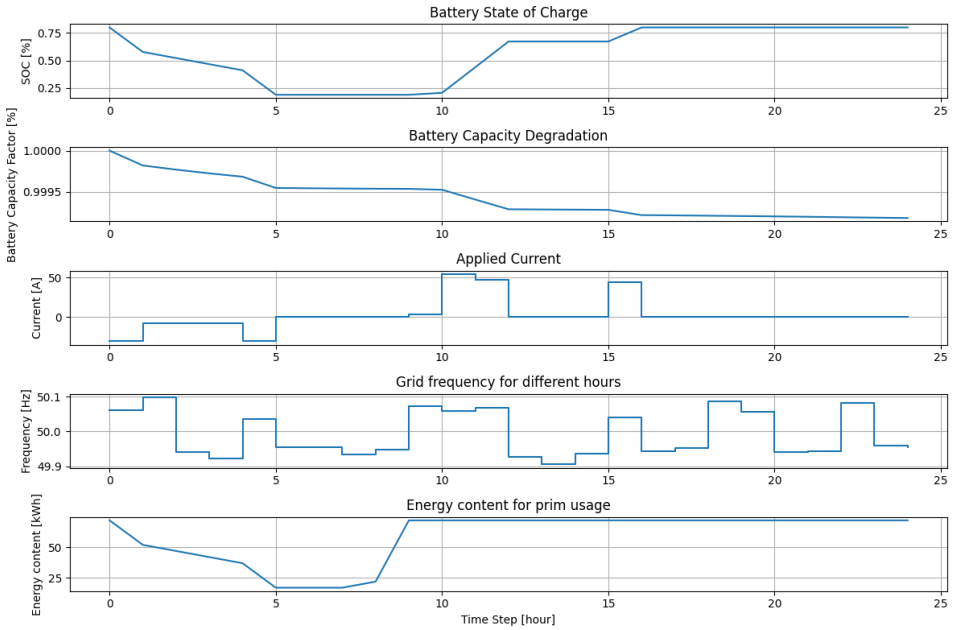

Figure B.15: NCA, GOT, 1 sept, unlimited

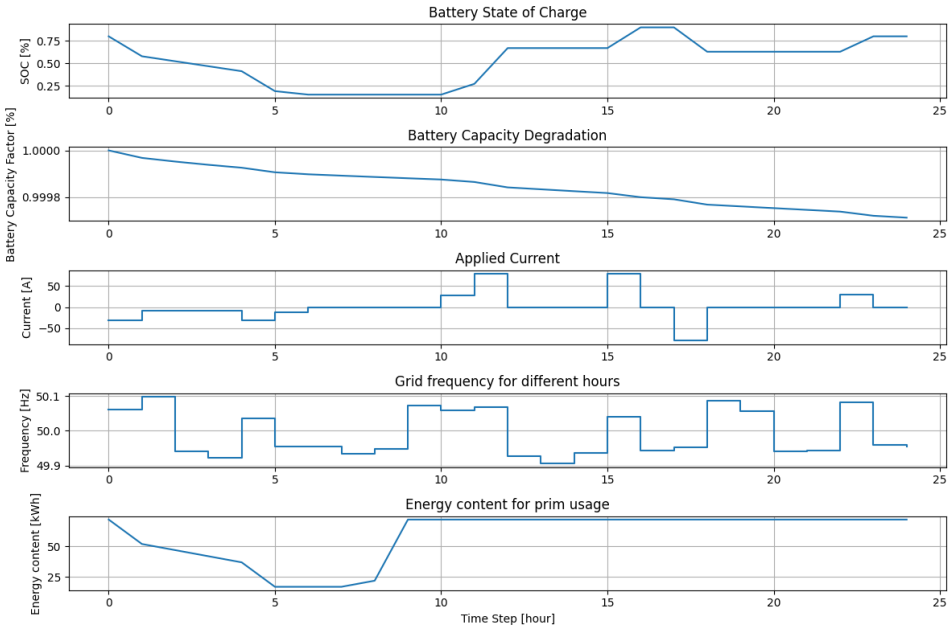

Figure B.16: LFP, GOT, 1 sept, unlimited

Use case 2

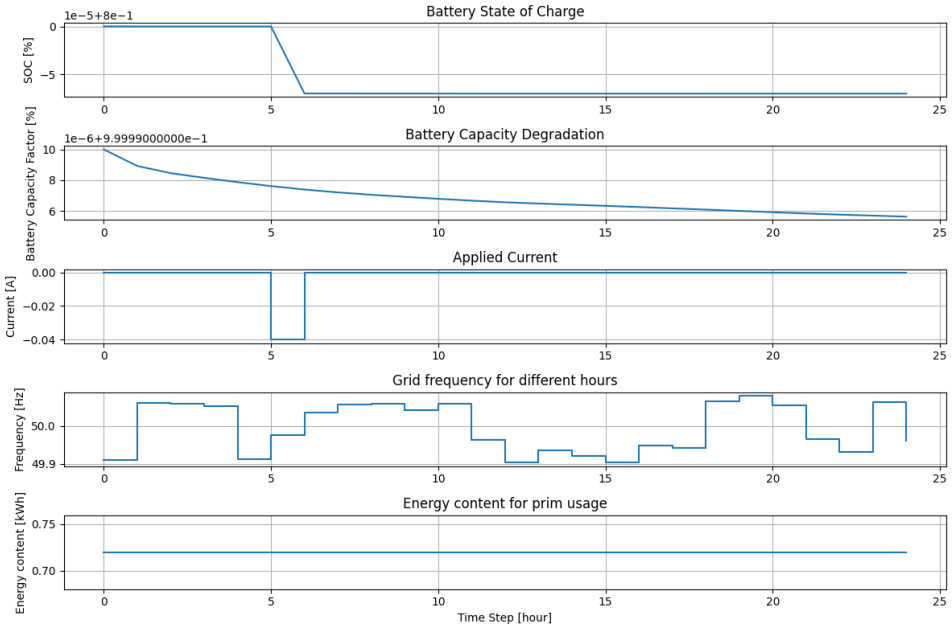

Figure B.17: NCA, LUL, 1 jan, limited

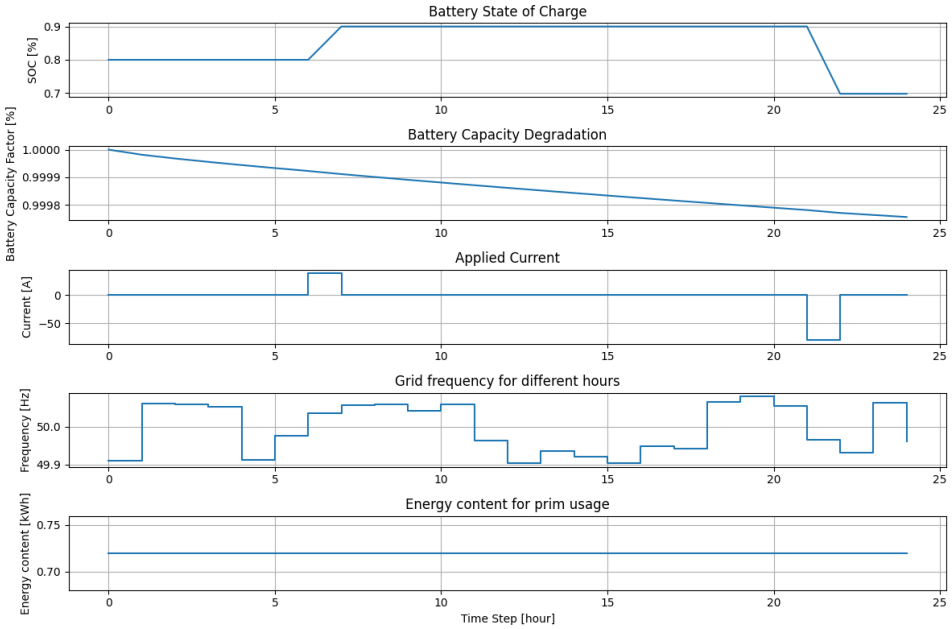

Figure B.18: LFP, LUL, 1 jan, limited

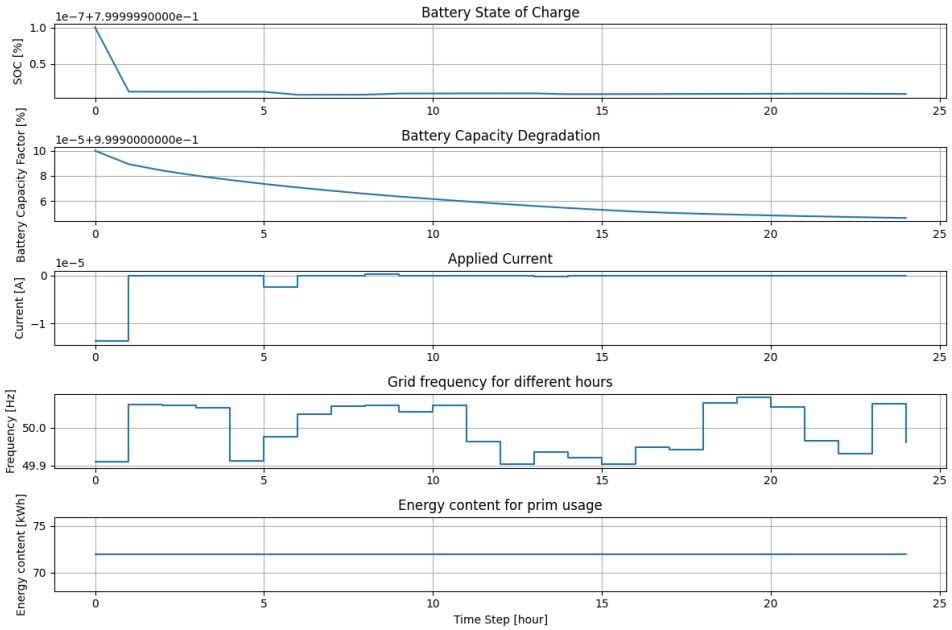

Figure B.19: NCA, GOT, 1 jan, limited

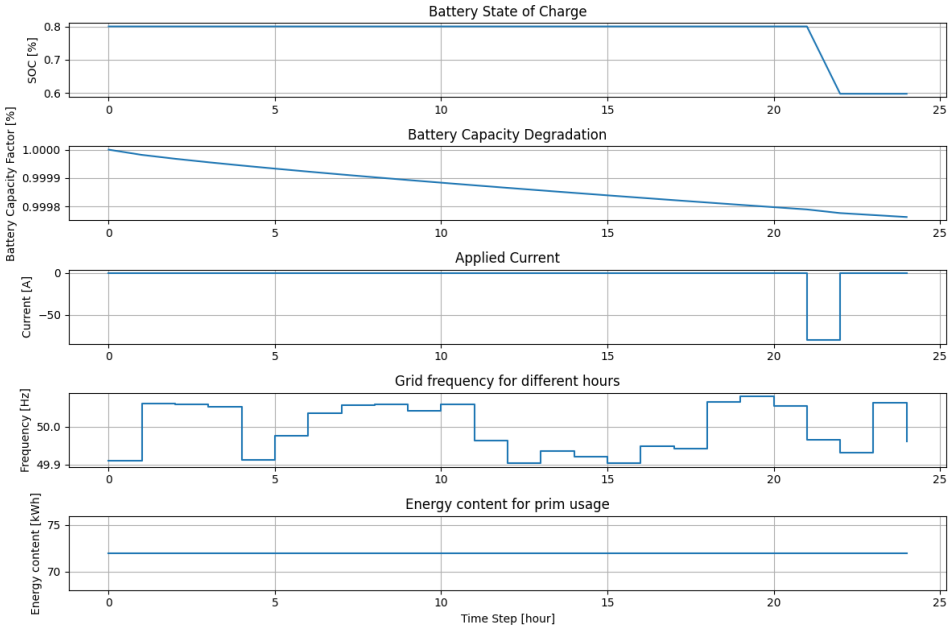

Figure B.20: LFP, GOT, 1 jan, limited

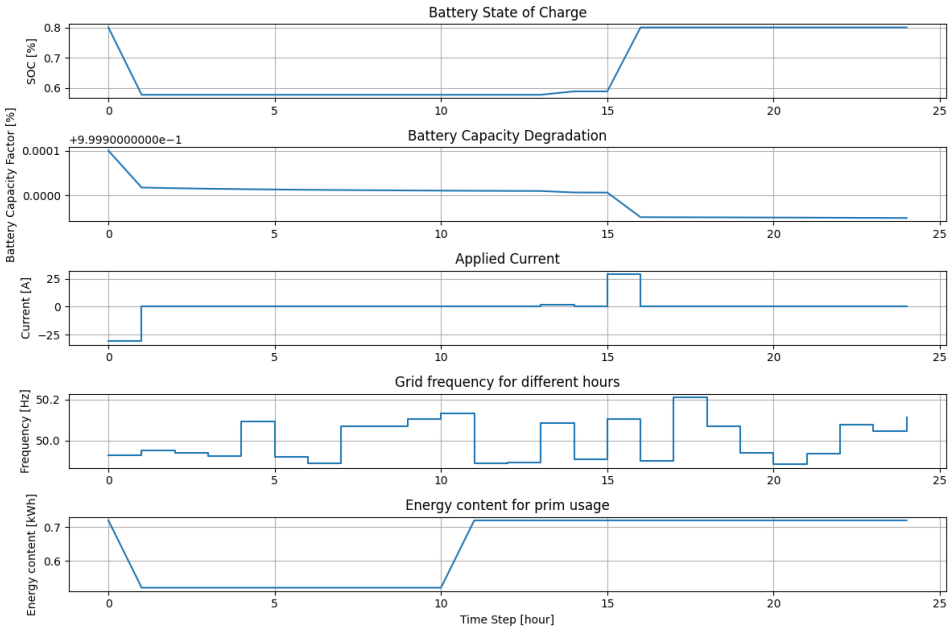

Figure B.21: NCA, LUL, 1 apr, limited

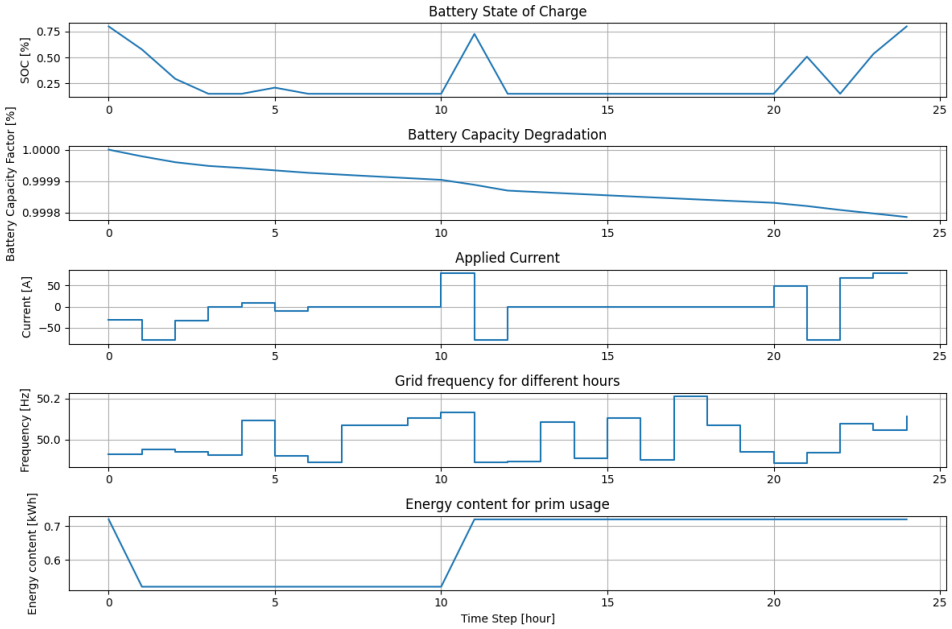

Figure B.22: LFP, LUL, 1 apr, limited

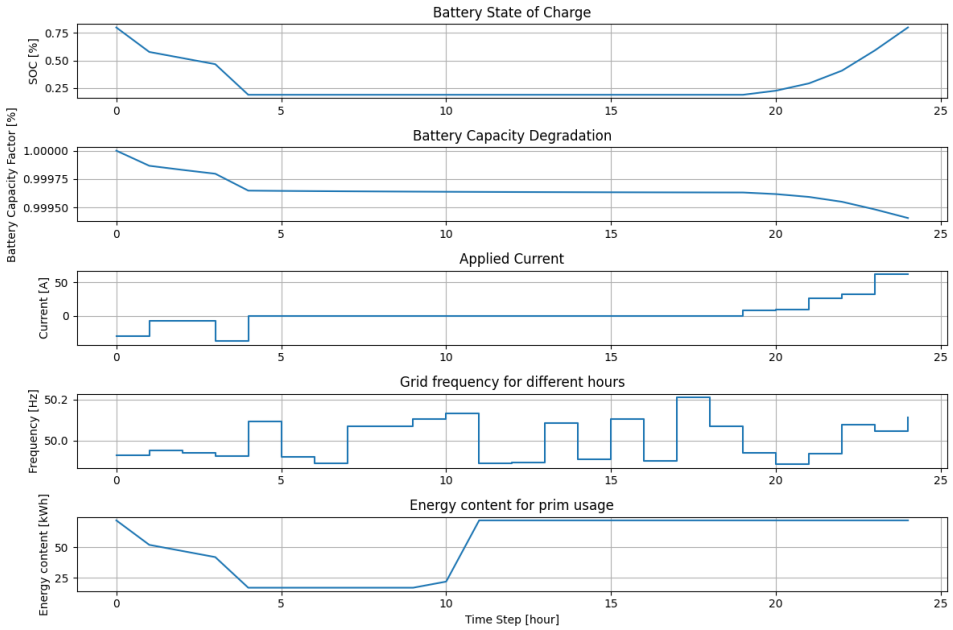

Figure B.23: NCA, GOT, 1 apr, limited

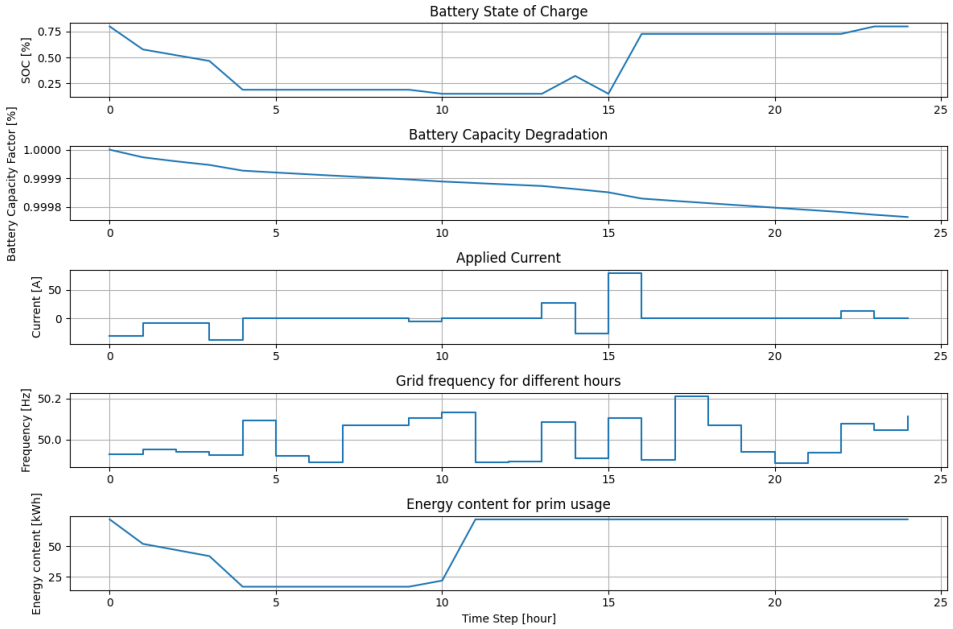

Figure B.24: LFP, GOT, 1 apr, limited

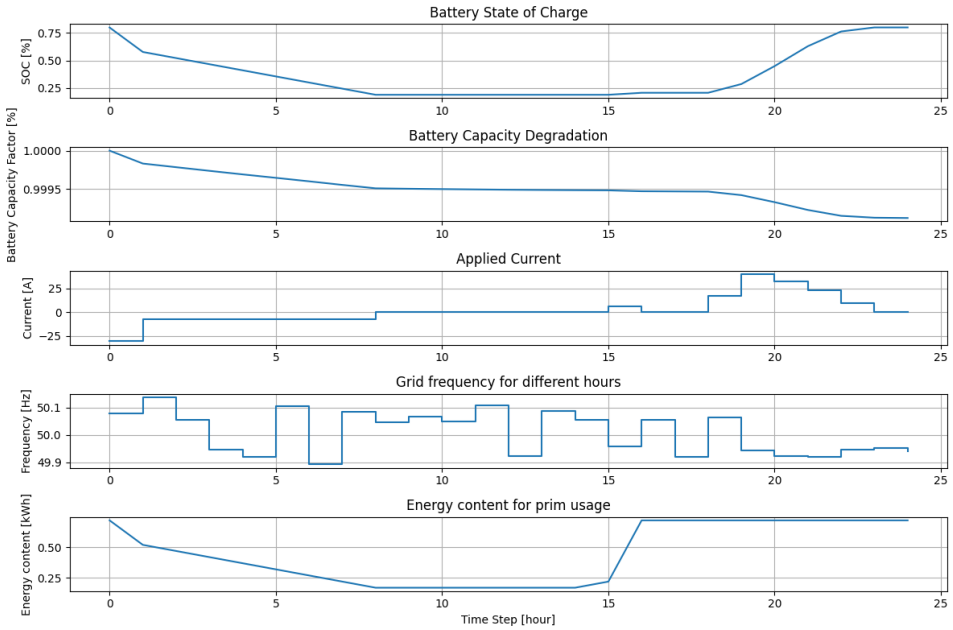

Figure B.25: NCA, LUL, 1 jun, limited

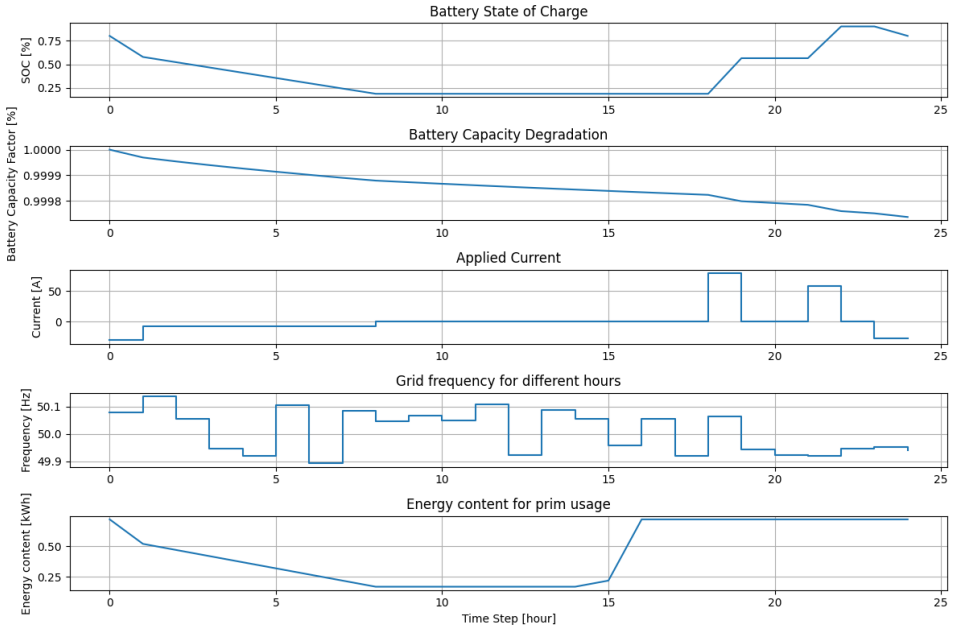

Figure B.26: LFP, LUL, 1 jun, limited

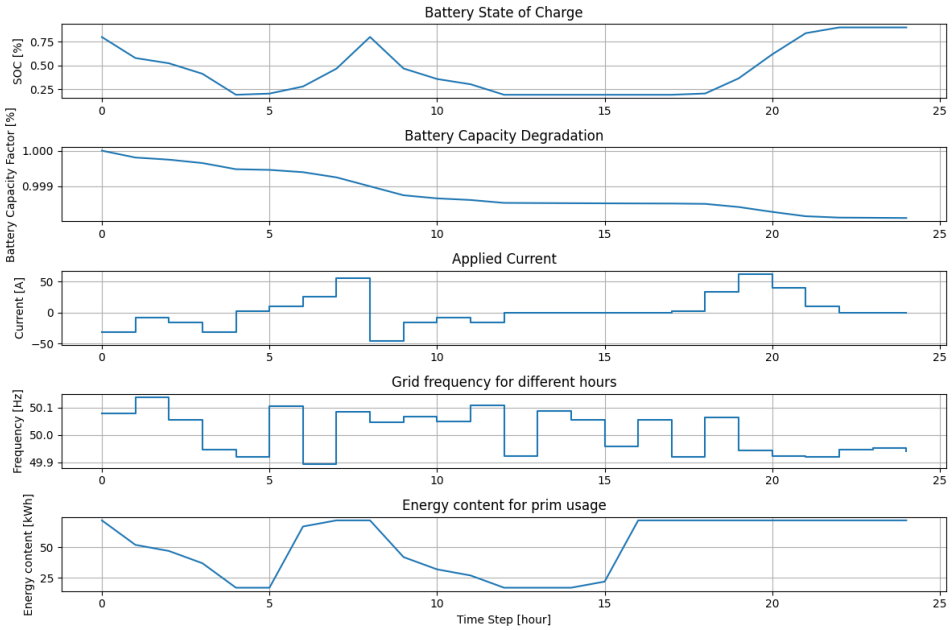

Figure B.27: NCA, GOT, 1 jun, limited

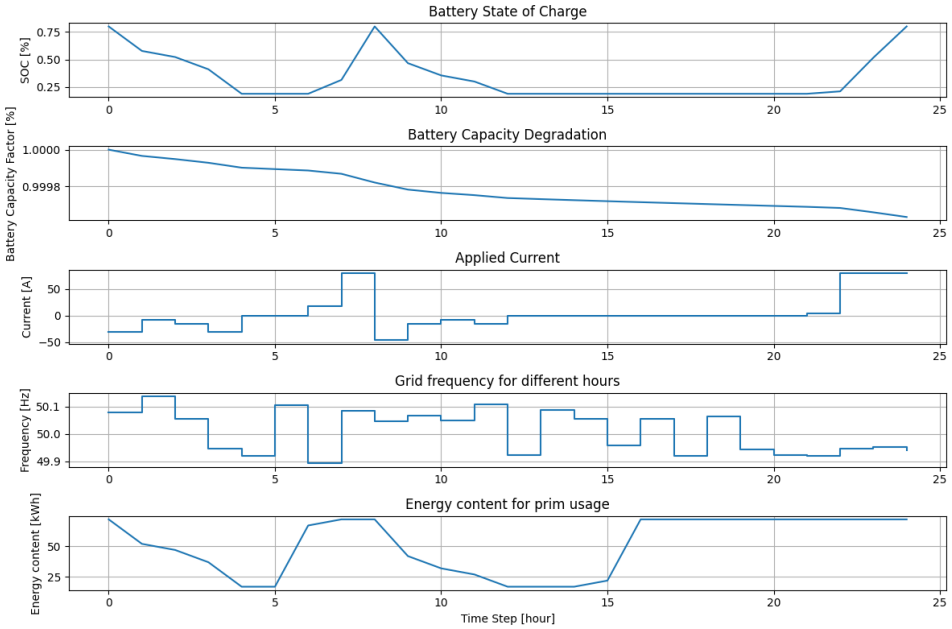

Figure B.28: LFP, GOT, 1 jun, limited

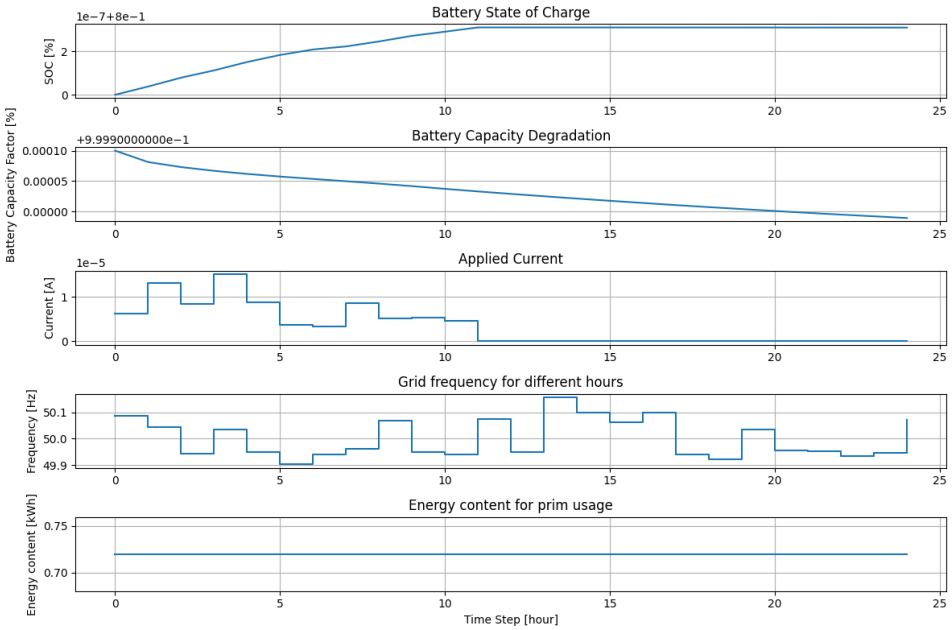

Figure B.29: NCA, LUL, 1 sept, limited

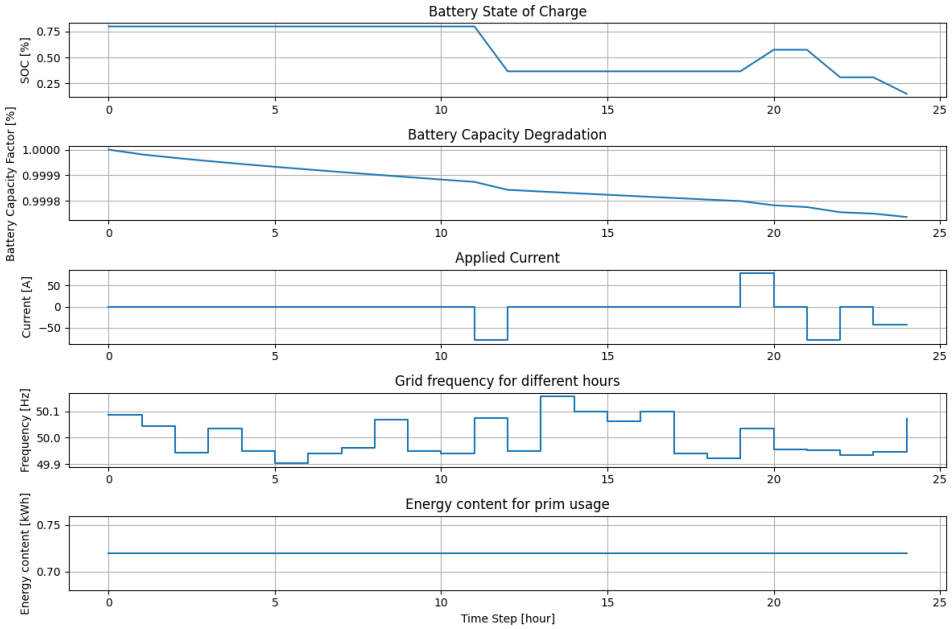

Figure B.30: LFP, LUL, 1 sept, limited

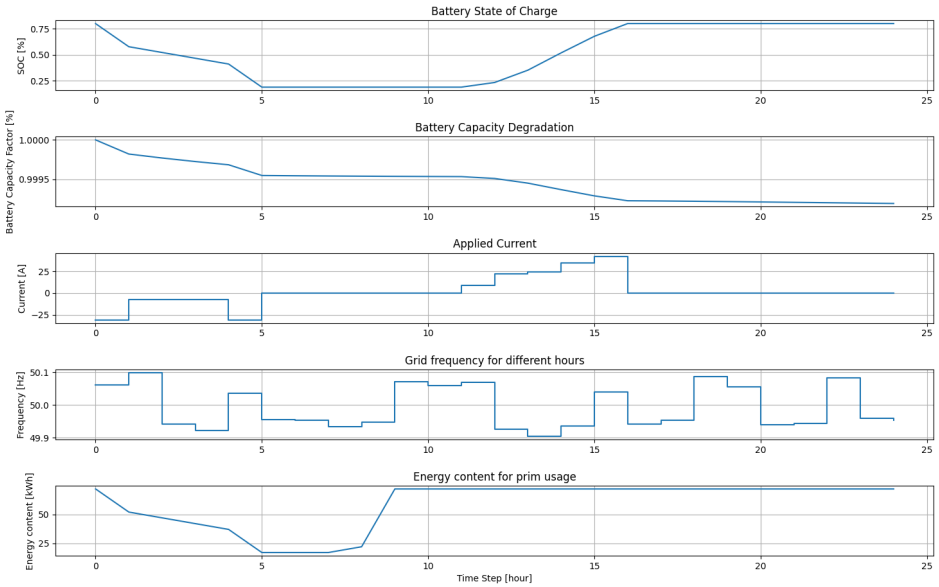

Figure B.31: NCA, GOT, 1 sept, limited

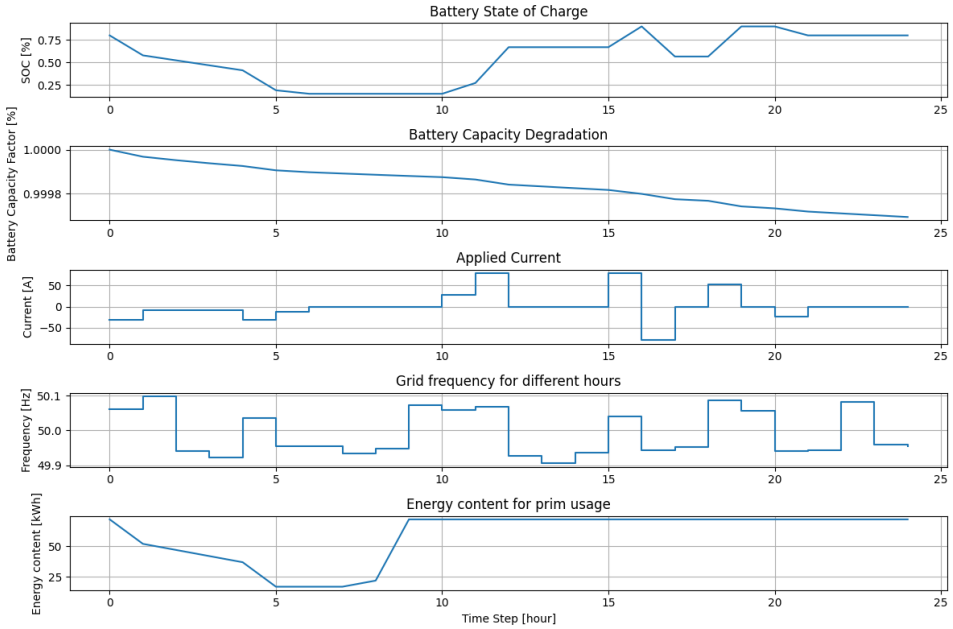

Figure B.32: LFP, GOT, 1 sept, limited

Longer runs

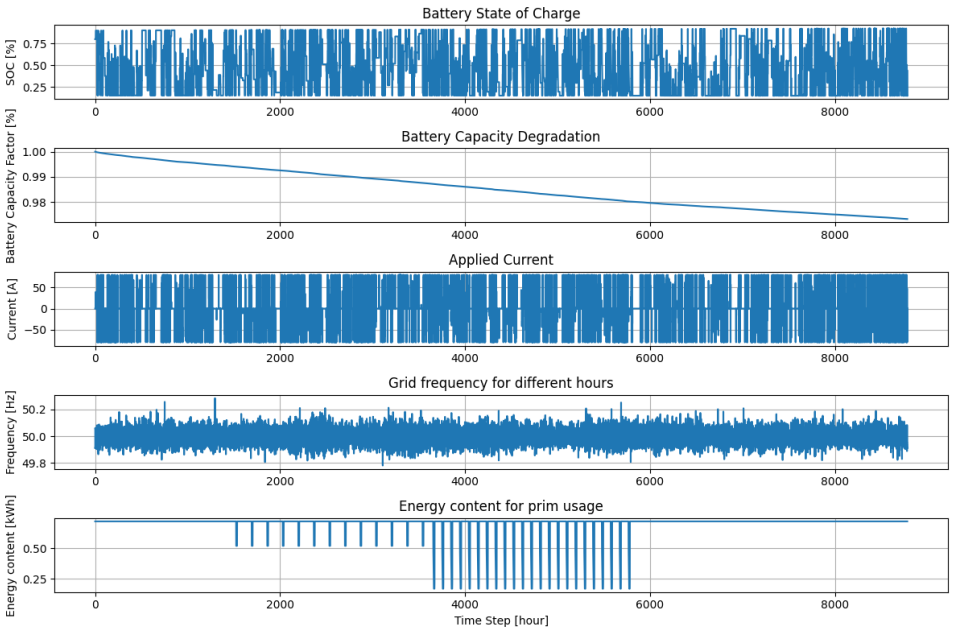

Figure B.33: Long run with: deg factor 1, warranty = 1, sim time = 1, limited

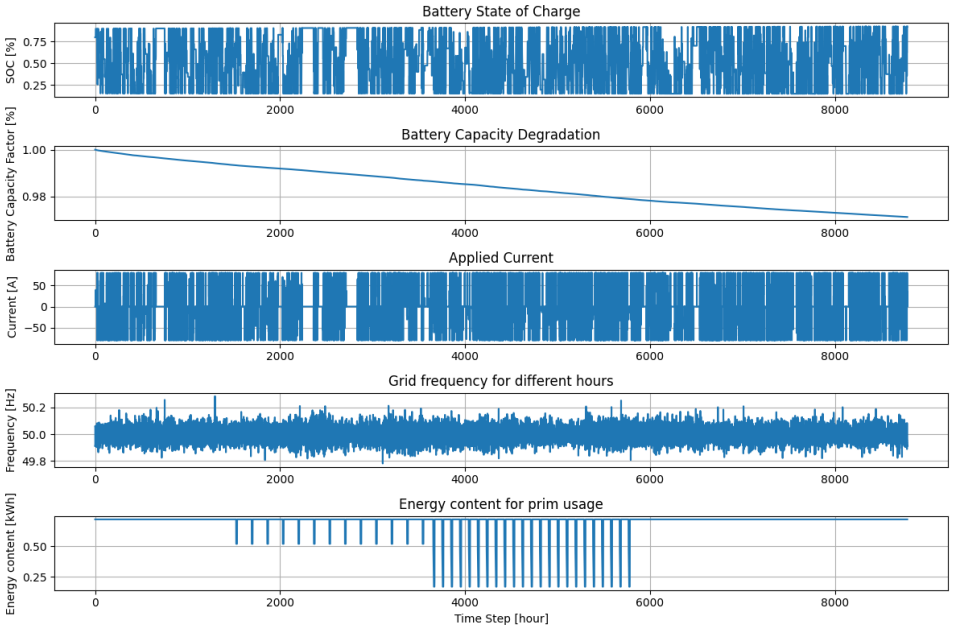

Figure B.34: Long run with: deg factor 1, warranty = 1, sim time = 1, unlimited

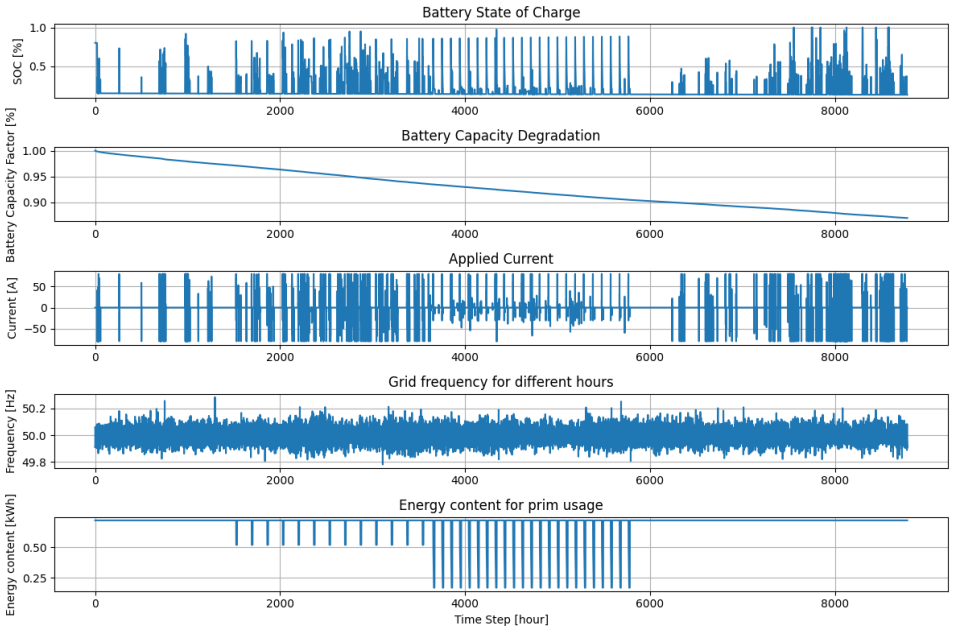

Figure B.35: Long run with: deg factor 5*1.39, warranty = 1, sim time = 1, limited

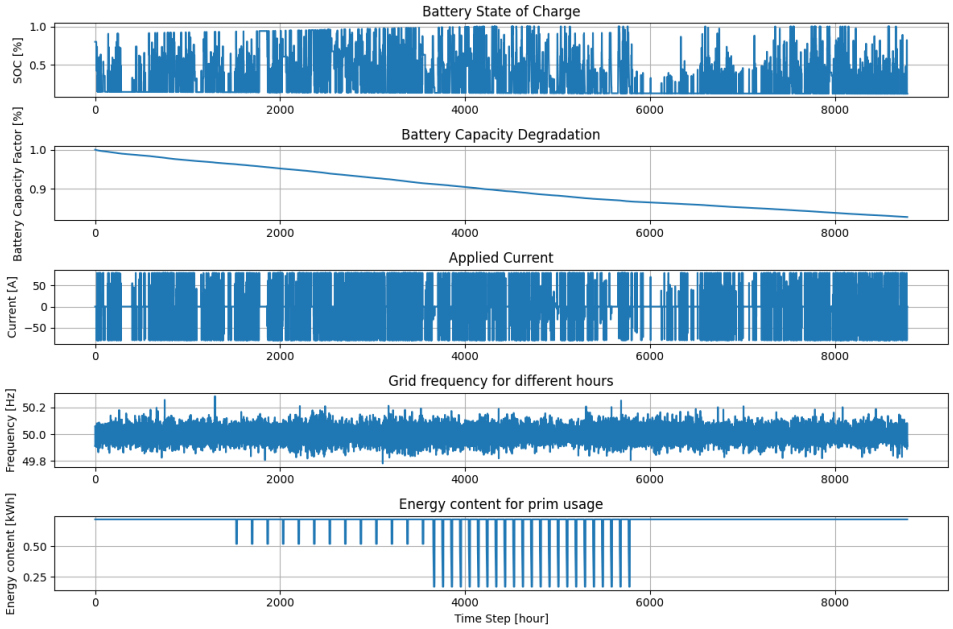

Figure B.36: Long run with: deg factor 5*1.39, warranty = 1, sim time = 1, unlimited

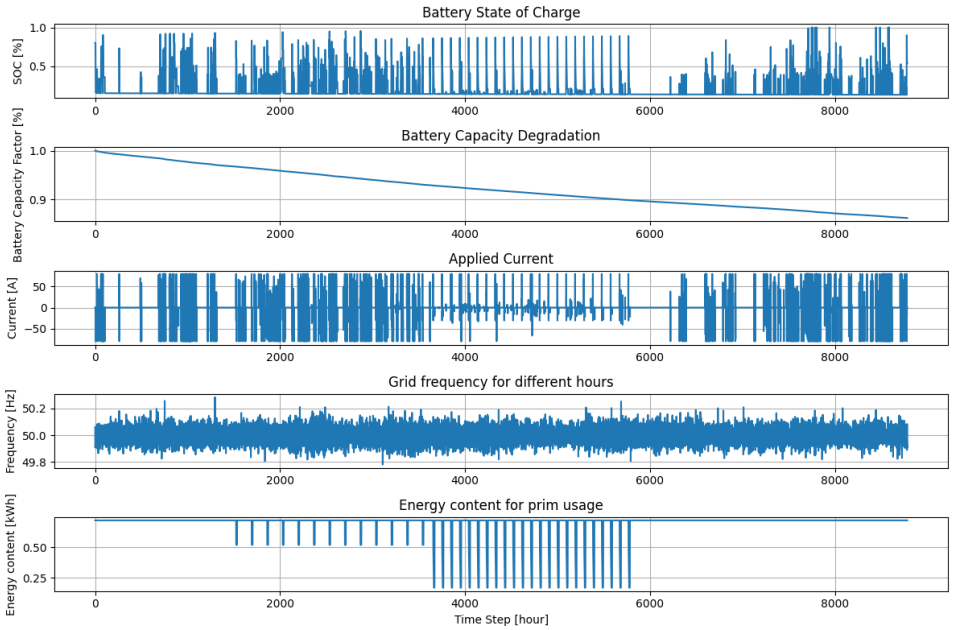

Figure B.37: Long run with: deg factor 5*1.45, warranty = 1, sim time = 1, limited

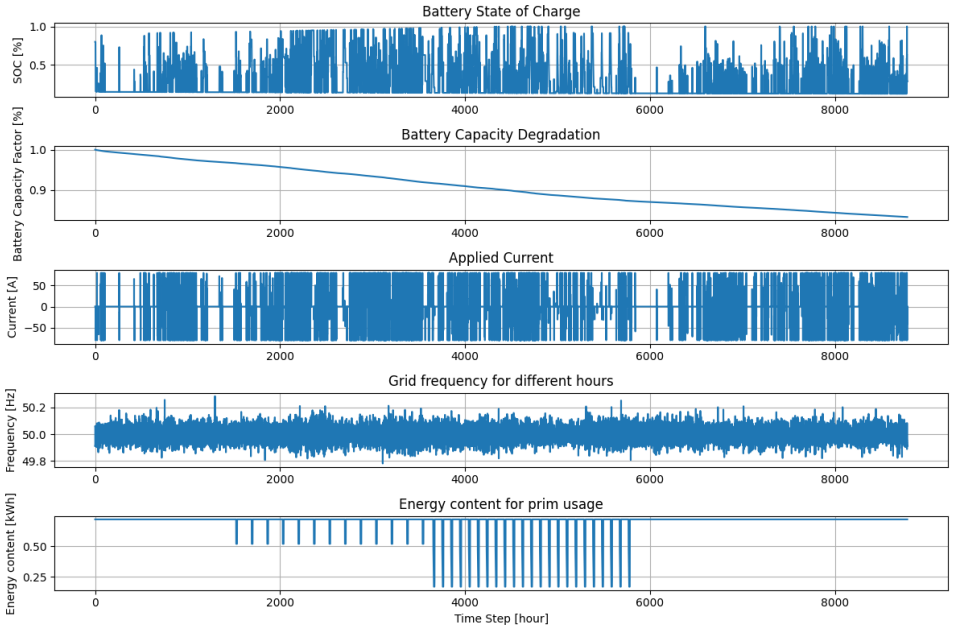

Figure B.38: Long run with: deg factor 5*1.45, warranty = 1, sim time = 1, unlimited

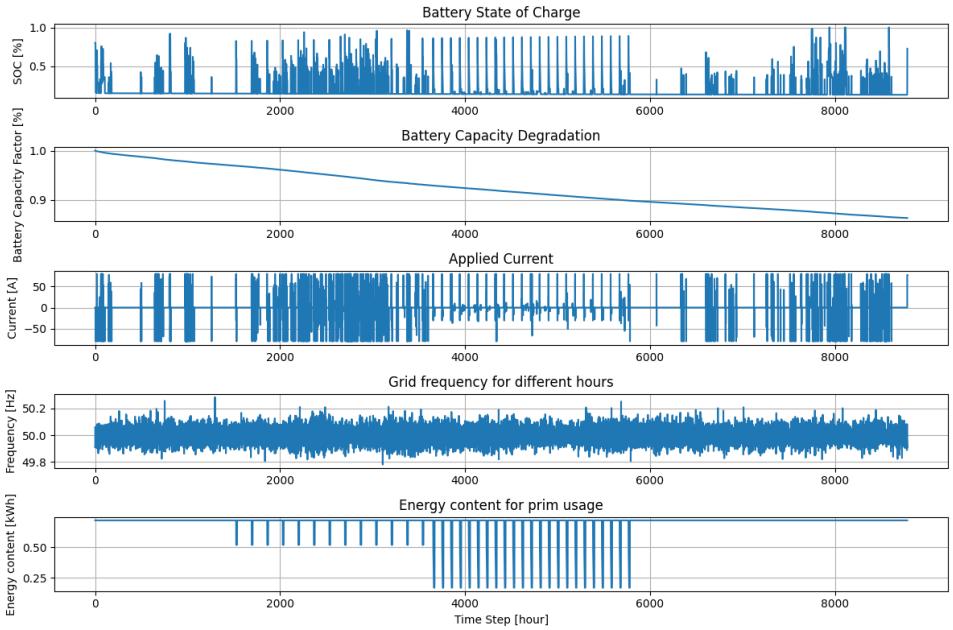

Figure B.39: Long run with: deg factor 5*[1.45, 1.65], warranty = 1, sim time = 1, limited

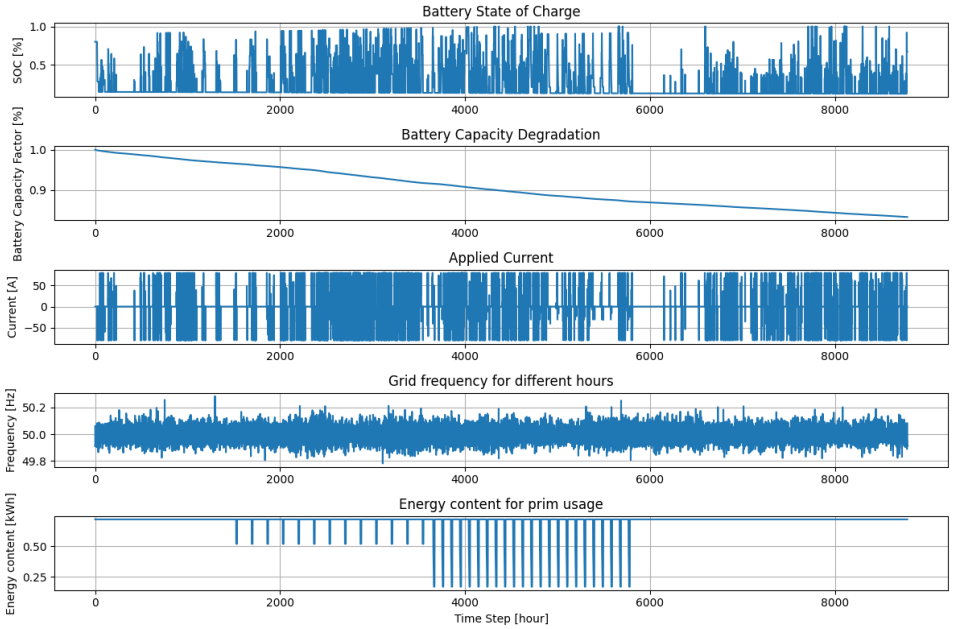

Figure B.40: Long run with: deg factor 5*[1.45, 1.65], warranty = 1, sim time = 1, limited

Department of Mechanics and Maritime Sciences
CHALMERS UNIVERSITY OF TECHNOLOGY
Gothenburg, Sweden
www.chalmers.se

CHALMERS
UNIVERSITY OF TECHNOLOGY